Investigations of the flume test and mini-slump test for thickened tailings disposal

by

Jinglong Gao

This thesis is presented for the degree of

Doctor of Philosophy

at

The University of Western Australia

School of Civil, Environmental and Mining Engineering

July 2015

DECLARATION FOR THESES CONTAINING PUBLISHED WORK AND/OR WORK PREPARED FOR PUBLICATION

In accordance with regulations of the University of Western Australia, this thesis is organised as a series of papers. This thesis contains published work and work prepared for publication, which have been co-authored. The bibliographical details of the work and where it appears in the thesis are outlined below.

Paper 1

The first paper is presented as Chapter 2 and is authored by the candidate and Professor Andy Fourie. The paper has been submitted.

J. Gao and A. B. Fourie, "Studies on thickened tailings deposition in flume tests using the CFD method," *International Journal of Mineral Processing*. Submitted.

The candidate (i) designed and carried out the CFD simulations; (ii) analysed the resulting data; and (iii) wrote the initial version of the paper. Professor Andy Fourie revised the paper and offered valuable discussions and suggestions.

Paper 2

The second paper is presented as Chapter 3 and is authored by the candidate and Professor Andy Fourie. The paper was published as:

J. Gao and A. B. Fourie, "Spread is better: An investigation of the mini-slump test," *Minerals Engineering,* vol. 71, pp. 120-132, 2015.

The candidate (i) planned and carried out the laboratory experiment; (ii) performed the CFD simulations for mini-slump tests; (iii) analysed the experimental and numerical data; and (iiii) wrote the initial version of the paper. Professor Andy Fourie wrote the abstract and revised the paper. He also offered valuable discussions and suggestions.

Paper 3

The third paper is presented as Chapter 4 and is authored by the candidate and Professor Andy Fourie. The paper has been accepted for publication.

J. Gao, A. Fourie, Using the flume test for yield stress measurement of thickened tailings, Minerals Engineering, 81 (2015) 116-127.

The candidate (i) performed the CFD simulations for flume tests; (ii) conducted theoretical analysis for flume tests (iii) analysed the simulation results; and (iiii) wrote the initial version of the paper. Professor Andy Fourie revised the paper and offered valuable discussions and suggestions.

Paper 4

The fourth paper is presented as Appendix A and is authored by the candidate and Professor Andy Fourie. The paper was published as:

J. Gao and A. Fourie, "Studies on flume tests for predicting beach slopes of paste using the computational fluid dynamics method," in *Proceedings of the 17th International Seminar on Paste and Thickened Tailings (Paste 2014)*, Vancouver, Canada, 2014.

The candidate (i) designed and performed the CFD simulations for flume tests; (ii) analysed the simulation results; and (iiii) wrote the initial version of the paper. Professor Andy Fourie revised the paper and offered valuable discussions and suggestions.

All the work was conducted under the supervision of Professor Andy Fourie.

Jinglong. Gao	[redacted]	30/07/2015
Print Name	Signature	Date
Andy Fourie	[redacted]	30/07/2015
Print Name	Signature	Date

ABSTRACT

Accurate prediction of the beach slope that results upon deposition is integral to realise the potential benefits of thickened tailings technology. Although there is notable improvement in understanding the deposition of thickened tailings, accurate beach slope prediction is still imprecise. A flume test which has been successfully used to predict the beach slope of conventional tailings for many years, has been found to produce unrealistically steeper slopes than those achieved in the field for thickened tailings. This different performance of flume tests for beach slope prediction between conventional and thickened tailings is generally attributed to the presence of a yield stress in thickened tailings, which is a key design parameter for thickened tailings disposal. Additionally, although there are a number of techniques to obtain the yield stress of thickened tailings, the mini-slump test has become the preferred method to quickly measure the yield stress in industry due to its simplicity. However the accuracy of mini-slump test is not very high due to some inherent defects.

Therefore the intentions of the thesis were to: (1) highlight the factors that influence the slope achieved in flumes, thereby developing a good understanding of thickened tailings deposition; (2) conduct a thorough study on the measurement of yield stress by slump testing to gain an appreciation of the advantages and limitations of the mini-slump test and provide useful guidelines for the operation and utilisation of the mini-slump test in

industry; (3) develop a cheap, easy and accurate technique for yield stress measurement of thickened tailings in both the laboratory and the field.

The objectives of this thesis have been fulfilled and the results are summarised as follows:

1. Computational Fluid Dynamics (CFD) simulations of laboratory flume tests on thickened tailings were carried out to highlight the factors that may impact on the final profiles (slopes) measured in the flumes. In particular, the software ANSYS FLUENT was used to conduct the simulations for both sudden-release (S-R) and discharge flume tests with thickened tailings treated as a Bingham fluid. The Volume of Fluid (VOF) model was used to track the free surface between air and Bingham fluid in the laminar regime. The numerical model was first validated against the analytical solution of sheet flow of Bingham fluid. It was then used to investigate the influence of several factors, including the volume of fluid, energy, rheological properties, flume width and the base angle of the flume on the slopes of the final profiles achieved in both S-R and discharge flume tests. The results show that an increase of volume, energy, flume width or base angle reduces the resulting slope angle. Moreover the yield stress of the fluid generally has more influence on the final profiles than the viscosity. In addition, the viscosity tends to have less influence on the formation of the final profiles if the inertial effects are relatively weak. Two dimensionless parameters were proposed to establish the relationship among the average slope, rheological properties and geometrical parameters

for a planar deposition of thickened tailings, which may have a potential to predict the beach slope of thickened tailings in the field. These results provide a better understanding of the process of deposition of thickened tailings in the field. The agreement between simulation results and laboratory observations in the literature gives confidence in the veracity of the computational results.

2. CFD simulations were used to investigate the mini-slump test with a cylindrical mould. Simulations with different mould lifting velocities were carried out to understand the influence of mould lifting velocity. The predicted slump and spread from mini-slump test simulations for three different scenarios ($v_{lifting}$ = 0.002 m/s, $v_{lifting}$ = 0.01 m/s, and without mould lifting process, i.e. instantaneous disappearance of the mould) were compared to those from laboratory experiments on kaolin. The rheological properties of the kaolin were measured using a vane rheometer and the data used directly in the modelling study. The results suggest that the lifting speed of the mould has a significant influence on the mini-slump test result, which must therefore be taken into account in both numerical simulations and laboratory tests. It was found that the variation of mould lifting velocity had a greater influence on slump than spread, indicating that spread is a more appropriate measurement for determining the yield stress in a mini-slump test. This was particularly true for relatively low yield stresses (e.g. 60 Pa or less), which are values typical of most thickened tailings deposits currently operating internationally.

3. In view of the relatively low accuracy of the mini-slump test for yield stress

measurement of thickened tailings in industry, the feasibility of using a laboratory flume test to measure the yield stress of thickened tailings was evaluated. The model of slow sheet flow (SSF) which has previously been used to model flume tests, and the Fourie and Gawu (FG) model, which was developed for interpretation of flume tests on thickened tailings, were compared. The SSF model, derived within the framework of long-wave approximation, is shown to only hold for flumes with frictionless sidewalls (or very wide flumes), whereas the FG model is valid for flumes of finite width and nonslip sidewalls. These findings were confirmed using CFD simulations of laboratory flume tests with nonslip and free-slip sidewalls on materials with yield stresses ranging from 20 to 60 Pa. Simulations to investigate the sensitivity of the final beach profile in the flume test to variations of yield stress and viscosity were performed. The results suggest that the final profile is very sensitive to yield stress variation but relatively insensitive to viscosity variation. This relative insensitivity to viscosity further justifies the use of the FG model for evaluation of yield stress from flume test data, as this model ignores the effect of viscosity. Simulations of mini-slump tests were conducted to demonstrate that different mould lifting velocities may introduce different inertial effects, thereby impacting the final profile and hence the yield stress extrapolated from slump tests. Moreover, comparison between the profiles predicted by several theoretical models for slump tests and CFD simulation results revealed that the existing models are not capable of capturing the final shape of the slumped material, which is inevitably distorted by the mould friction

to some extent. Consequently, the accuracy of the yield stress extrapolated from mini-slump tests is not high. The small errors in yield stresses calculated from the CFD simulation results using the FG model suggest that yield stresses may be determined from flume tests with very high accuracy using the FG model.

NOMENCLATURE

Symbol	Description	Unit
A	Volume of thickened tailings per width	m^2
a	Length of the patched fluid in S-R flume tests	m
b	Height of the patched fluid in S-R flume tests	m
BS_a	Average beach slope	%
D	Final spread in a mini-slump test	m
D_0	Diameter of the cylindrical mould	m
D_c	Diameter of the cylindrical container used in the viscosmeter test	m
D_v	Diameter of the vane in the viscosmeter test	m
E_p	Potential energy per unit width of fluid in S-R flume tests	J/m
E'_p	Potential energy per unit volume of fluid in S-R flume tests	J/m^3
f_s	layer split factor	
f_c	Layer collapse factor	
F_r	Froude number	
g	Gravitational acceleration	m/s^2
H	Characteristic thickness of thickened tailings deposited on an inclined plane	m
H_0	Thickness of the yield stress fluid at the deposition point	m
H_v	Height of the vane in the viscosmeter test	m
h	Initial height of the fluid in the reservoir plus the height of the reservoir above the horizontal (Chapter 2)	m
h_{ideal}	Ideal cell height specified for the moving boundary	m
h_j	Height of layer j of a cell	m
h_{TTD}	Height of thickened tailings disposal (TTD) system	m
I_{av}	Typical inertial stress	Pa
ISL_{av}	Typical inertial stresses with respect to the vertical direction	Pa
ISP_{av}	Typical inertial stresses with respect to the radial direction	Pa
K	Consistency factor	$Pa \cdot s^n$
L	Overall length of the final profile of Bingham fluid	m
L'	Neglected distance of final profile for linear fit near the inlet of flume tests	m
n	Power-law index	
p	Static pressure	Pa
Q	Discharging flow rate in a discharge flume test	m^3/s

R_e	Reynolds number	
R_{IY}	Typical inertial stress – yield stress ratio	
R_{vy}	Ratio of slope variations caused by increased viscosity and increased yield stress	
r	Radius of the footprint of TTD system	m
S	Area of the patched fluid in S-R flume tests	m^2
SL_f	Final slump in a mini-slump test	m
SP_f	Final spread in a mini-slump test	m
ΔS_v	Variation of slope resulting from increased viscosity	%
ΔS_y	Variation of slope resulting from increased yield stress	%
s'	Dimensionless slump	
T_f	Flow time required to reach the final equilibrium state	s
$u(r)$	Axial velocity of fluid in pipe	m/s
u_0	Inlet velocity of pipe flow	m/s
V	Volume of the tested material in a mini-slump test	m^3
v	Instantaneous initial suspension velocity (Chapter 2)	m/s
v_{inlet}	Discharge velocity in the discharge flume test	m/s
$v_{lifting}$	Lifting velocity of the mould in a mini-slump test	m/s
$\boldsymbol{v_q}$	Velocity vector field for the q^{th} phase	m/s
$\vec{v}$	Velocity field	m/s
w	Flume width	m
Z_1	Distance between the top end of vane and the fluid surface	m
Z_2	Distance between the low end of vane and the bottom of cylindrical container	m
τ	Shear stress	Pa
$\bar{\bar{\tau}}$	Stress tensor	Pa
τ_y	Yield stress of yield-stress fluid	Pa
τ_y'	Dimensionless yield stress	
$\dot{\gamma}$	Shear rate	1/s
$\dot{\gamma}_c$	Critical shear rate	1/s
μ	Shear viscosity	Pa·s
μ_0	Plastic viscosity	Pa·s
μ_∞	Constant viscosity approached at the infinite shear limit	Pa·s
η	Apparent viscosity	Pa·s
ρ	Fluid density	kg/m^3
ρ_1	Density of phase 1	kg/m^3
ρ_2	Density of phase 2	kg/m^3
θ	Average base angle	%
α_q	Volume fraction of the q^{th} fluid in a cell	

ACKNOWLEDGEMENTS

First of all, I would like to sincerely express gratitude to my supervisor, Professor Andy Fourie, for all your time, support, and valuable discussions and comments throughout this study. I deeply appreciate that you offered weekly meetings to me, especially considering how busy you were as the head of school. I also greatly appreciate your help to revise the papers I drafted. Without your valuable discussions and adequate supervision, I could hardly imagine finishing my PhD research timely.

Professor Linming Dou and Anye Cao in China University of Mining & Technology (CUMT) are gratefully acknowledged for their support and encouragement during my PhD application.

I also gratefully acknowledge Chinese Scholarship Council (CSC) and University of Western Australia (UWA) for providing scholarships to support my PhD study.

I would sincerely acknowledge the Pawsey Supercomputing Centre (PSC) with funding from Australian Government and the Government of Western Australia for providing advanced supercomputing resources.

I am indebted to the IT staff in UWA: Keith Russell, Sebastian Daszkiewicz as well as the staff in PSC: Daniel Grimwood, David Schibeci, Ashley Chew. Thank them for their help to solve the problems I encountered when I utilised the supercomputer. I would not

have been able to run the simulations on the supercomputer in PSC thereby finishing the simulations in this thesis in time without their help.

I would like to express my sincere thanks to the technical staff in UWA: Binaya Bhattarai, Nathalie Boukpeti, Ying Guo; Claire Bearman. It is their help that make my laboratory experiment possible.

Finally I would like to thank my family for all the support. Heartfelt thanks to my wife who is extremely considerate and supportive to me.

TABLE OF CONTENTS

1. GENERAL INTRODUCTION

This thesis focuses on two widely used tests in the mining industry, i.e. the mini-slump test and the flume test. The mini-slump test is typically used to measure the yield stress of thickened tailings, which is a key design parameter in the surface disposal of thickened tailings (sometimes termed paste) while the flume test is used to predict the beach slope of tailings in the field. Despite finding widespread application in the mining industry, the two tests still have many problems in their application which needs to be resolved. This chapter introduces background information on the application of a mini-slump test and a flume test in the mining industry as well as the definition of thickened tailings used in this work. The problems identified from this discussion provided the motivation for topics covered in this thesis. These topics and the structure of the thesis are summarised in Section 1.7.

1.1 Conventional tailings slurry and thickened tailings

A mechanical crushing and grinding operation is typically involved in the processing of ores, usually resulting in a slurry with fine solid particles, followed by an extraction process to separate the valuable fraction from the uneconomic fraction. The leftover materials are referred to as tailings and discharged into tailings storage facilities after transportation from the processing plant. As chemical reagents are often employed to extract the desired mineral, the tailings slurry discharged into the disposal area is often

hazardous, depending on the ore composition and the reagents used.

A tailings slurry produced in the mining industry typically has a low solid concentration as it undergoes minimal thickening [1]. This slurry is also referred to as a conventional tailings slurry, which behaves like a Newtonian fluid. Due to the low solid concentration, conventional tailings are often segregating, that is, larger particles in the slurry will settle out before smaller ones. There are a number of problems identified with the disposal of conventional tailings, usually including the large consumption of water, difficult closure, high risk of leachate seepage into the underlying soil and catastrophic facility failure [2-7]. It is these problems that have provoked workers into finding a new way to tackle conventional tailings.

Since Robinsky [8-10] introduced the concept of thickened tailings and put it into practice at Kidd Creek Mine near Timmins, Ontario in 1973, it has drawn widespread interest from the mining industry and become increasingly popular because of its inherent advantages over conventional tailings slurry [11-13]. Typically a thickened tailings is produced by dewatering a conventional tailings slurry. Unlike conventional slurry which behaves as a Newtonian fluid, the high density, thickened tailings generally possesses a yield point [14-16], which is referred to as the yield stress [17, 18]. As a yield stress fluid, the thickened tailings acts like a rigid body (neglect the elastic deformation if any) when the applied stress is lower than the yield stress, while it flows like a viscous fluid when the

stress applied exceeds the yield stress.

It is noted that the term “thickened tailings” in this work is used to describe tailings in which the particles do not settle and are fine enough that the homogeneous fluid approach can be applied to them. In addition, the thickened tailings investigated in this thesis possess obvious yield points which could be approximated by the Bingham plastic model. Considering that the yield stress in thickened tailings disposal operations in most cases ranges from 20 Pa to 50 Pa, the yield stress range focused on in this thesis is roughly from 20 to 60 Pa.

1.2 Methods for tailings disposal and resulting beach slopes

There are a number of methods for tailings disposal: tailings impoundments, thickened tailings disposal (TTD) systems (which is also referred to as a tailings stack or a Central Thickened Discharge (CTD) scheme), dry stacks, underground backfilling, open-pit backfilling, subaqueous disposal, etc. Since this work focuses on thickened tailings with yield stress values less than 60 Pa, the dry stack option, where filtered tailings are dewatered to moisture contents that can no longer be transported by pipelines but by truck or conveyor, is not discussed [19]. Additionally, the underground backfilling, open-pit backfilling and subaqueous disposal schemes represent the minority of the tailings disposal methods, compared to the tailings impoundment and TTD system, and therefore are not presented in the following discussion.

As the most commonly used tailings storage facility, a tailings impoundment has a form of basin which is typically confined by a constructed embankment and natural boundaries. Once the tailings slurry is transported from the mill to the impoundment through pipelines, a single point discharge technique or multi-spigot technique can be used to deposit the tailings into the impoundment. Because of the resulting particle segregation and energy dissipation, the tailings slurry discharged from the spigots generates a beach over time. The slope of the beach, which dictates the storage capacity of the impoundment, is of importance for the design and operation of a tailings impoundment [20-22]. **Figure 1** presents a photograph of a tailings impoundment taking advantage of a natural depression.

Figure 1 Photograph of a tailings impoundment with part of its boundary formed by natural depression (http://www.tailings.info/assets/images/content/valleyimpound-ment.jpg).

Since Robinsky [9, 10] proposed the TTD system as an alternative to the conventional

disposal of tailings, this tailings disposal scheme has been gaining in popularity because of its advantages over the conventional disposal of tailings [23-25]. In the TTD system, tailings are thickened before being discharged from elevated spigot locations to form a cone-shaped mound [23]. **Figure 2** shows a photograph of a TTD system and **Figure 3** illustrates schematically the resulting (idealised) geometry and relevant parameters for the beach slope calculation.

Figure 2 Photograph of a thickened tailings disposal (TTD) system (http://www.tailsafe.com/photos/partner_paste-technolgy/03-06-12_paste-technolgy_pa.gif).

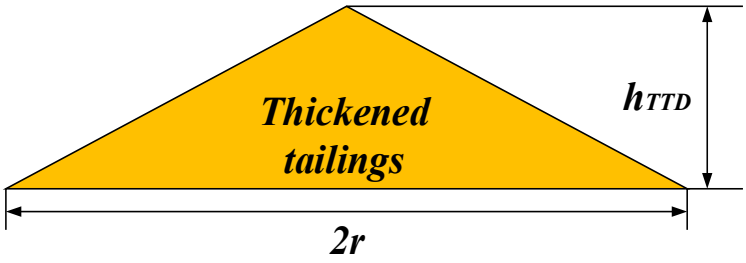

Figure 3 A sketch for TTD system and the relevant parameters for beach slope calculation.

The average beach slope (BS_a) of a TTD system is given by:

$$BS_a = h_{TTD}/r * 100\% \quad (1)$$

where h_{TTD} is the height of the mound and r is the radius of the footprint. It is noted that the beach slope is never linear in practice.

The beach slope is even more important for the TTD system than for a conventional tailings impoundment, as discussed by Fitton [22]. Firstly, the beach slope determines the mound height, thereby dictating the storage capacity of the TTD system. Secondly, the beach slope determines the footprint of the facility. Overestimation of the beach slope may result in a real footprint that is larger than the designed one while underestimation can lead to a waste of land, as discussed by Fourie and Gawu [26]. Either way, the likely consequences for the operation of a TTD system would be severe. Therefore it is of crucial importance to predict the beach slope with some degree of certainty and hence forecast the required area for the footprint accurately.

1.3 Flume test and beach slope prediction

There are two types of flume test investigated in this thesis: sudden-release (S-R) flume

tests and discharge flume tests. In an S-R laboratory flume test, the fluid to be tested is stored in a reservoir located at one end of the flume. Then the gate of the reservoir is quickly lifted to release the fluid. The fluid will collapse and flow due to gravity. This flume test is typically used to simulate the dam-break flow problem [27-32] although it sometimes was also used to investigate thickened tailings deposition [33-35]. In a discharge flume test, the tailings is discharged into one end of the flume through a pipe to achieve a profile at rest, which is normally used to predict the beach slope of tailings in the field [36-45].

As discussed in Section 1.2, it is critically important to accurately predict the beach slope for thickened tailings disposal operations. This is often performed using a laboratory flume test. Although the flume test has been used for many years to predict the beach slope of conventional tailings with acceptable accuracy [36, 46], it has tended to seriously overestimate the beach slope of thickened tailings developed in the field [26, 35, 47]. Both laboratory work and theoretical analysis have been conducted to explain the disparity of beach slopes of thickened tailings between flume tests and field observations [26, 37, 38]. However, very little work has been conducted using computational fluid dynamics (CFD) to investigate flume tests for thickened tailings. Consequently a thorough investigation on thickened tailings deposition in flume tests using CFD simulations was conducted in this thesis to highlight factors that have previously been neglected when interpreting flume test data, thereby offering a comprehensive

explanation for the disparity of beach slopes between flume tests and field observations.

1.4 Mini-slump test for yield stress measurement of thickened tailings

The yield stress is perhaps the most essential parameter for thickened tailings disposal as it directly influences the design and operation of thickened tailings disposal systems [1, 15, 48-51]. Relatively slight variations in yield stress can lead to significant changes in beach slope [51]. The yield stress not only strongly influences the beach slope in the field, which is a key parameter for thickened tailings storage facility design and operation, but also plays a crucial role in the preparation and transportation of thickened tailings [52-54]. Consequently it is crucial to determine the yield stress of thickened tailings accurately.

The slump test using a miniature cylindrical mould is widely used in the mining industry to obtain quick and easy measurements of the yield stress of thickened tailings [50, 54-56]. However, the accuracy of this method tends to be influenced by the mould lifting process, which is normally operated manually. Accordingly both experimental and numerical work in this thesis was carried out to investigate the impact of the mould lifting process on the final spread and slump that are used to calculate the yield stress. **Figure 4** demonstrates a photograph of slump test with a cylindrical mould on a mixture of kaolin clay and water.

Figure 4 Photograph of a slump test with a miniature cylindrical mould.

1.5 Yield stress measurement of thickened tailings using a flume test

As discussed in Section 1.4, the accurate measurement of yield stress of thickened tailings is of critical importance for thickened tailings disposal, from preparation through transportation, and to final deposition. However, this vital rheological parameter, i.e. the yield stress of thickened tailings, is often estimated by a mini-slump test in industry [50, 55, 56], which is of relatively low accuracy. Although the yield stress can be accurately obtained by using delicate electronic equipment, such as the vane viscometer and rheometer, these instruments are expensive and often unavailable on a mine site. In addition, the utilisation of these sensitive and expensive instruments on site is hardly practical considering the operating environment in the field. It is therefore of great significance to develop a cheap, accurate, easy method for the yield stress measurement of thickened tailings. Such an inexpensive technique can then be used routinely on a mine

site for quality control purposes.

Accordingly this thesis explores the feasibility to measure the yield stress of thickened tailings by using a laboratory flume test, which is typically used for beach slope prediction, as discussed in Section 1.3.

1.6 Flow model selection for thickened tailings

Thickened tailings is typically treated as a viscoplastic fluid (which is also referred to as a yield-stress fluid) which flows with a deformation localized along the surfaces where the yield stress is reached. Once the yield stress has been overcome, the material flows at a finite rate which increases with the difference between the local stress and the yield stress. There are several rheological models used to describe the flow behaviour of time-independent yield-stress fluids [57], such as Bingham model, Herschel-Bulkley model and Casson model [58], which can be summarised by the following generic form:

$$\tau = \tau_y + f(\dot{\gamma}),\ \tau > \tau_y \tag{2}$$

where τ_y is the yield stress of yield-stress fluids and f is a positive function of $\dot{\gamma}$.

For Bingham model, $f(\dot{\gamma}) = \mu_0\dot{\gamma}$, in which μ_0 is the plastic viscosity, and for Herschel-Bulkley model, $f(\dot{\gamma}) = K\dot{\gamma}^n$, where K and n are the consistency factor and power-law index, respectively, which can be determined by laboratory tests. The Casson model corresponds to $f(\dot{\gamma}) = \mu_\infty\dot{\gamma} + 2\sqrt{\mu_\infty\tau_y\dot{\gamma}}$, in which μ_∞ is the constant viscosity

approached at the infinite shear limit.

In addition to Casson model which is usually used to describe blood [59-61], both Bingham and Herschel-Bulkley rheological models have been applied to tailings slurry [62]. The Bingham model, rather than the Herschel-Bulkley model was used in this work to represent the rheological behaviour of thickened tailings due to the following reasons:

- Although the flow behaviour of thickened tailings is best described using a Herschel–Bulkley model, which contains three parameters: a yield stress term, a power law and a consistency index term, the Bingham model provides an acceptable approximation to the flow behaviour for the purposes of the slope prediction work for thickened tailings [63].
- During both slump test and flume test, the tailings initially flow with a high velocity and slow before stopping. The variation in the velocity is so large that it was necessary to use a constant, representative Bingham viscosity in analyses rather than a shear rate dependent viscosity [33, 63].
- The application of the three parameter Herschel–Bulkley model is more tedious and less certain [58], which tends to result in significant error.
- Finally, this work focused on the final profile of thickened tailings, a yield stress fluid, whose final profile is mostly, if not only, influenced by yield stress [64]. In other words, the final profiles of the yield stress fluid described by both Bingham

model and Herschel–Bulkley model is very similar as long as the same yield stress is used and the inertial effects are within reason. Consequently although the two parameter Bingham Plastic model is unlikely to accurately define the flow behaviour of tailings mixtures at relatively low shear rate, the flow behaviour at this low shear rate (hence low inertial effects) will not influence the final profile if the yield stress in both Bingham plastic and Herschel-Bulkley model is the same.

Therefore the selection of the Bingham model which includes both yield stress and viscosity will not invalidate the findings from this work.

1.7 Thesis outline

Beach slope prediction for thickened tailings is vital in waste management and this is often done by using a laboratory flume test. However, the slopes achieved in flumes are unrealistically steeper than those in the field. Therefore the investigation on this issue was conducted firstly in this thesis (Chapter 2). Being aware of the importance of yield stress in beach slope prediction, an investigation of the mini-slump test which is widely used to approximate the yield stress of thickened tailings in the mining industry was carried out (Chapter 3). In light of the fact that the accurate measurement of the yield stress of thickened tailings is critical to the operation of a tailings storage facility, and the mini-slump test used in industry can only roughly estimate the yield stress, studies were conducted to evaluate the feasibility of using a flume test to measure the yield stress of

thickened tailings, which may result in an accurate, cheap and easy method for yield stress measurement (Chapter 4).

This thesis is organised as a series of journal papers, except for the first and final chapters. The first chapter (Chapter 1) is a general introduction which introduces the background information and clarifies the organisation and structure of the thesis. The final chapter (Chapter 5) summarises the findings of the thesis, establishes the significance of the work conducted in this thesis and presents some recommendations for the future work. **Figure 5** illustrates the flow chart of the thesis.

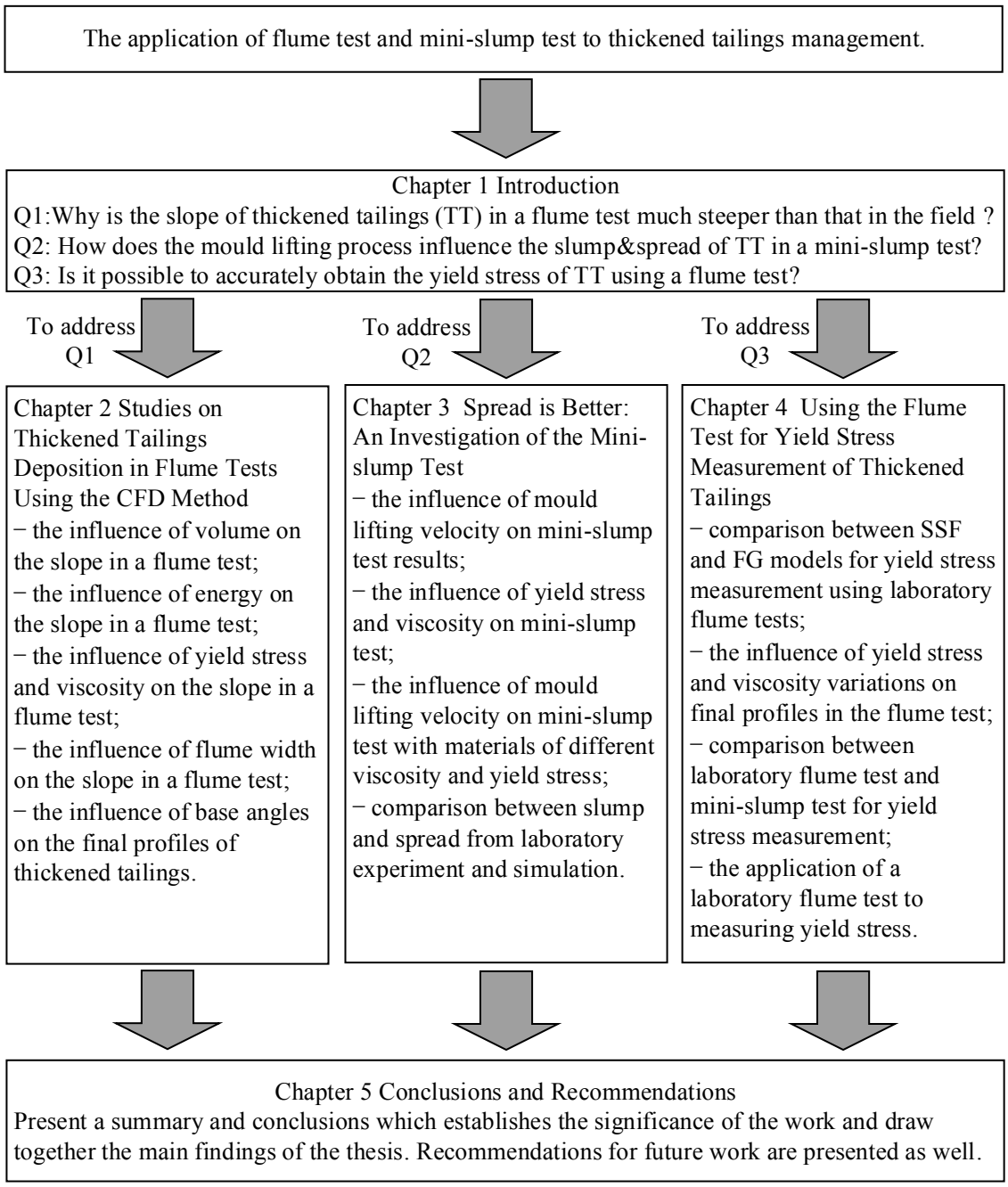

Figure 5 Organisation and structure of the thesis.

The published and submitted papers that have arisen from this thesis and the corresponding chapters are listed as follows. It is noted that the conference paper, titled "Studies on flume tests for predicting beach slopes of paste using the computational fluid

dynamics method" is placed in Appendix A as there is some overlap of the content between this conference paper and the journal paper presented in Chapter 2.

Chapter 2: J. Gao and A. B. Fourie, "Studies on thickened tailings deposition in flume tests using CFD method," *International Journal of Mineral Processing*. Submited.

Chapter 3: J. Gao and A. B. Fourie, "Spread is better: An investigation of the mini-slump test," *Minerals Engineering,* vol. 71, pp. 120-132, 2015.

Chapter 4: J. Gao, A. Fourie, Using the flume test for yield stress measurement of thickened tailings, Minerals Engineering, 81 (2015) 116-127.

Appendix A: J. Gao and A. Fourie, "Studies on flume tests for predicting beach slopes of paste using the computational fluid dynamics method," in *Proceedings of the 17th International Seminar on Paste and Thickened Tailings (Paste 2014)*, Vancouver, Canada, 2014.

2. STUDIES ON THICKENED TAILINGS DEPOSITION IN FLUME TESTS USING THE CFD METHOD

Abstract

Computational Fluid Dynamics (CFD) simulations of laboratory flume tests on thickened tailings were carried out to highlight the factors that may impact on the slopes of final profiles achieved in such flumes. In particular, the software ANSYSFLUENT was used to conduct the simulations for both sudden-release (S-R) and discharge flume tests with thickened tailings treated as a Bingham fluid. The coupled level-set and volume of fluid model was used to track the free surface between air and Bingham fluid in the laminar regime. The numerical model was first validated against the analytical solution of a sheet of Bingham fluid on a flat plane at flow stoppage. It was then used to investigate the influence of several factors, including the volume of fluid, energy, rheological properties, flume width and the base angle of the flume on the average slopes of the final profiles achieved in both S-R and discharge flume tests. The results show that an increase of volume, energy, flume width or base angle reduces the resulting slope angle. Moreover the yield stress of the fluid generally has more influence on the final profiles than the viscosity. In addition, the viscosity tends to have less influence on the formation of the final profiles if the inertial effects are relatively weak. Finally two dimensionless parameters were proposed to establish the relationship between the average slope, rheological properties and geometrical parameters for planar deposition of thickened

tailings in both S-R and discharge flume tests. These results provide a better understanding of the deposition of thickened tailings in the field. The agreement between simulation results and laboratory observations in the literature gives confidence in the veracity of the computational results.

Keywords: Thickened tailings; Flume test; Beach slope; CFD modelling.

2.1 Introduction

The beach slope generated by tailings slurry after it is discharged into a tailings storage facility (TSF) is of great importance for the design and operation of a TSF in the mining industry [20, 65]. Therefore the beach slope prediction is important for TSFs, and it becomes even more crucial for thickened tailings disposal (which is also referred to as a 'tailings stack' or 'central thickened discharge' scheme) with the TSF constructed on sloping ground because the beach slope of thickened tailings can determine the feasibility of the entire scheme in such case [22].

The discharge flume test, where the tailings are admitted through a pipe to the flume to form a beach profile, has been used for many years to simulate hydraulic deposition of conventional tailings where the particle size distribution is non-uniform along the beach as a result of sequential sedimentation during tailings deposition. The coherence between experimental results and field observations implies that discharge flume tests are at least sufficient to qualitatively simulate conventional tailings deposition [36, 46].

Technical advancements in tailings thickening have enabled the growing implementation

of thickened tailings disposal owing to its many inherent advantages over conventional tailings, which may include low water consumption, reduced risk of ground water contamination, significant safety improvement, easier rehabilitation, etc. [51, 63]. Unlike conventional tailings which typically have a low solids concentration and where larger particles settle out prior to finer ones during deposition and transportation, thickened tailings are in general more concentrated and non-segregating, with yield stresses in most cases ranging from 20 Pa to 50 Pa [66]. Notwithstanding successful simulation for conventional tailings deposition, flume tests have turned out to be problematic for direct beach slope prediction of thickened tailings. Beach slopes in the field are typically around 2% to 3% with 5% scarcely being achieved for thickened tailings (or paste) schemes implemented word-wide [4, 24]. However the slopes for thickened tailings developed in flume tests tend to be unrealistically steeper than those in the field [26, 35, 37, 47, 67, 68]. A significant amount of work has been carried out to explain the enormous disparity between beach slopes of thickened tailings in flume tests and field observations. Sofra and Boger [33, 63] carried out a series of sudden-release (S-R) laboratory flume tests to identify the factors, including yield stress, viscosity, hydraulic head and slope of the underlying base, affecting the deposition behaviour of three types of thickened tailings (red mud, titanium dioxide suspension and hydrous sodium lithium magnesium silicate) with the yield stress varying from 17 to 210 Pa. They used a flume made from clear glass with a length of 2 m and a width of 0.2 m. In the sudden-release (S-R) laboratory flume test, the fluid to be tested was stored in a reservoir located at one end of the flume initially.

Then the gate of the reservoir was quickly lifted to release the fluid. A beach profile was finally formed in the flume as a result of the balance between driving and resisting forces. Through dimensional analysis they found that the slope of thickened tailings with different rheology and density is a function of the dimensionless yield stress, Reynolds and Froude numbers. They observed that the angle of repose decreased when the tailings volume increased by filling the reservoir to a greater height. They concluded that the increased hydrostatic head resulted in the reduced angle. However it is likely that the flatter slopes result from both the higher hydraulic head and the greater volume (see Sections 2.3.1 and 2.3.2).

Simms [37] used the theoretical solution for slow spreading flow (SSF) of Bingham fluid to explain the disparity in beach slopes of thickened tailings achieved in discharge flume tests and in the field. He found that the overall slope of the deposit is significantly influenced by both the scale of flow and the underlying topography. The influence of flume width and initial energy of tailings was not discussed. Henriquez et al. [38] pursued the method proposed in Simms [37] to study the dynamic flow behaviour and multilayer deposition of gold paste tailings. Both discharge and S-R flume tests were conducted in their work. They observed that the S-R flume tests yielded thinner and longer final profiles (It is noteworthy that the ‘profile’ and ‘slope’ are different: ‘profile’ is the shape of entire surface, from deposition point to end of flow, while slope is a linear value – usually fitted to some portion of the profile.), especially with a larger volume of tailings used compared to the discharge flume tests, which was attributed to the significant and

rapid release of potential energy. Besides the flow-scale dependency of beach slope, they reported that the lubrication of the flume walls with a hydrophobic grease did not influence the final equilibrium profile of the flows, which indicates that the greasing did not change the sidewall friction of the acrylic flume significantly. Additionally the effect of deposition rate, which may influence the final profile, was not studied in their work. Mizani et al. [69] carried out discharge flume tests on high density tailings from a gold mine to investigate stack geometry of thickened tailings in the laboratory. A flume made of acrylic with length and width of 2430 mm and 152 mm respectively and a rubber inlet tube with an inner diameter of 7.3 mm were employed in their work. They reported that the final profile was sensitive to flow rate when it was below 1.6 litres per minute (LPM) in the flume tests. It is worth noting that the SSF model which is derived within the framework of long-wave approximation, was used to describe the final profile of thickened tailings in laboratory flume tests by several workers [34, 37, 69], which may be inappropriate as the assumption of long-wave approximation typically cannot be fulfilled in a laboratory flume test [70].

Fourie and Gawu [26] developed a mathematical model taking the friction of flume sidewalls into account to explain the much steeper slope angles yielded by flume tests for thickened tailings. The model reveals that the slope of thickened tailings in a flume test will decrease with an increasing flume width. Moreover, they found that the slope decreases with an increase of the volume of thickened tailings. However, the inertial effects which may influence the profiles in flume tests were not discussed.

Compared to the large number of experimental and theoretical studies in the literature, very little work has been conducted using computational fluid dynamics (CFD) to investigate flume tests for the deposition of thickened tailings. To develop a clear understanding of the flow behaviour of thickened tailings, CFD simulations for both S-R and discharge flume tests were performed to assess the influence of several factors, including tailings volume, energy, yield stress, viscosity, flume width and base angle on the final profiles achieved in the two types of flume test. It is emphasised that yield stress roughly ranges from 20 to 60 Pa in actual thickened tailings disposal operations [66]. Therefore we only focused on the yield stresses (see **Table 3** and **Table 4**) within this range in the present work.

Similar to the argument made by Kupper et al. [45] who used the laboratory flume test to study hydraulic fill, we emphasise that the flume test is not a scaled version of any prototype but a fundamental test which provides a cheap and easy way to understand the physical phenomenon of thickened tailings flow. It is stressed that the intention of this work is not to compare CFD models with experimental data from flumes, or directly predict the beach slope in the field using laboratory flume tests. Rather, it is to highlight the factors that influence the flow of thickened tailings and provide useful insight into the deposition of thickened tailings, particularly in laboratory flume tests.

It is noted that the flume width in the planar simulations for both S-R and discharge flume test should be considered as infinite. Therefore both S-R flume tests and discharge flume tests with 2D geometries are different from the laboratory flume test where typically a

narrow flume is used. In other words, the 2D flume test simulations do not take the sidewall friction into account.

In this paper the numerical model (CFD) is described first, followed by its validation. Thereafter the influence of energy, volume, yield stress, viscosity, flume width and base angle on the final profile achieved in flume tests is investigated by using CFD simulations. After that, two dimensionless parameters were proposed to establish a relationship between the average slope, rheological properties and geometrical parameters for planar deposition of thickened tailings based on both S-R and discharge flume tests. Finally some conclusions are reached.

2.2 Numerical model and validation

A commercially available CFD code, ANSYS FLUENT was used to perform the simulations. Considering the low flow velocity in a flume test, both thickened tailings and air in the work are assumed to be incompressible, therefore the continuity and momentum equations are simplified as:

$$\nabla \cdot (\vec{v}) = 0 \tag{1}$$

$$\rho \frac{\partial \vec{v}}{\partial t} + \rho \nabla \cdot (\vec{v}\,\vec{v}) = -\nabla p + \nabla \cdot (\bar{\bar{\tau}}) + \rho \vec{g} \tag{2}$$

where $\vec{v}$ is the velocity field, ρ is the density, p is the pressure, $\vec{g}$ is the gravitational acceleration and $\bar{\bar{\tau}}$ is the stress tensor, which is given by:

$$\bar{\bar{\tau}} = \mu(\nabla \vec{v} + \nabla \vec{v}^{T}) \tag{3}$$

where μ is the shear viscosity of the fluid.

The thickened tailings in this work is modelled using the Bingham constitutive law [17]:

$$\eta = \begin{cases} \mu_0 + \frac{\tau_y}{\dot{\gamma}}, & \tau \geq \tau_y \\ \infty, & \tau < \tau_y \end{cases} \tag{4}$$

where η is the apparent viscosity, μ_0 is the plastic viscosity, τ_y is the yield stress of Bingham fluid, and $\dot{\gamma}$ is the shear rate. It is noted that the plastic viscosity is also referred to as viscosity in the present work.

To overcome the problem of discontinuity of viscosity, the Bingham law is implemented in ANSYS FLUENT with the following form [71]:

$$\eta = \begin{cases} \mu_0 + \frac{\tau_y}{\dot{\gamma}}, & \dot{\gamma} \geq \dot{\gamma}_c \\ \mu_0 + \frac{\tau_y(2-\dot{\gamma}/\dot{\gamma}_c)}{\dot{\gamma}_c}, & \dot{\gamma} < \dot{\gamma}_c \end{cases} \tag{5}$$

where $\dot{\gamma}_c$ is the critical shear rate.

The critical shear rate ($\dot{\gamma}_c$) should be as small as possible to reproduce the flow behaviour of a Bingham fluid. However excessively small $\dot{\gamma}_c$ may lead to numerical instability. Gao and Fourie [72] reported that the proper critical shear rate ($\dot{\gamma}_c$) is primarily dependent on the yield stress of Bingham fluid and a value of 0.005 s^{-1} for $\dot{\gamma}_c$ is appropriate for the yield stress ranging from approximately 18 to 60 Pa. As discussed in Section 2.1, the yield stress (see **Table 3**) of interest in this work is roughly within this range. Therefore the critical shear rate of 0.005 s^{-1} was employed in the simulations.

The surface tension effect was neglected in this work as a result of the high yield stresses of interest. Roussel et al. [73] studied the surface tension effects of several pastes in mini-

cone tests. They found that the surface tension effects can be safely neglected if the spread is smaller than 0.35 m, which is corresponding to a yield stress of approximately 1.5 Pa. In the present work, the yield stress ranges from 18.61 to 62.62 Pa, as shown in **Table 3**, which are much higher than 1.5 Pa. Therefore neglecting the surface tension in the simulations is justified.

The interface between air and thickened tailings was tracked by using the coupled level-set and volume of fluid (VOF) model provided in ANSYS FLUENT [74]. The coupled level-set and VOF model which overcomes the deficiencies of the level-set method and VOF method [75-78] is specifically designed for two-phase flows without mass transfer. In a two-phase system, the level-set function $\varphi(x,t)$ which is also known as the signed distance function or oriented distance function, is defined as the distance of a given point x from the interface [79]:

$$\varphi(x,t) = \begin{cases} +|d| & if\ x \in the\ primary\ phase \\ 0 & if\ x \in \Gamma \\ -|d| & if\ x \in the\ secondary\ phase \end{cases} \quad (6)$$

where d is the distance from the interface of the two phases and Γ is the interface, given by:

$$\Gamma = \{x|\varphi(x,t) = 0\} \quad (7)$$

The evolution of the level-set function is given in a similar fashion as the VOF model [77, 78]:

$$\frac{\partial \varphi}{\partial t} + \nabla \cdot (\vec{v}\,\varphi) = 0 \quad (8)$$

Detailed information on the coupled level-set function and VOF method can be found

elsewhere [78, 80].

The numerical model in ANSYS FLUENT for flume test simulations of Bingham fluid has been discussed previously [70]. Velocity profiles of Bingham fluid in a circular pipe from both an analytical solution and the CFD simulation were compared to validate the Bingham model [72].

Further validation of the model for flume test simulations is carried out in the present work, by comparing the final profile of the thickened tailings achieved in a planar simulation of flume test with the analytical solution for a thin layer of Bingham fluid on a flat plane [81, 82]:

$$\frac{dy}{dx} = -\frac{\tau_y}{\rho g y} \tag{9}$$

where y is the elevation of the free surface at a particular x. It is emphasised that Eq.(9) is based on static equilibrium at flow cessation of a Bingham fluid with extensional stresses and surface tension neglected. Given the material properties (i.e. ρ and τ_y) and a single point (e.g. flow distance at the end of the final profile) on the final profile, the entire profile of a Bingham fluid on a flat plane can be obtained by solving Eq.(9).

A 2D planar simulation of a discharge flume test was performed to obtain the final profile of a Bingham fluid on a horizontal base. The same geometry, mesh and setup that were used in Section 2.3.1.2 were employed here with a fluid discharge time of 16 s. In ANSYS FLUENT, the shear stress ($\eta\dot{\gamma}$) will be null if the shear rate vanishes. Therefore the yield stress fluid cannot completely stop in the ANSYS FLUENT simulations. However, it is

acceptable to assume that the flow of a yield stress fluid has stopped if the interface moves slowly enough [72]. It is found that the reduction of the slope of the final profile was very minor once the spreading speed of the front was less than 0.3 mm/s in the flume test simulations. In addition, for simulations with a relatively large fluid volume or higher viscosity, the decline rate of the spreading speed below 0.3 mm/s is very slow. Taking both accuracy and computing time into account, it was considered a reasonable compromise to stop the simulations when the spreading speed of the front toe is slower than 0.3 mm/s. **Figure 1** illustrates the final profiles of the 2D flume test from both the analytical solution and simulation. The good agreement indicates that the numerical model in ANSYS FLUENT and the critical shear rate of 0.005 s^{-1} are capable of modelling the planar deposition of Bingham fluids.

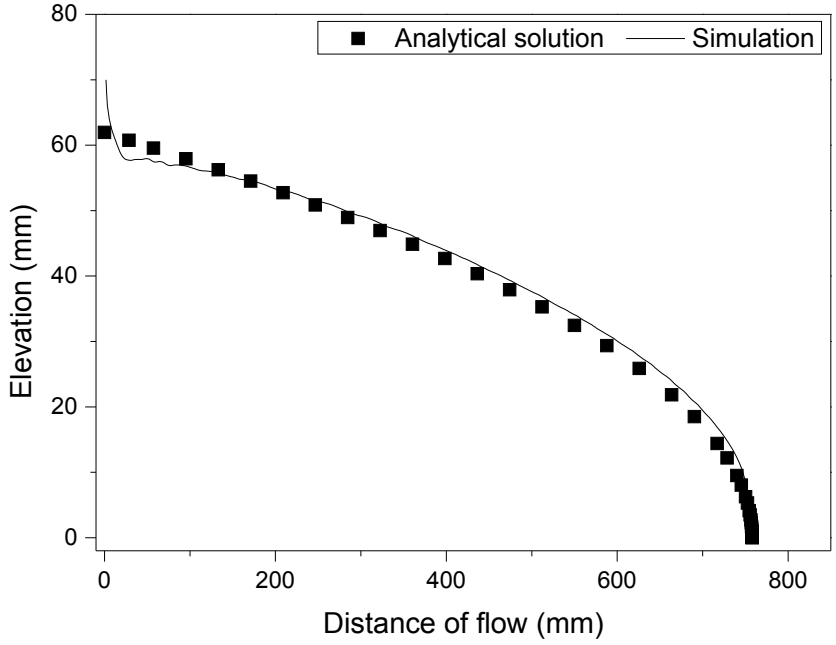

Figure 1 Comparison of analytical and simulated final profiles in a 2D flume test. The parameters of the material used were: 33.28 Pa, 0.4 Pa·s and 1342.6 kg/m^3.

2.3 Results and discussion

This section firstly investigates the influence of several factors, including fluid volume, energy, yield stress, viscosity, flume width and base angle, on the final profile achieved in flume tests. Then a dimensional analysis was performed to establish the relationship between average beach slope and several dimensionless parameters.

There are two types of flume tests used in the work: S-R flume test (see **Figure 2**(a)) and discharge flume test (see **Figure 2**(b)). For the simulations of S-R flume test, a certain amount of fluid is patched at one end of the flume at t=0, as shown in **Figure 2**(a). Non-slip conditions were applied to all the walls of the flume except for the inlets and outlets. Care was taken to prevent the Bingham fluids from flowing out of flumes so that entire profiles could be achieved in both types of flume test. The properties of the three main materials used in this work ((a) 33.28 Pa, 0.4 Pa·s and 1342.6 kg/m^3; (b) 18.61 Pa, 0.32 Pa·s and 1315.0 kg/m^3; (c) 50.1 Pa, 0.64 Pa·s and 1367.4 kg/m^3) are based on two mixtures of kaolin and tap water. The determination of the material properties can be found elsewhere [72]. It is noted that there is no comparison between experimental results and numerical results in the present work.

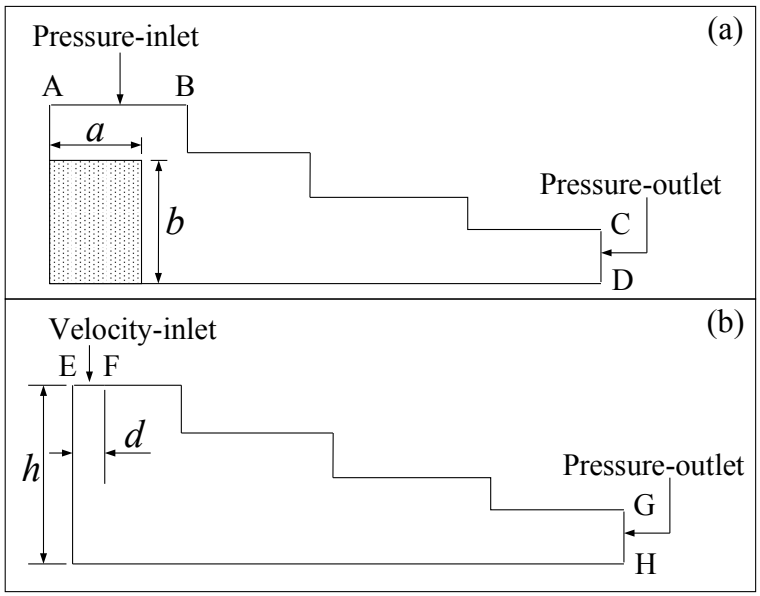

Figure 2 Sketch of geometries for 2D planar flume tests. (a) S-R flume test (b) Discharge flume test. The shaded area in panel (a) is the fluid patched in the flume at t=0. The empty area is occupied by air for both flumes. The walls, except for the inlets and outlets, are treated as non-slip walls.

The slope of the final profile was obtained by a linear fit of a certain percentage of the whole final profile. **Figure 3** shows the sketch for obtaining the slope of a convex profile achieved in a discharge flume test. To determine the part of the profile to be used for a linear fit, the influence distance (L') of the inlet discharge is removed first. Then 20% of the remainder ($L - L'$) at the front toe is removed as well to reduce the influence of the sharp curvature at the front toe of the profile on the linear fit. Therefore the range used for a linear fit is (L', x), where x is given by:

$$x = 0.8L + 0.2L' \tag{10}$$

where L is the overall length of the final profile, as shown in **Figure 3**.

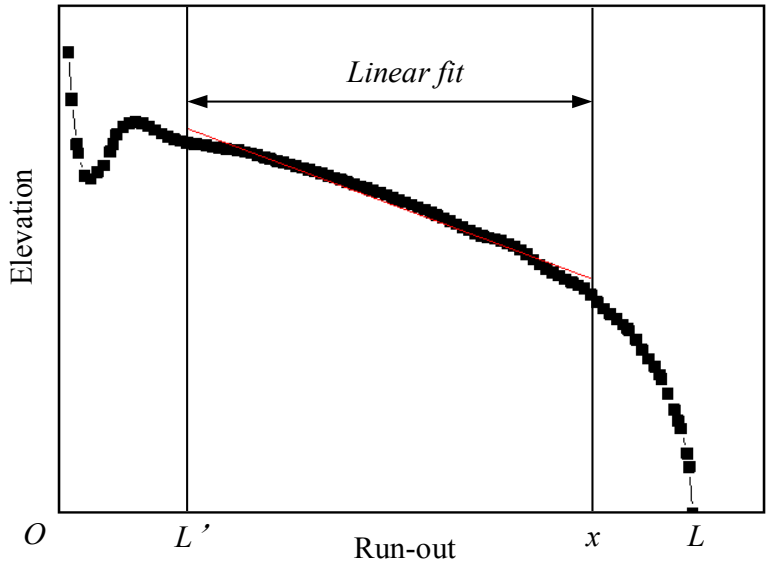

Figure 3 Sketch for the slope obtainment of a profile in flume test by linear fit. x is given by $0.8L + 0.2L'$.

It is noted that the variation of influence distance (L') near the inlet may change the slope obtained by linear fitting of the same profile. Consequently the slopes presented in particular figures in the work used similar L' to enable the slopes to be rationally compared.

The isoline (2D simulations) or isosurface (3D simulations) of the fluid volume fraction at 0.5 is determined to be the interface between the two phases (Bingham fluid and air).

To guarantee the grid-independence of the 2D simulation results, square cells used to discretise the computational domain were refined from $5\text{mm} \times 5\text{mm}$, to $2\text{mm} \times 2\text{mm}$ and finally to $1\text{mm} \times 1\text{mm}$ for all the 2D simulations in the work. It was found that the $2\text{mm} \times 2\text{mm}$ cells are not only fine enough to ensure the grid-independence of results but also of higher efficiency in computation than the $1\text{mm} \times 1\text{mm}$. Thus the

simulation results of a computational mesh consisting of $2\text{mm} \times 2\text{mm}$ cells are discussed in the work. In addition, mesh-independence investigations were performed for all the 3D simulations as well, as discussed in Section 2.3.4.

2.3.1 The influence of volume on the slope in a flume test

2D simulations for both S-R and discharge flume tests with horizontal bases, as shown in **Figure 2**, were carried out to investigate the influence of tailings volume on the slopes of the final profiles. Step-like flumes were employed to trim the computational domain thereby reducing the computing time. Contours of fluid volume fraction were saved during simulations and inspected after the simulations to ensure that the Bingham fluid did not contact the irrelevant walls of the steps.

2.3.1.1 The influence of volume on the slope in an S-R flume test

Using the flume bottom as the reference level, the potential energy of the Bingham fluid per unit width in **Figure 2**(a) is given by:

$$E_p = \frac{1}{2}\rho g a b^2 = \frac{1}{2}\rho g S b \tag{11}$$

where a and b are the length and height of the patched area respectively, S is the area of the patched material, which is given by $S = ab$.

Thus the potential energy per unit volume reads:

$$E'_p = \frac{1}{2}\rho g b \tag{12}$$

Eq.(12) indicates that the increase of the length of patched area (a) with a fixed height (b)

in a S-R flume test does not vary the potential energy per unit volume of the patched fluid.

To facilitate the analysis of the influence of fluid volume on the achieved slope, it is preferable to ensure that the potential energy per unit volume is similar in each S-R flume test since the potential energy may influence the slope as well (see Section 2.3.2). Accordingly the variation of volume of Bingham fluid in the four simulations reported in this section was realised by incrementally extending the length of patched area (a in **Figure 2**(a)) from 50 mm to 100 mm, and then 200 mm and finally 400 mm, with the height (b in **Figure 2**(a)) fixed at 130 mm.

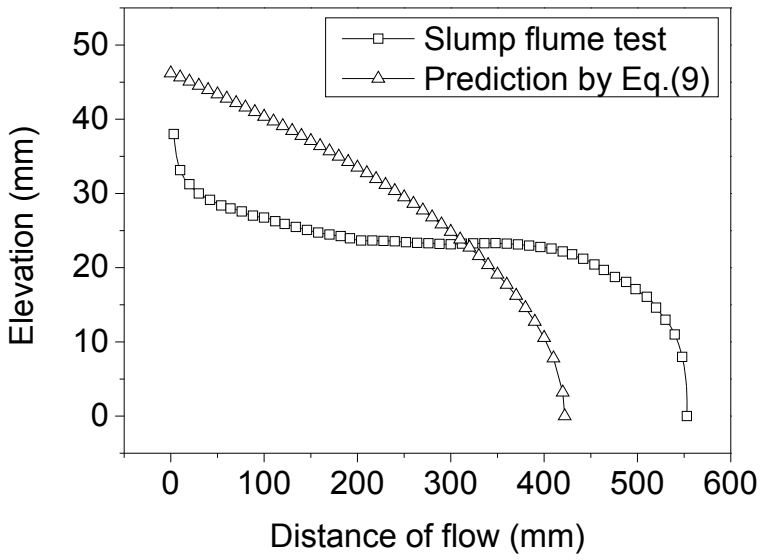

Figure 4 Final profiles of the prediction by Eq.(9) and the 2D planar simulation of S-R flume test with a patched area of $130\ \text{mm(Height)} \times 100\ \text{mm(Length)}$. The input material properties were: 33.28 Pa, 0.4 Pa·s and 1342.6 kg/m^3.

Figure 4 illustrates the final profiles from S-R flume test and the prediction by Eq.(9). It is clear that the profile from the S-R flume test is thinner and longer than that of the

prediction. Since there are no inertial effects in the prediction by Eq.(9), it is argued that the inertial effects in the S-R flume test were very high which 'pushed' the final profile to flow further, thus concealing the volume influence. It is noteworthy that the phenomenon that S-R flume tests tend to result in distorted profiles due to significant release of potential energy was also observed in the laboratory by Henriquez and Simms [34].

To reduce the inertial effects, the viscosity of the Bingham fluid in the simulations of the S-R flume test was increased from 0.4 Pa·s to 10 Pa·s. **Figure 5** summarizes the final profiles from the four simulations of S-R flume tests with different patched areas as well as the corresponding slopes. The final profiles in **Figure 5**(a) with a higher viscosity (10 Pa·s) tend to be convex while the profile in **Figure 4** from S-R flume test simulation with a lower viscosity (0.4 Pa·s) is initially concave. This difference indicates that the inertial effects in the simulations of S-R flume test on material of relatively high viscosity were weak, which was conducive to the investigation of volume influence.

Figure 5(b) demonstrates the slope variation according to the length of patched area in 2D simulations of S-R flume test. It is worth noting that the length of the patched area is an indicator of the fluid volume per unit width in this section since the height of the patched area (130 mm) was fixed. As shown in **Figure 5**(b), the slopes achieved in S-R flume test simulations decrease with the increase of Bingham fluid volume, which indicates that the beach slope of Bingham fluid in a S-R flume test is flow-scale dependent.

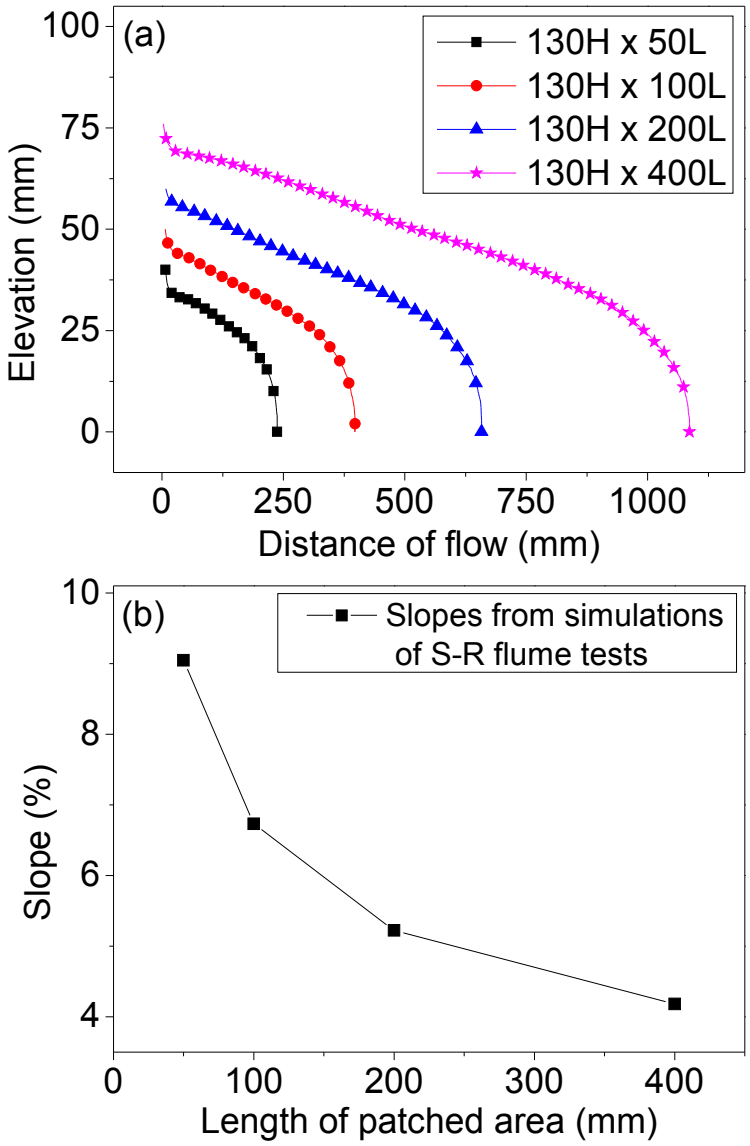

Figure 5 Final profiles from S-R flume test simulations with different patched areas (a) and the variation of the corresponding slopes according to the length of the patched area (b). '130H×50L' means the height and length of the patched area are 130 mm and 50 mm respectively, and so on. The height of the patched areas was fixed at 130 mm while the length of the patched areas increased from 50 to 400 mm. The input material properties were: 33.28 Pa, 10 Pa·s and 1342.6 kg/m^3.

2.3.1.2 The influence of volume on the slope in a discharge flume test

Four 2D simulations of the discharge flume test were performed to investigate the volume influence on the slope. The inlet size (d in **Figure 2**(b)) was 20 mm with an inlet velocity of 0.1 m/s. The height of the discharging point (h in **Figure 2**(b)) was 100 mm. The fluid volume varied among the four simulations by employing different discharging time: 2 s, 4 s, 8 s and 16 s. The material properties used in the simulations were: 33.28 Pa, 0.4 Pa·s and 1342.6 kg/m^3. **Figure 6** shows the final profiles from the four simulations and the corresponding slopes. It is clear from **Figure 6** (b) that the slopes of the final profiles from discharge flume test simulations decrease with the increase of fluid volume, which was observed in laboratory discharge flume tests by several workers [26, 34, 69].

Overall both results from the S-R flume test and discharge flume test suggest that the slope of Bingham fluid declines with an increase of the volume of deposition material. This scale-dependency feature of Bingham fluid is very important as it may prevent us from directly extrapolating the slope obtained using small-scale deposition tests to the field [69]. Although this finding, as with some others in this study, is perhaps intuitively obvious, many flume studies have been conducted without accounting for the effects of variables such as flow volume. Quantification of the influence of these variables, as is done in this paper, should result in more considered flume tests in future.

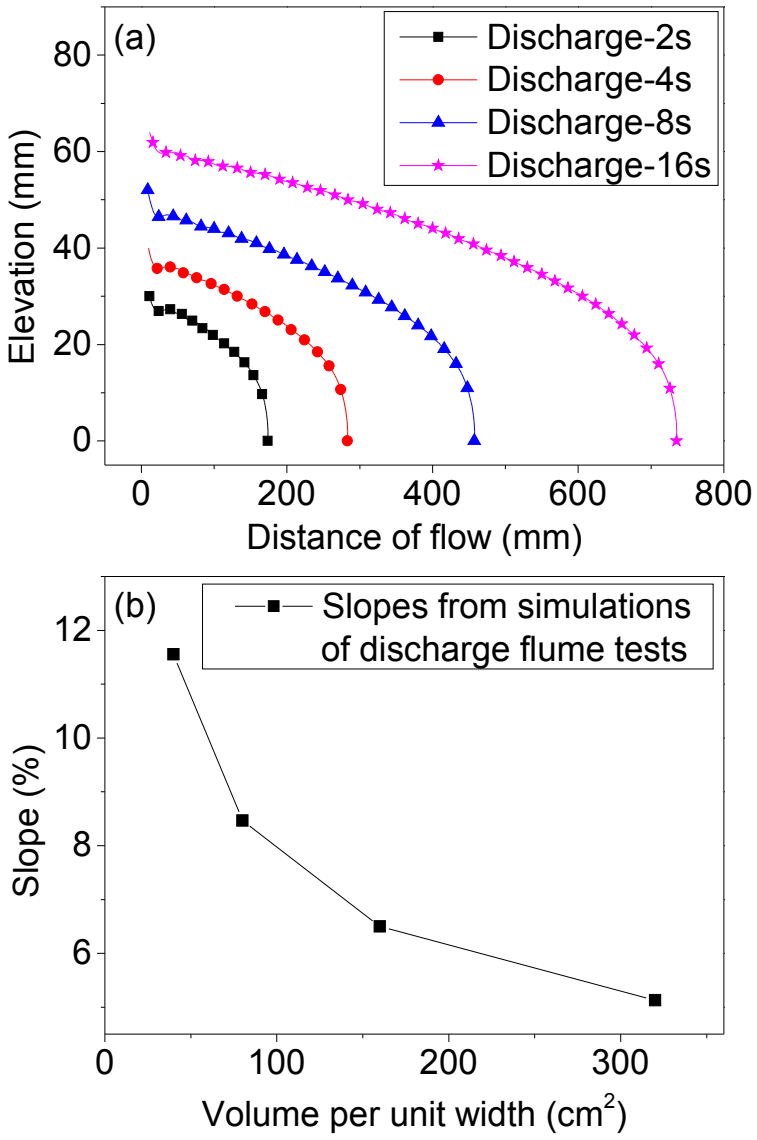

Figure 6 Final profiles from 2D simulations of discharge flume tests with different discharge time (a) and the variation of the corresponding slopes according to the volume per unit width (b). The input material properties were: 33.28 Pa, 0.4 Pa·s and 1342.6 kg/m^3.

2.3.2 The influence of energy on the slope in a flume test

To investigate the energy influence on the final slope of Bingham fluid, 2D simulations of both discharge and S-R flume tests were carried out.

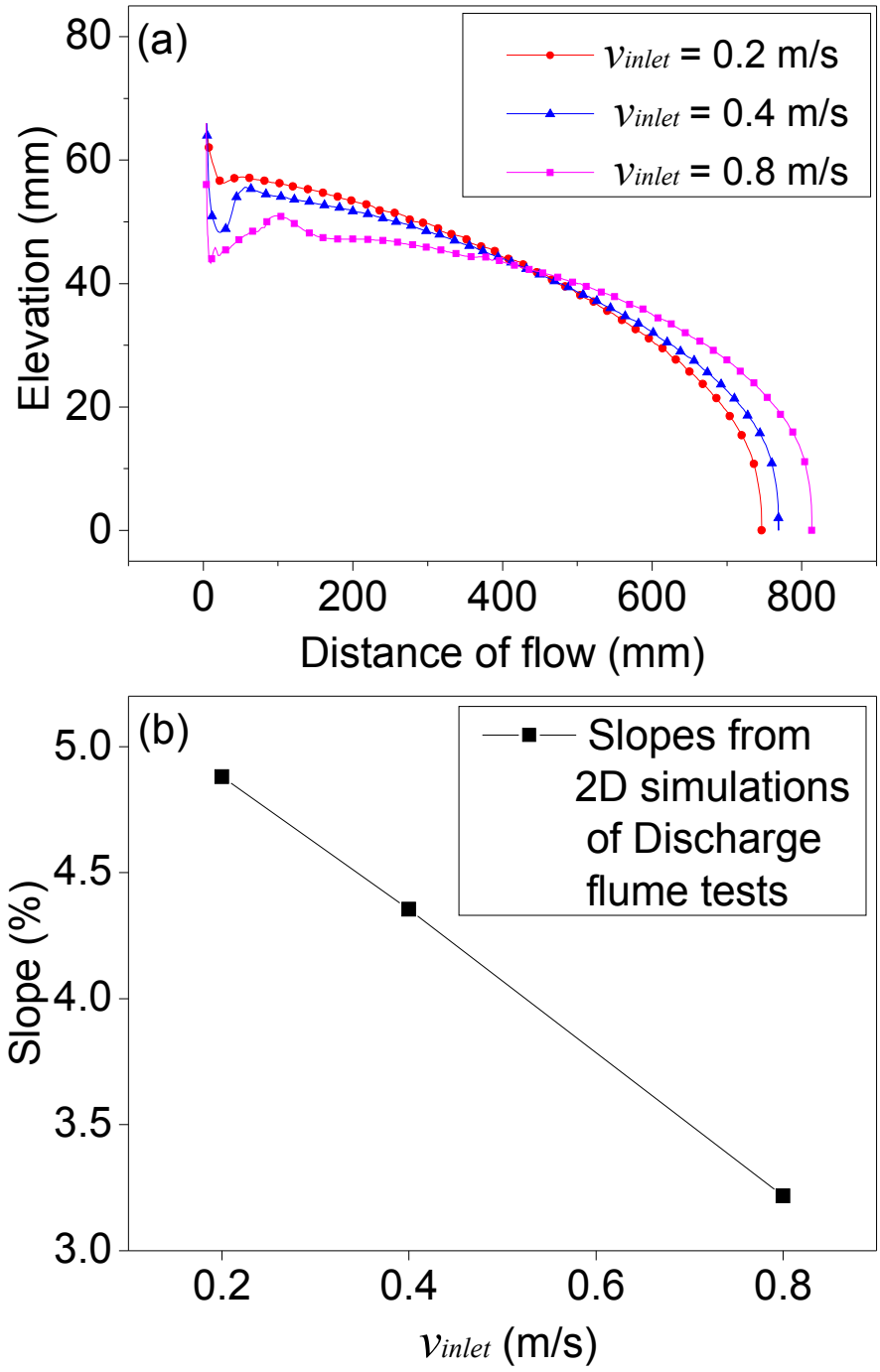

Figure 7 Final profiles from 2D simulations of discharge flume tests with different inlet velocities and the corresponding slopes. The input material properties were: 33.28 Pa, 0.4 Pa·s and 1342.6 kg/m^3.

For the discharge flume test simulations, the geometry employed was the same as that in

Section 2.3.1.2. The inlet velocities for the three simulations were 0.2 m/s, 0.4 m/s and 0.8 m/s respectively. In Section 2.3.1 it was demonstrated that the volume of fluid has an influence on the slope of the final profile achieved in a flume test, therefore the same fluid volume was employed for the three simulations by varying the discharge time. **Figure 7** shows the final profiles from the 2D planar simulations of the flume tests with the same fluid volume discharged at different velocities and the corresponding slopes. As can be seen clearly from **Figure 7**(b), the slope of the final profile decreases with the increment of the discharging velocity. This was observed in laboratory flume tests by Mizani et al. [69].

Three 2D simulations of S-R flume tests with the same patched area of 32,000 mm^2 were carried out to investigate the influence of the initial potential energy on the final profiles. Since the patched area (S) was fixed, the variation of the height (b) of the patched area may result in different potential energy per unit width, according to Eq.(11). The patched areas for the three simulations were $80\ \text{mm} \times 400\ \text{mm}$, $160\ \text{mm} \times 200\ \text{mm}$ and $320\ \text{mm} \times 100\ \text{mm}$ (Height × Length). **Figure 8** illustrates the final profiles and their corresponding slopes from the three S-R flume test simulations of different potential energy and the prediction by Eq.(9). As shown in **Figure 8**, with an increase of the height of the patched area the distance of flow extends and the slope of the final profile decreases. Since there are no inertial effects in the prediction, the dramatic difference in the profiles between the prediction and simulations, as illustrated in **Figure 8** (a), were induced by the inertial effects in S-R flume tests. It indicates that the sudden release of fluid with

higher potential energy introduces more inertial effects, thereby leading to extension of flow distance and reduction of slope.

Simulation results for both discharge and S-R flume tests reveal that the increase of energy reduces the slope of the final profile, which was observed in laboratory flume tests as well [63, 69].

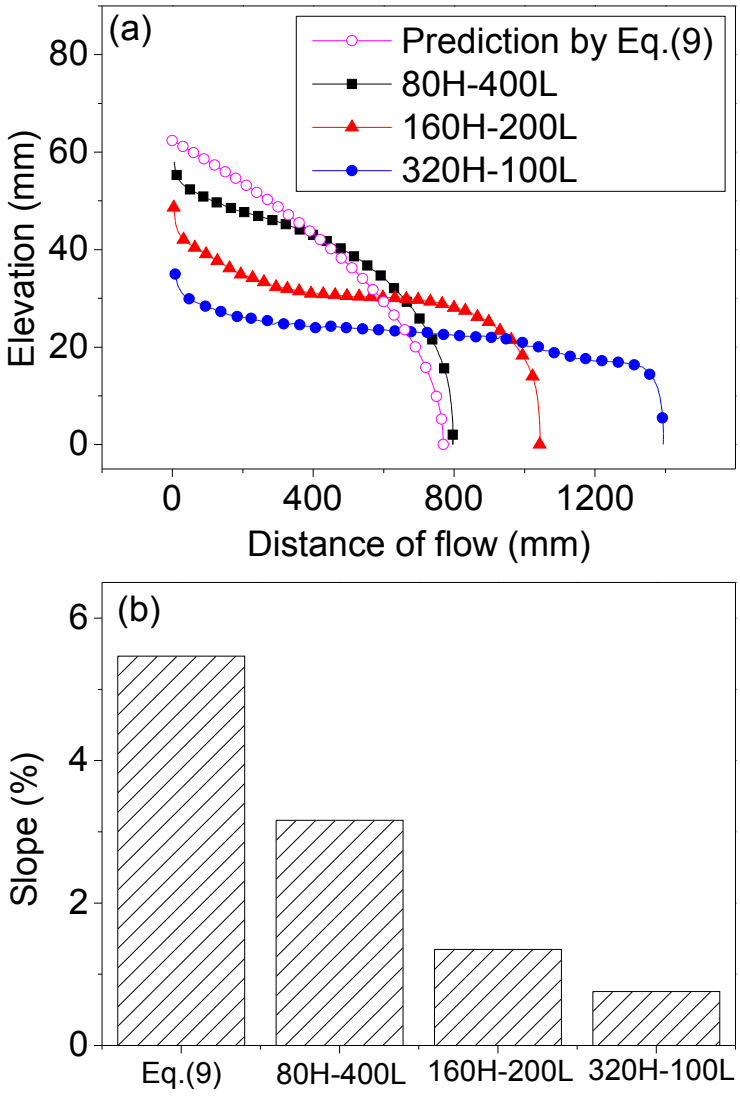

Figure 8 Final profiles (a) and corresponding slopes (b) from 2D simulations of S-R flume tests and the prediction by Eq.(9). '80H-400L' means the height and length of the

patched area are 80 mm and 400 mm respectively, and so on. The input material properties were: 33.28 Pa, 0.4 Pa·s and 1342.6 kg/m^3.

2.3.3 The influence of yield stress and viscosity on the slope in a flume test

Twelve 2D simulations in four groups were carried out to study the influence of yield stress and viscosity on the slope achieved in both S-R flume tests and discharge flume tests. Detailed information of the simulations are listed in **Table 1**.

Table 1. Detailed information of flume test simulations for the investigation of yield stress and viscosity influence on final profiles

Groups	Cases	Yield stress(Pa)	Viscosity(Pa·s)	Energy conditions	Flume test
Group1	Case0	18.61	0.32	$v_{inlet} = 0.1\mathrm{m/s}$	Discharge
	Case1	1.25 × 18.61	0.32		
	Case2	18.61	1.25 × 0.32		
Group2	Case0	18.61	0.32	$v_{inlet} = 0.4\mathrm{m/s}$	
	Case1	1.25 × 18.61	0.32		
	Case2	18.61	1.25 × 0.32		
Group3	Case0	18.61	0.32	Patched shape: 46mm × 300mm (Height × Length)	S-R
	Case1	1.25 × 18.61	0.32		
	Case2	18.61	1.25 × 0.32		
Group4	Case0	18.61	0.32	Patched shape: 69mm × 200mm (Height × Length)	
	Case1	1.25 × 18.61	0.32		
	Case2	18.61	1.25 × 0.32		

As shown in **Table 1**, Group 1 and Group 2 simulate discharge flume tests with inlet velocities of 0.1 m/s and 0.4 m/s respectively and Group 3 and Group 4 are for S-R flume tests with rectangular patched shapes ($46\mathrm{mm} \times 300\mathrm{mm}$ and $69\mathrm{mm} \times 200\mathrm{mm}$). Each group contains three simulations designated as Case 0, Case 1 and Case 2. Case 1 and Case 2 have a 25% higher yield stress and a 25% higher viscosity, respectively compared

to Case 0 which is the base case. The six simulations for discharge flume tests have the same volume of fluid, as is the case for the six simulations for S-R flume tests. The slopes obtained from the simulations listed in **Table 1** are illustrated in **Figure 9**. **Figure 10** summarizes the slope variations from the base cases (Case 0 in each group) induced by the increase of yield stress and viscosity.

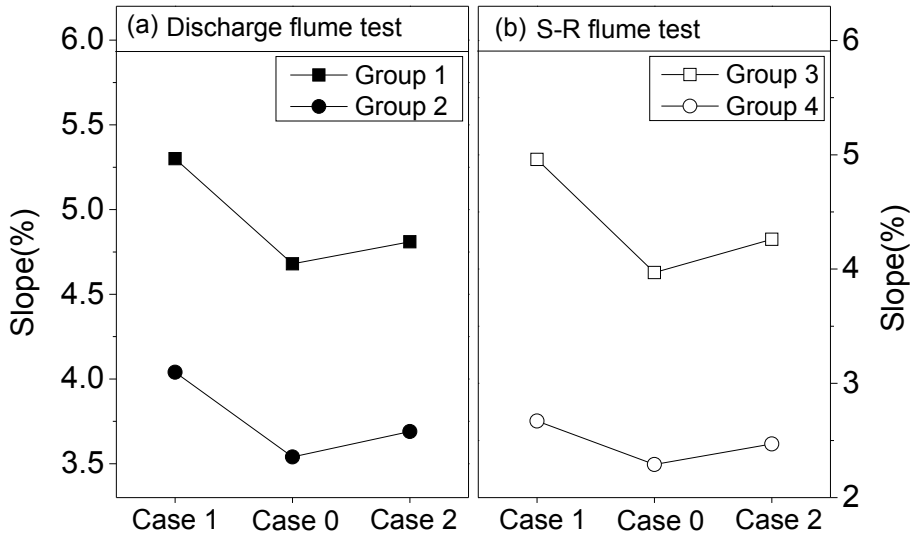

Figure 9 Slopes from simulations of discharge flume tests (a) and S-R flume tests (b) for yield stress and viscosity influence investigation. Detailed information of the simulations are listed in **Table 1**.

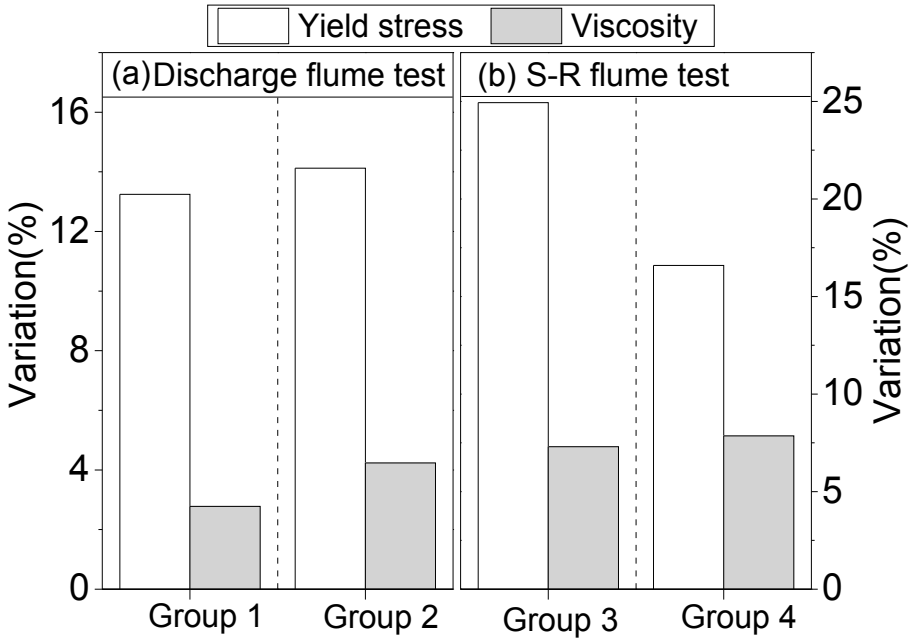

Figure 10 Slope variations from Case 0 caused by 25% increase of yield stress and viscosity in simulations of discharge flume tests (a) and S-R flume tests (b). Detailed information of the simulations are listed in **Table 1**.

It can be concluded from the comparison of slopes between Group 1 and Group 2, and Group 3 and Group 4 that higher energy resulted in a smaller slope for both kinds of flume tests, as shown in **Figure 9**. Moreover in each group the smallest slopes are always from the base cases (Case 0) rather than the cases with higher yield stresses or viscosities, which indicates that the slope of the Bingham fluid was influenced by both yield stress and viscosity.

Although both yield stress and viscosity influenced the slope, the 25% increase of yield stress resulted in a much greater variation of slope from the base case than the 25% increased viscosity, as demonstrated in **Figure 10**. The results suggest that yield stress plays a more dominant role in the formation of the beach profile of thickened tailings in

the flume tests, and presumably also with field deposition.

To understand the influence of viscosity in different scenarios with respect to inertial effects, the ratio (R_{vy}) of slope variations caused by increased viscosity and increased yield stress in each group is used to depict the relative importance of viscosity and yield stress:

$$R_{vy} = \frac{\Delta S_v}{\Delta S_y} \tag{13}$$

where ΔS_v and ΔS_y are the variations of slope resulting from increased viscosity (Case 2) and yield stress (Case1), compared to Case 0 in the same group.

For example, the variations of slope caused by viscosity and yield stress increase in Group 1 is 2.8% and 13.3%, as shown in **Figure 10**. Thus the ratio of the slope variations between Case 2 and Case 1 in Group 1 is 0.21 (2.8%/13.3%). Following this method, the ratio of slope variations by increased viscosity (Case2) and yield stress (Case 1) for the other groups can be calculated and are summarized in **Figure 11**. As can be seen in **Figure 11**, all ratios for both discharge and S-R flume tests are less than unity which suggests that the viscosity plays a less important role in the slope formation than the yield stress. Furthermore, the ratios for scenarios where the energy is relatively high (Group 2 and Group 4) are larger than the corresponding scenarios of low energy (Group 1 and Group 3) for both types of flume test. The results suggest that the importance of viscosity in the final profile formation of a Bingham fluid increases with the increase of inertial effects during the deposition process, although it is less important than the yield stress generally.

On the other hand, we may infer that the influence of viscosity can be negligible if the inertia effects are sufficiently low during the deposition of Bingham fluid [70]. Considering the energy release in a dam-break is significant and quick, the inertial effects are expected to be strong. Therefore the viscosity could be an important factor in a real dam-break.

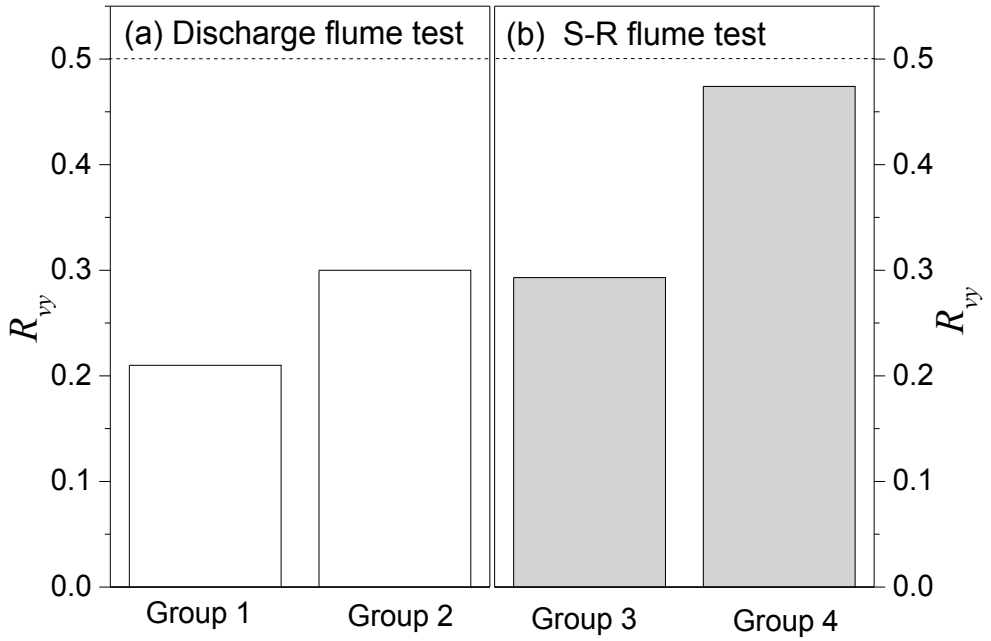

Figure 11 Ratio of slope variations between Case 2 and Case 1 for simulations of discharge flume tests (a) and S-R flume tests (b). The Bingham fluids employed in Case 2 and Case 1 have higher viscosity and yield stress respectively than Case 0, as shown in **Table 1**.

2.3.4 The influence of flume width on the slope in a flume test

3D simulations of both S-R and discharge flume tests with three different flume widths (100 mm, 200 mm and 400 mm) were carried out to investigate the influence of flume width on the final profiles achieved in flume tests. **Figure 12** illustrates the geometries of

the 3D simulations of S-R and discharge flume tests. Nonslip wall conditions were applied to sidewalls and bottoms of the flume.

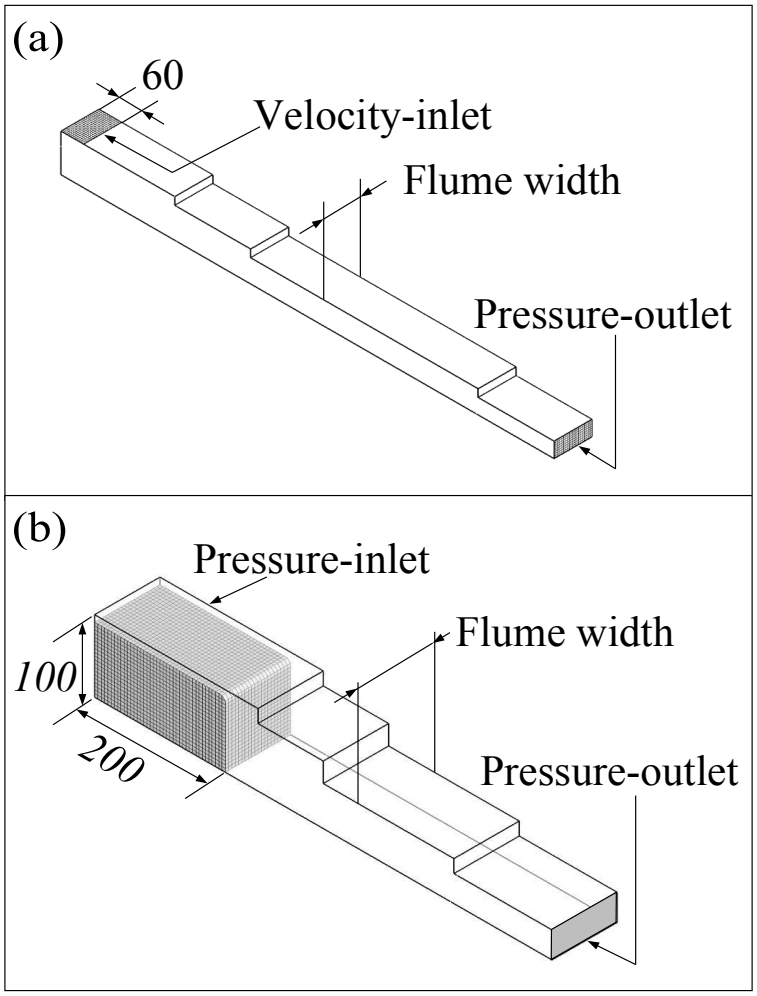

Figure 12 Sketches for the 3D simulations of the discharge flume test with a flume-wide inlet (a) and the S-R flume test at the initial state (b). The shaded volume in panel (b) is the initial volume patched in the flume at t=0. Non-slip conditions are applied to the walls except for the outlets and inlets.

To make the simulation results for discharge flume tests with different flume widths comparable, the width of the inlet of the discharge flume test was identical to the flume width with an inlet length at 60 mm, as shown in **Figure 12** (a). Furthermore the three

simulations of discharge flume tests shared the same inlet velocity (0.5 m/s), discharging time (1 s) and material properties. With these measures, both flow rate and fluid volume per unit width of the discharge flume tests with different flume widths are equivalent. Therefore the difference in the final profiles of the three simulations, if any, should be caused by the flume width.

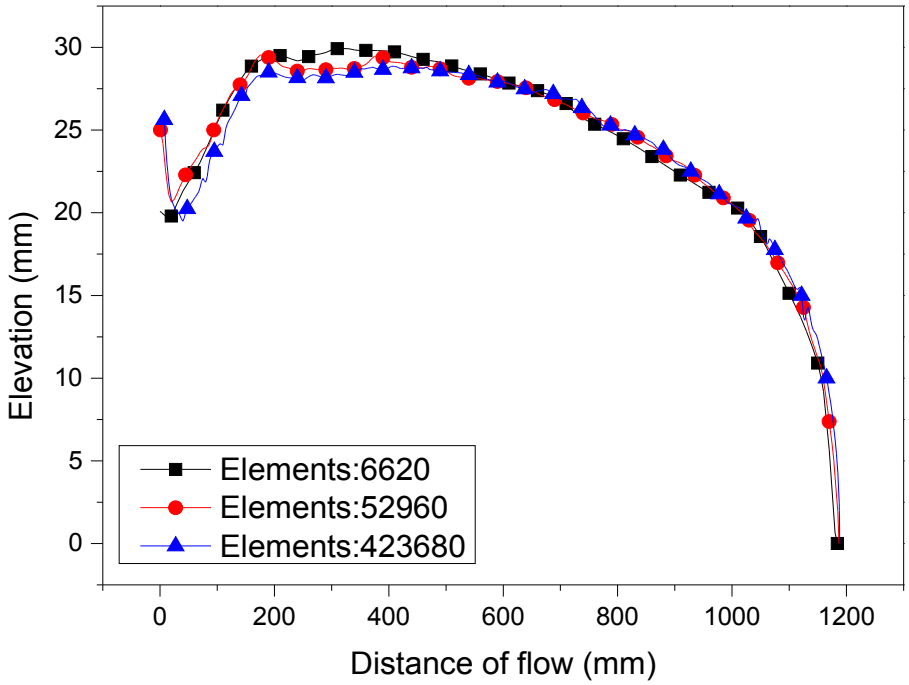

Figure 13 Final profiles from 3D simulations of different number of elements for the discharge flume test with flume width at 200 mm.

The initial shapes of the fluid in the S-R flume test simulations were rectangular cuboids of which the height and length were fixed at 100 mm and 200 mm respectively with widths consistent with the flume widths, as shown in **Figure 12** (b). Thus both the volume of fluid per unit width and the potential energy of fluid per unit volume (see Eq.(12)) were identical in the three S-R flume test simulations, thereby facilitating the analysis of the

flume width influence.

Regular hexahedron elements were used to discretise the 3D geometries and care was taken to reduce the difference in sides of the elements to improve the convergence rate and accuracy of the simulations. Mesh-independence investigations were performed for all the 3D simulations in the present work but only the discharge flume test with a width at 200 mm, as an example, is presented for the sake of conciseness. **Figure 13** summarises the three final profiles of the 3D simulations using different numbers of elements for the discharge flume test with the flume width at 200 mm. The corresponding slopes and the slope variations from the base case (Case 3: 423680 elements) are listed in **Table 2**. As shown in **Figure 13**, the final profiles from simulations of different numbers of elements are very similar. Further analysis suggests that, compared to the big difference in slopes between Case 1 and Case 3 (14.78%), the difference between Case 2 and Case 3 is relatively minor (1.74%), although the number of elements of Case 3 is eight times more than that of Case 2, as shown in **Table 2**. Accordingly the mesh resolution of Case 2 is sufficiently high with both accuracy and computing time taken into account.

Table 2 Comparison of the slopes from 3D simulations of different number of elements for the discharge flume test with the flume width at 200 mm.

Cases	Elements	Slope (%)	Slope variation from Case 3 (%)
Case 1	6620	1.646	14.78
Case 2	52960	1.459	1.74
Case 3	423680	1.426	-

Figure 14 and **Figure 15** show the final profiles and the corresponding slopes from the simulations of discharge and S-R flume tests with flume widths of 100 mm, 200 mm and 400 mm. It is evident that the slopes of the final profiles in both types of flume tests decrease with increasing flume width, which was demonstrated theoretically by Fourie and Gawu [26]. This is a very useful result which may partially account for the unrealistic steeper slopes achieved in laboratory flume tests for thickened tailings than those observed in the field. Moreover it suggests that the analytical solution (Eq.(9)) which was initially developed for sheet flow of Bingham fluid is not suitable for laboratory flume test on thickened tailings, as discussed by Gao and Fourie [70].

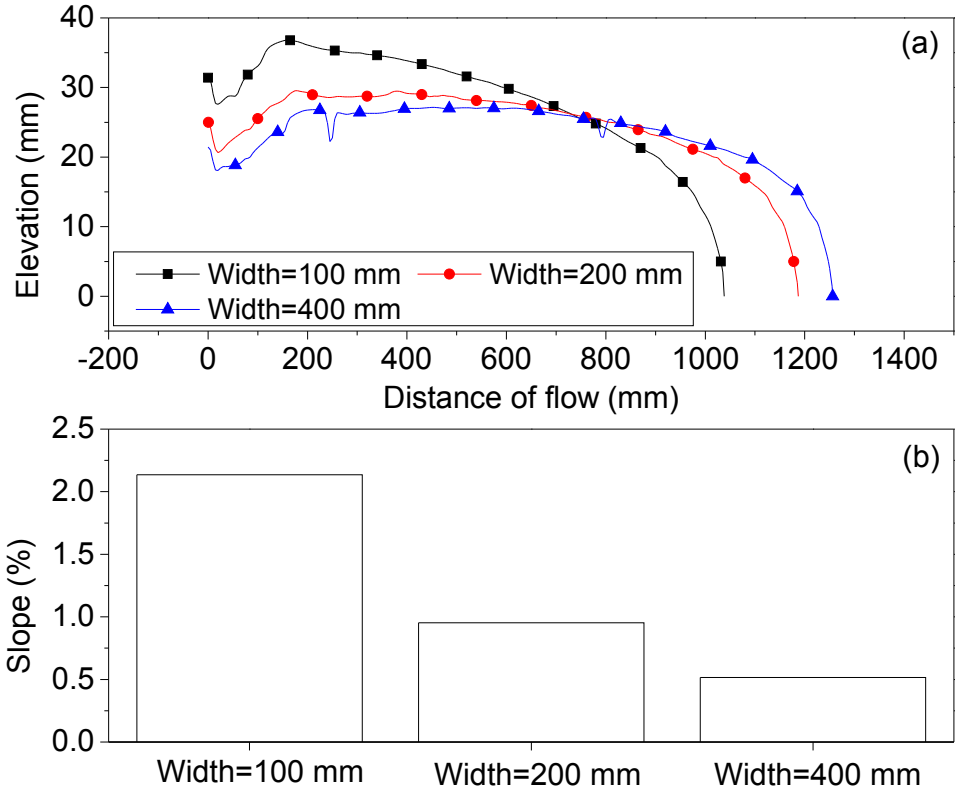

Figure 14 Final profiles (a) and the corresponding slopes (b) from discharge flume test simulations (3D) of different flume widths. The inlet velocity was 0.5 m/s with a discharging time of 1 s. The input material properties were: 18.61 Pa, 0.32 Pa·s and 1315.0 kg/m^3.

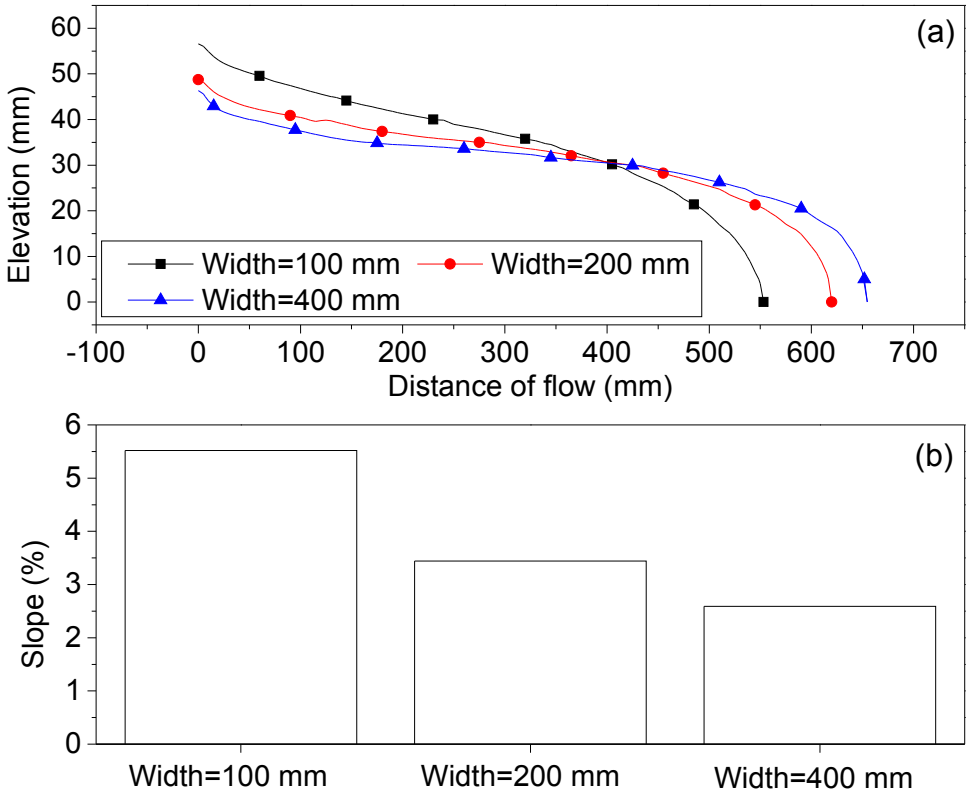

Figure 15 Final profiles (a) and the corresponding slopes (b) from S-R flume test simulations (3D) of different flume widths. The input material properties were: 33.28 Pa, 0.4 Pa·s and 1342.6 kg/m^3.

2.3.5 The influence of base angles on the final profiles of thickened tailings

To investigate the influence of the base angle on the final profiles of thickened tailings, simulations (2D) of both S-R and discharge flume tests with different base angles (0, 1%, 2%, and 3%) were conducted. The volume of fluid was identical for all the simulations in this section. The inlet size (d in **Figure 2**(b)), the height of the inlet (h in **Figure 2**(b)) and the inlet velocity was the same as those in Section 2.3.1.2. For the simulations of S-R flume tests, the initial shape of the fluid patched in the flumes is 80 mm (b in **Figure 2**(a)) × 400 mm (a in **Figure 2**(a)).

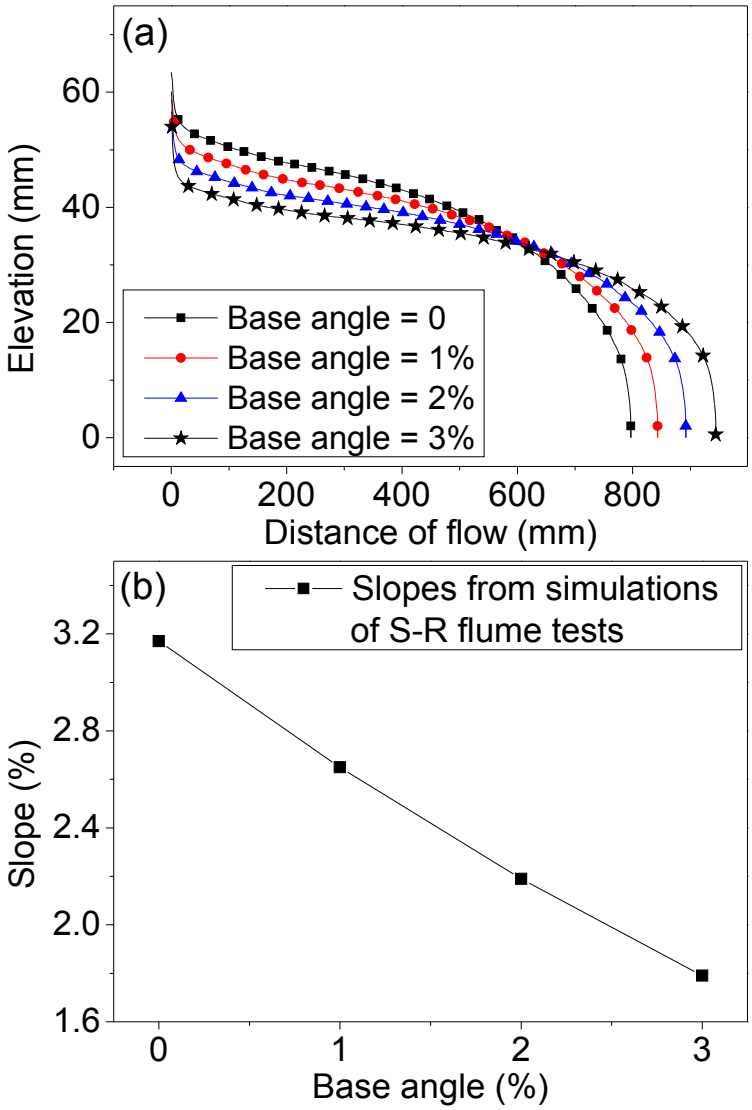

Figure 16 Final profiles (a) and the corresponding slopes (b) from simulations (2D) of S-R flume test with different base angles. The material properties were: 33.28 Pa, 0.4 Pa·s and 1342.6 kg/m^3.

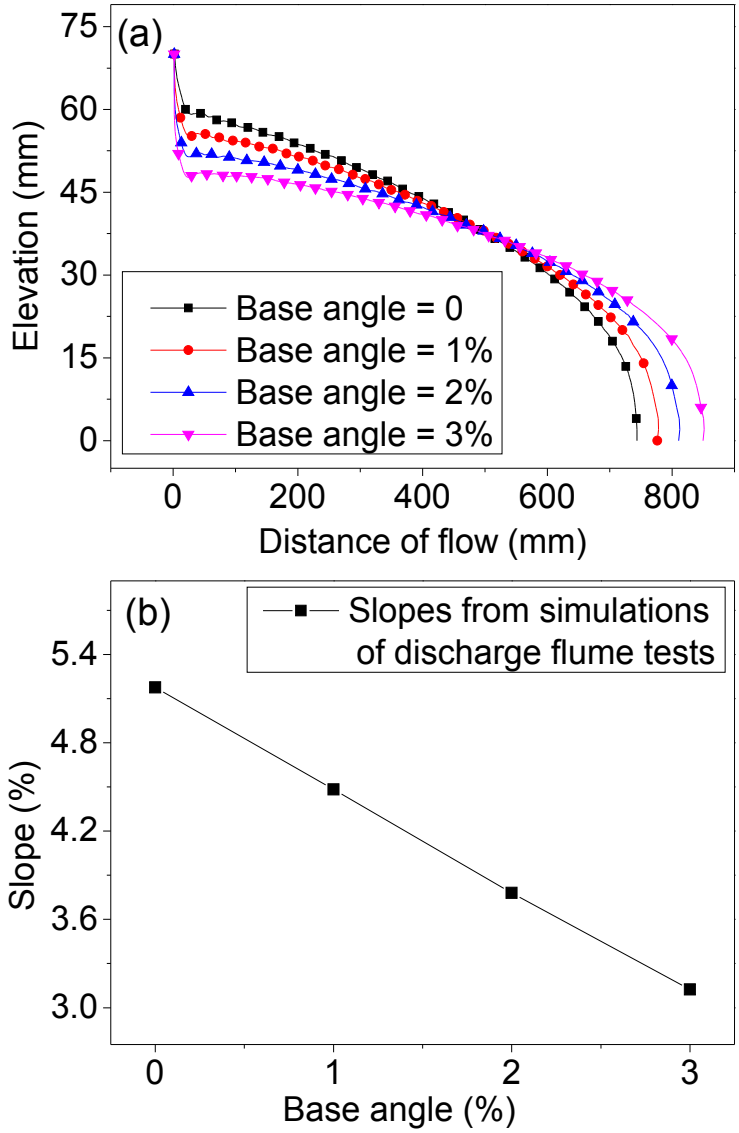

Figure 17 Final profiles (a) and the corresponding slopes (b) from simulations (2D) of discharge flume test with different base angles. The material properties were: 33.28 Pa, 0.4 Pa·s and 1342.6 kg/m^3.

Figure 16 shows the final profiles and the corresponding slopes from the 2D simulations of S-R flume tests with four different base angles and **Figure 17** shows results for discharge flume tests. It is evident that the final profiles tend to be longer and flatter with increasing base angles. More interestingly, the slope of the profile seems to be a linear

function of the base angle for both types of flume tests, as shown in **Figure 16** (b) and **Figure 17** (b). Sofra and Boger [63] carried out S-R flume tests with different base angles on Laponite slurries of yield stress ranging from 17 to 110 Pa. A linear relation between base angles and slopes of final profiles was observed, which confirms the CFD simulations. In addition, the impact of base angle on the resulting slope implies that the beach slope of thickened tailings in the field is likely to be influenced by the underlying topography, as reported by other researchers [37, 69].

2.3.6 Dimensional analysis

To develop a better understanding of the planar (2D) deposition of thickened tailings, a dimensional analysis was performed to find out the relationship between the relevant parameters and the average beach slopes. The relationship obtained from small-scale deposition may provide useful insight into the deposition of thickened tailings in the field.

A dimensional analysis using the Buckingham π theorem [83] was performed by Sofra and Boger [63, 84] to determine the important dimensionless parameters for thickened tailings deposition based on laboratory S-R flume tests using different dense suspensions. Three relevant dimensionless groups were identified: dimensionless yield stress ($\frac{\tau_y}{\rho v^2}$), Reynolds number (R_e) and Froude number (F_r):

$$R_e = \frac{\rho v w}{\mu} \tag{14}$$

$$F_r = \frac{v^2}{g w} \tag{15}$$

where w is the flume width and v is the instantaneous initial suspension velocity, which

was calculated by assuming that all of the potential energy of the fluid in the reservoir is converted to kinetic energy:

$$\rho g h = \frac{1}{2}\rho v^2 \tag{16}$$

Therefore:

$$v = \sqrt{2gh} \tag{17}$$

where h is the initial height of the fluid in the reservoir plus the height of the reservoir above the horizontal.

They also reported an appropriate form of the relationship between these groups and the average beach slope (BS_a):

$$BS_a = f_1\left(\frac{\tau_y F_r}{\rho v^2 R_e}\right) = f_1\left(\frac{\mu_0 \tau_y}{\rho^2 W^2 g v}\right) \tag{18}$$

For the 2D planar simulations of flume tests carried out in the present work, the flume width (w) is deemed to be infinite, which renders Eqs.(14)-(15) inapplicable due to the presence of flume width in these equations. Moreover, although the assumption that all of the potential energy of the fluid in the reservoir is converted to kinetic energy is valid in the work of Sofra and Boger [63, 84] as a result of the relatively low viscosity of the suspensions (0.0058–0.0382 Pa·s) they used, the assumption does not hold for the materials with very high viscosities, such as the runs 7-10 in **Table 3** where the viscosity is 10 Pa·s. This is because the high viscosity results in significant frictional losses, thereby voiding Eq.(17). Additionally both tailings volume and base angle which influence the average beach slope were not taken into account in their dimensional analysis [33, 63].

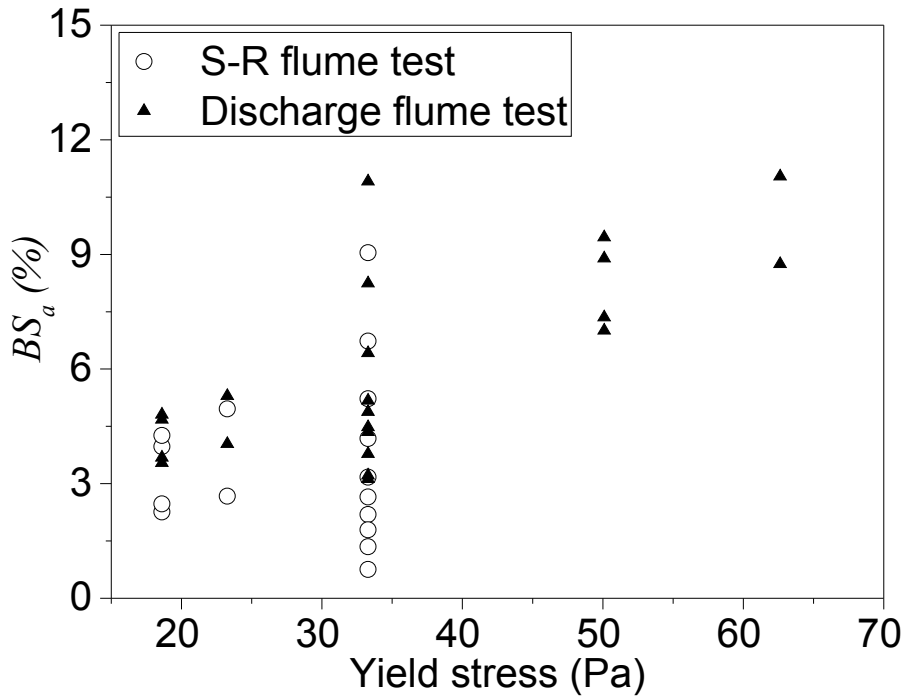

Figure 18 The average beach slope vs. yield stress from the planar simulation results of both S-R and discharge flume tests.

Figure 18 shows the variation in the average beach slope with the yield stress, according to the planar simulations of both S-R and discharge flume tests performed in the present work. There are several different slopes for one yield stress, clearly indicating that the yield stress is not the only parameter influencing the slope of thickened tailings.

To find out the important dimensionless groups for planar thickened tailings deposition, dimensional analysis was conducted for both S-R and discharge flume tests in the present work (see Appendices 2A and 2B).

2.3.6.1 Dimensional analysis for S-R flume tests

For the S-R flume tests, the average beach slope is given by (see Appendix 2A):

$$BS_a = f(\theta, \frac{\tau_y}{\sqrt{A}\rho g}, \frac{b}{\sqrt{A}}, \frac{\mu_0}{A^{0.75}\rho\sqrt{g}}) \quad (19)$$

where A is the volume of thickened tailings ($A=ab$), b is the height of the patched area (see **Figure 2**(a)) and θ is the average base angle.

An appropriate combination of the dimensionless groups in Eq. (19) is determined based on the data of S-R flume tests listed in **Table 3**:

$$BS_a = f_1\left(\frac{\tau_y - \rho g H sin\theta}{\sqrt{A}\rho g} \times \left(\frac{\mu_0}{A^{0.75}\rho\sqrt{g}}\right)^{0.3} \div \frac{b}{\sqrt{A}}\right) = f_1\left[\frac{{\mu_0}^{0.3}(\tau_y - \rho g H sin\theta)}{\rho^{1.3} g^{1.15} A^{0.225} b}\right] \quad (20)$$

where H is the characteristic thickness of thickened tailings deposited on an inclined plane and is determined to be 0.038 m for both S-R and discharge flume tests based on the simulation results.

Application of the combined dimensionless group in Eq. (20) to the data from S-R flume tests in **Figure 19** shows that there is a clear linear relation between the average beach slope and the proposed combination of relevant parameters:

$$BS_a = 793.04 \frac{{\mu_0}^{0.3}(\tau_y - \rho g H sin\theta)}{\rho^{1.3} g^{1.15} A^{0.225} b} \quad (21)$$

The high coefficient of determination ($R^2 \approx 0.99$) indicates that the statistical model (Eq. (21)) fits the data very well. Moreover the relevant parameters for the process of S-R flume tests have been included by the proposed dimensionless group.

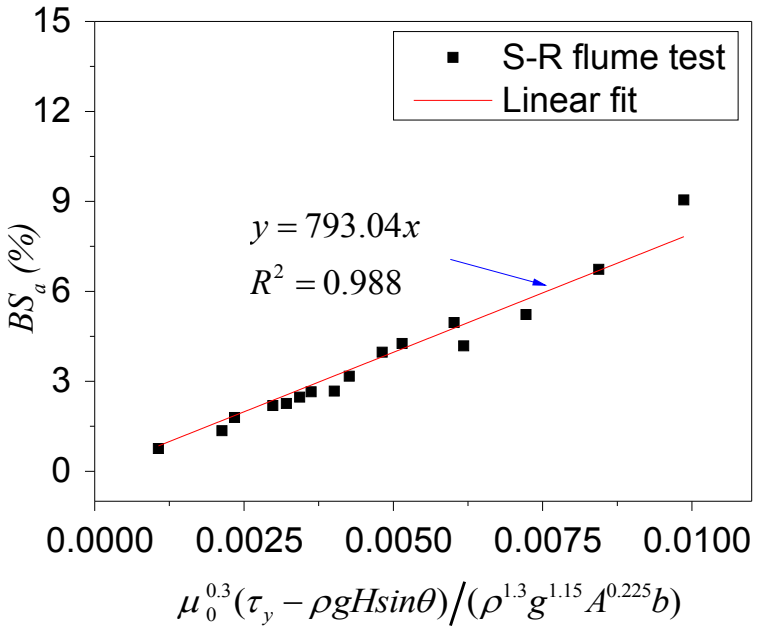

Figure 19 Average beach slope as a function of $\frac{\mu_0{}^{0.3}(\tau_y-\rho gHsin\theta)}{\rho^{1.3} g^{1.15} A^{0.225} b}$ for S-R flume tests.

Table 3 Data from simulations of S-R flume tests.

Runs	$tan\theta$	τ_y	μ_0	ρ	a	b	A	H	L	$\frac{\mu_0{}^{0.3}(\tau_y - \rho gHsin\theta)}{\rho^{1.3} g^{1.15} A^{0.225} b}$	BS_a
Units	-	Pa	Pa·s	kg/m^3	m	m	m^2	m	m	-	%
1	0	33.28	0.4	1342.6	0.4	0.08	0.032	-	0.7970	4.264E-03	3.17
2	0.01	33.28	0.4	1342.6	0.4	0.08	0.032	0.038	0.8433	3.624E-03	2.65
3	0.02	33.28	0.4	1342.6	0.4	0.08	0.032	0.038	0.8924	3.055E-03	2.19
4	0.03	33.28	0.4	1342.6	0.4	0.08	0.032	0.038	0.9442	2.551E-03	1.79
5	0	33.28	0.4	1342.6	0.2	0.16	0.032	-	1.0436	2.132E-03	1.35
6	0	33.28	0.4	1342.6	0.1	0.32	0.032	-	1.3941	1.066E-03	0.756
7	0	33.28	10	1342.6	0.05	0.13	0.0065	-	0.2463	9.865E-03	9.045
8	0	33.28	10	1342.6	0.1	0.13	0.013	-	0.4155	8.440E-03	6.731
9	0	33.28	10	1342.6	0.2	0.13	0.026	-	0.6812	7.222E-03	5.224
10	0	33.28	10	1342.6	0.4	0.13	0.052	-	1.0865	6.179E-03	4.182
11	0	18.61	0.32	1315	0.3	0.046	0.0138	-	0.5199	4.814E-03	3.969
12	0	23.26	0.32	1315	0.3	0.046	0.0138	-	0.4769	6.018E-03	4.958
13	0	18.61	0.4	1315	0.3	0.046	0.0138	-	0.5146	5.148E-03	4.259
14	0	18.61	0.32	1315	0.2	0.069	0.0138	-	0.6035	3.210E-03	2.258
15	0	23.26	0.32	1315	0.2	0.069	0.0138	-	0.5535	4.012E-03	2.671
16	0	18.61	0.4	1315	0.2	0.069	0.0138	-	0.5857	3.432E-03	2.47

2.3.6.2 Dimensional analysis for discharge flume tests

For the discharge flume tests, the relation between the average beach slope and the dimensionless groups are (see Appendix 2B):

$$BS_a = g(\theta, \frac{A\tau_y}{\rho Q^2}, \frac{\mu_0}{\rho Q}, \frac{A^{1.5}g}{Q^2}) \tag{22}$$

where Q is the discharging flow rate in a discharge flume test.

Further investigation suggests that the appropriate combination of the dimensionless groups for discharge flume tests listed in **Table 4** is as follows:

$$BS_a = g_1\left(\frac{A(\tau_y - \rho g H sin\theta)}{\rho Q^2} \times \left(\frac{\mu_0}{\rho Q}\right)^{0.3} \div \frac{A^{1.5}g}{Q^2}\right) = g_1\left[\frac{{\mu_0}^{0.3}(\tau_y - \rho g H sin\theta)}{\rho^{1.3} g A^{0.5} Q^{0.3}}\right] \tag{23}$$

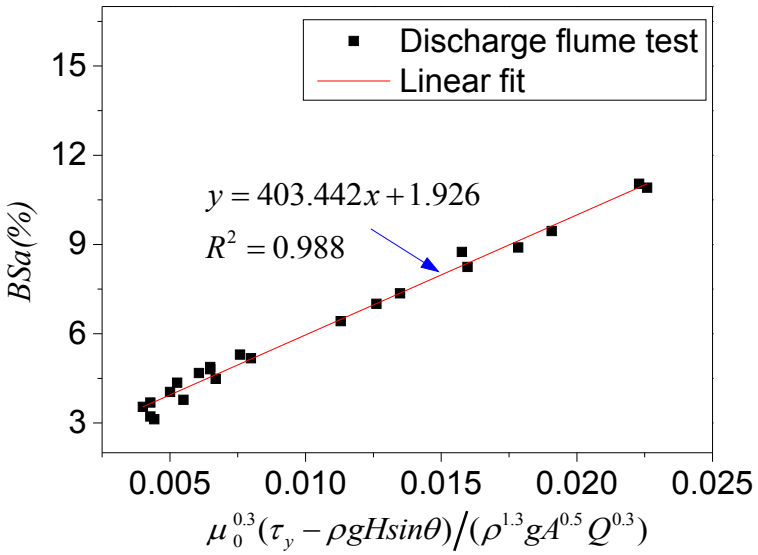

Figure 20 Average beach slope as a function of $\frac{{\mu_0}^{0.3}(\tau_y - \rho g H sin\theta)}{\rho^{1.3} g A^{0.5} Q^{0.3}}$ for discharge flume tests.

Figure 20 illustrates the linear relationship between the average beach slope and the proposed combination of relevant parameters in Eq. (23) for the discharge flume tests:

$$BS_a = 403.442 \frac{{\mu_0}^{0.3}(\tau_y - \rho g H sin\theta)}{\rho^{1.3} g A^{0.5} Q^{0.3}} + 1.926 \quad (24)$$

The high coefficient of determination ($R^2 \approx 0.99$) indicates that the linear function (Eq. (24)) can be used to predict the average beach slope of thickened tailings in the planner discharge flume tests with high accuracy. Additionally it suggests that the proposed dimensionless group in Eq. (23) involves the relevant parameters for discharge flume tests.

Table 4 Data from simulations of discharge flume tests.

Runs	$tan\theta$	τ_y	μ_0	ρ	Q	A	H	L	$\frac{{\mu_0}^{0.3}(\tau_y - \rho g H sin\theta)}{\rho^{1.3} g A^{0.5} Q^{0.3}}$	BS_a
Units	-	Pa	Pa·s	kg/m^3	m^2/s	m^2	m	m	-	%
1	0	33.28	0.4	1342.6	0.002	0.004	-	0.1739	2.259E-02	10.91
2	0	33.28	0.4	1342.6	0.002	0.008	-	0.2833	1.597E-02	8.243
3	0	33.28	0.4	1342.6	0.002	0.016	-	0.4576	1.129E-02	6.421
4	0	33.28	0.4	1342.6	0.002	0.032	-	0.7436	7.987E-03	5.175
5	0	33.28	0.4	1342.6	0.004	0.032	-	0.7466	6.487E-03	4.88
6	0	33.28	0.4	1342.6	0.008	0.032	-	0.7691	5.269E-03	4.355
7	0	33.28	0.4	1342.6	0.016	0.032	-	0.8136	4.280E-03	3.217
8	0	18.61	0.32	1315	0.002	0.016	-	0.5563	6.069E-03	4.68
9	0	23.26	0.32	1315	0.002	0.016	-	0.5150	7.586E-03	5.298
10	0	18.61	0.4	1315	0.002	0.016	-	0.5550	6.489E-03	4.807
11	0	18.61	0.32	1315	0.008	0.016	-	0.6143	4.004E-03	3.543
12	0	23.26	0.32	1315	0.008	0.016	-	0.5686	5.005E-03	4.041
13	0	18.61	0.4	1315	0.008	0.016	-	0.6031	4.281E-03	3.685
14	0.01	33.28	0.4	1342.6	0.002	0.032	0.038	0.7781	6.688E-03	4.482
15	0.02	33.28	0.4	1342.6	0.002	0.032	0.038	0.8121	5.499E-03	3.78
16	0.03	33.28	0.4	1342.6	0.002	0.032	0.038	0.8512	4.427E-03	3.123
17	0	50.1	0.64	1367.4	0.008	0.016	-	0.4146	1.261E-02	7.007
18	0	62.62	0.64	1367.4	0.008	0.016	-	0.3887	1.576E-02	8.751
19	0	50.1	0.8	1367.4	0.008	0.016	-	0.4094	1.349E-02	7.356
20	0	50.1	0.64	1367.4	0.008	0.008	-	0.2621	1.784E-02	8.898
21	0	62.62	0.64	1367.4	0.008	0.008	-	0.2443	2.229E-02	11.04
22	0	50.1	0.8	1367.4	0.008	0.008	-	0.2575	1.907E-02	9.451

2.3.6.3 Discussions of the proposed model

Theoretically the proposed model (Eqs.(21) and (24)) has the potential to predict the average beach slope in the field, similar to the "master profile" proposed by Blight et al. [36, 39], which has been successfully used to model the beach slope of conventional tailings. However there are still several issues that need to be addressed before the proposed model can be applied to the field confidently. First, the flow of thickened tailings on the tailings beach is complex [85, 86], and lateral spreading is likely to occur [63]. It is necessary to investigate lateral spreading considering that the proposed method is based on planar simulations. Moreover, it is not easy to determine the rheological parameters in the field, such as the yield stress, viscosity and density, because of the variation of thickener output [26, 87]. In addition, although the value of 0.038 m for characteristic thickness of the deposited tailings, which is necessary for the beach slope prediction with a non-zero base angle, works very well for the flume tests, further investigations into this value for the field deposition of thickened tailings are required. Notwithstanding these issues, the proposed model provides good insights into the factors influencing the beach formation of thickened tailings and offers some interesting possibilities for beach slope prediction of thickened tailings

2.4 Conclusions

Based on the present work, several conclusions may be reached regarding flume tests on thickened tailings:

1. The average beach slope of thickened tailings achieved in a planar flume can be predicted using the proposed models (Eqs. (21) and (24)). The models may have a potential to predict the average beach slope of thickened tailings in the field, although further investigations are required.
2. The slope of the final profile of a yield-stress fluid decreases with an increasing fluid volume, which indicates that the beach slope of thickened tailings is flow-scale dependent. In other words, it is not advisable to use small-scale tests for direct extrapolation to field applications.
3. Higher energy results in longer and flatter final profiles of thickened tailings.
4. Generally, the yield stress of thickened tailings has more influence on the slope than does viscosity. The importance of viscosity for the final profile formation of thickened tailings increases with an increase of inertial effects during the deposition process. Therefore, it is inferred that the influence of viscosity can be negligible if the inertia effects are sufficiently low in the deposition of thickened tailings. Conversely, viscosity may be a dominant variable in the dam-break simulations.
5. The flume width has a significant influence on the slope of thickened tailings in a laboratory flume test. A smaller flume width increases the slope of thickened tailings in a flume. This is an important result as it demonstrates the inadvisability of using slopes achieved in laboratory flume tests to directly extrapolate to beach slopes in field deposition.
6. An increasing base angle results in the reduction of the resulting slope, which

suggests that the beach slope of thickened tailings is influenced by base topography in the field.

7. The agreement between simulation results and laboratory observations in the literature gives confidence in the veracity of the computational results. Consequently, CFD simulations provide a potentially effective method to investigate the flow problem of thickened tailings.
8. Quantification of the influence of the factors, as is studied in this paper, should result in more considered flume tests in future.

Acknowledgements

This work was supported by resources provided by the Pawsey Supercomputing Centre with funding from the Australian Government and the Government of Western Australia; the first author gratefully acknowledges the China Scholarship Council (CSC) and The University of Western Australia for financial support.

Appendix 2A. Dimensional analysis of S-R flume tests

The variables that govern the flow of thickened tailings in an S-R flume test are listed in **Table 2A1**.

Table 2A1. Variables for dimensional analysis of the 2D S-R flume test.

Variables	Symbol	Units	Dimensions
Average beach slope	BS_a	(°)	$M^0L^0T^0$
Base angle	θ	(°)	$M^0L^0T^0$
Yield stress	τ_y	Pa	$M^1L^{-1}T^{-2}$
Volume of tailings	A	m^2	$M^0L^2T^0$
Height of patched area	b	m	$M^0L^1T^0$
Plastic viscosity	μ_0	Pa·s	$M^1L^{-1}T^{-1}$
Density	ρ	kg/m^3	$M^1L^{-3}T^0$
Gravitational acceleration	g	m/s^2	$M^0L^1T^{-2}$

We choose A, ρ and g as the repeating variables, which can be justified by:

$$\begin{vmatrix} 0 & 2 & 0 \\ 1 & -3 & 0 \\ 0 & 1 & -2 \end{vmatrix} = -2 \neq 0 \qquad (2A1)$$

Therefore the Π terms are:

$$\Pi_1 = \frac{BS_a}{A^{a1}\rho^{b1}g^{c1}} \qquad (2A2)$$

$$\Pi_2 = \frac{\theta}{A^{a2}\rho^{b2}g^{c2}} \qquad (2A3)$$

$$\Pi_3 = \frac{\tau_y}{A^{a3}\rho^{b3}g^{c3}} \qquad (2A4)$$

$$\Pi_4 = \frac{b}{A^{a4}\rho^{b4}g^{c4}} \qquad (2A5)$$

$$\Pi_5 = \frac{\mu_0}{A^{a5}\rho^{b5}g^{c5}} \qquad (2A6)$$

Since the Π terms are dimensionless, it is readily to determine the indexes (a_i, b_i, c_i) in Eqs. (2A2) - (2A6). Thus we have:

$$\Pi_1 = BS_a \quad (2A7)$$

$$\Pi_2 = \theta \quad (2A8)$$

$$\Pi_3 = \frac{\tau_y}{\sqrt{A}\rho g} \quad (2A9)$$

$$\Pi_4 = \frac{b}{\sqrt{A}} \quad (2A10)$$

$$\Pi_5 = \frac{\mu_0}{A^{0.75}\rho\sqrt{g}} \quad (2A11)$$

The relation between the Π terms can be expressed as:

$$BS_a = f(\theta, \frac{\tau_y}{\sqrt{A}\rho g}, \frac{b}{\sqrt{A}}, \frac{\mu_0}{A^{0.75}\rho\sqrt{g}}) \quad (2A12)$$

Appendix 2B. Dimensional analysis of discharge flume tests

The variables that govern the flow of thickened tailings in a discharge flume test are listed in **Table 2B1**.

Table 2B1. Variables for dimensional analysis of the discharge flume test.

Variables	Symbol	Units	Dimensions
Average beach slope	BS_a	(°)	$M^0L^0T^0$
Base angle	θ	(°)	$M^0L^0T^0$
Yield stress	τ_y	Pa	$M^1L^{-1}T^{-2}$
Volume of tailings	A	m^2	$M^0L^2T^0$
Flow rate	Q	m^2/s	$M^0L^2T^{-1}$
Plastic viscosity	μ_0	Pa·s	$M^1L^{-1}T^{-1}$
Density	ρ	kg/m^3	$M^1L^{-3}T^0$
Gravitational acceleration	g	m/s^2	$M^0L^1T^{-2}$

Tailings volume A, discharging flow rate Q and density ρ are chosen as the repeating variables, which can be justified by:

$$\begin{vmatrix} 0 & 2 & 0 \\ 0 & 2 & -1 \\ 1 & -3 & 0 \end{vmatrix} = -2 \neq 0 \qquad (2B1)$$

Therefore the Π terms are:

$$\Pi_1 = \frac{BS_a}{A^{a1}Q^{b1}\rho^{c1}} \qquad (2B2)$$

$$\Pi_2 = \frac{\theta}{A^{a2}Q^{b2}\rho^{c2}} \qquad (2B3)$$

$$\Pi_3 = \frac{\tau_y}{A^{a3}Q^{b3}\rho^{c3}} \qquad (2B4)$$

$$\Pi_4 = \frac{\mu_0}{A^{a4}Q^{b4}\rho^{c4}} \qquad (2B5)$$

$$\Pi_5 = \frac{g}{A^{a5}Q^{b5}\rho^{c5}} \qquad (2B6)$$

The indexes (a_i, b_i, c_i) may be determined by equating the coefficients in Eqs. (2B2)-

(2B6). Thus we have:

$$\Pi_1 = BS_a \tag{2B7}$$

$$\Pi_2 = \theta \tag{2B8}$$

$$\Pi_3 = \frac{A\tau_y}{\rho Q^2} \tag{2B9}$$

$$\Pi_3 = \frac{\mu_0}{\rho Q} \tag{2B10}$$

$$\Pi_4 = \frac{A^{1.5}g}{Q^2} \tag{2B11}$$

The average beach slope can be expressed as:

$$BS_a = g(\theta, \frac{A\tau_y}{\rho Q^2}, \frac{\mu_0}{\rho Q}, \frac{A^{1.5}g}{Q^2}) \tag{2B12}$$

3. SPREAD IS BETTER: AN INVESTIGATION OF THE MINI-SLUMP TEST

Abstract

In the rapidly evolving application of surface deposition of high density, thickened tailings (paste), a key design parameter is the yield stress. A method widely used in industry to obtain quick and easy measurements of the yield stress is the slump test. This paper investigates current techniques for interpreting the cylindrical slump (or mini-slump) test. The lifting process of the cylindrical mould was taken into account in numerical simulations using a computational fluid dynamics (CFD) approach. Simulations with different mould lifting velocities were carried out to understand the influence of mould lifting velocity. Therefore, the influence of plastic viscosity and yield stress on mini-slump test results was studied using a mould lifting velocity of 0.01 m/s, which is representative of rates used in laboratory tests. The predicted slump and spread from mini-slump test simulations for three different scenarios ($v_{lifting} = 0.002$ m/s, $v_{lifting} = 0.01$ m/s, and without mould lifting process, i.e. instantaneous disappearance of the mould) were compared to those from laboratory experiments on kaolin. The rheological properties of the kaolin were measured using a vane rheometer and the data used directly in the modelling study. The results suggest that the lifting speed of the mould has a significant influence on the mini-slump test result, which must therefore be taken

into account in both numerical simulations and laboratory tests. It was found that the variation of mould lifting velocity had a greater influence on slump than spread, indicating that spread is a more appropriate measurement for determining the yield stress in a mini-slump test. This was particularly true for relatively low yield stresses (e.g. 60 Pa or less), which are values typical of most thickened tailings deposits currently operating internationally.

Keywords: Thickened tailings; Yield stress; Slump test; CFD modelling; Spread.

3.1 Introduction

The slump test was originally developed for the determination of the "workability" or consistency of fresh concrete, and has been used in many fields as a result of its simplicity of operation and acceptable accuracy. In slump testing, a conical or cylindrical mould is carefully filled with the material to be tested, and then the mould is raised vertically at a constant velocity. The slump, which is defined as the difference between the height of the mould and the height of the slumped material after flow stops, is measured. An alternative measure is a comparison of the final, spread diameter of the material with that of the cylinder. The slump (or spread) can be used to estimate the yield stress of the tested material [50, 73, 88]. Furthermore, to approximate the plastic viscosity of the tested material, partial or complete slump time is sometimes also measured and recorded [89-92], although this is relatively uncommon.

Since Tanigawa and co-workers [93, 94] simulated the slump test with their CFD codes, much work on simulation of both conical or cylindrical slump tests, based on single phase fluid flow, has been reported. Christensen [64] used finite element method (FEM) based CFD codes to simulate the Abrams' cone slump test. He concluded that the final slump height was governed solely by the Bingham yield stress, while the plastic viscosity only influenced the slump time to reach an equilibrium condition.

Roussel and Coussot [95] carried out simulations of both the ASTM cone and paste cone

slump test with the commercial CFD code FLOW-3D. Good agreement between model and experimental results was reported. However, in their simulations, the mould lifting process was not taken into account, meaning that the mould 'disappeared' at the commencement of iteration. To remove inertial effects, a relatively large plastic viscosity was used in their work, i.e. plastic viscosity = 300 Pa·s for the ASTM cone and plastic viscosity=10 Pa·s for the paste cone [96]. This "artificial" plastic viscosity may indeed enable the model and the experimental results to coincide, but it is preferable to use actual, measured values of viscosity for comparisons of model versus experimental data as the increased viscosity may result in some information, such as flow time, from the simulations being irrelevant. Furthermore, as shown in this paper, viscosity does indeed affect the predicted slump height and spread, so artificially increasing the viscosity is not advisable.

Thrane [97] simulated the ASTM cone slump test with the mould lifting velocity taken into account and found that the lifting velocity of the cone influenced the time to reach equilibrium, and if not accounted for, incorrect interpretation of physical properties of the tested paste may result. However, poor agreement between simulation and experimental results was obtained. To make the predicted and experimental spread results comparable, applied plastic viscosity or yield stress in the simulation, which should have been determined by experiment, had to be changed. No cogent reasons for the clear disparity of results between simulation and experimental results were given.

Tregger et al. [91] used a FEM based, commercially available CFD code to simulate the mini-slump test and found the final spread was underestimated. They argued that this discrepancy should mainly be attributed to the coarse mesh used. The mould lifting process was not simulated in their work.

Recently Bouvet et al. [92] conducted mini-conical slump flow test simulations with the commercial code COMSOL. Again the lifting process was neglected. In their work, the yield stress τ_y (20 Pa and 1 Pa for paste no.1 and paste no.2, respectively) used in the simulations was obtained from Eq.(1) for the mini-cone slump test proposed by [88].

$$\tau_y = \frac{225\rho g V^2}{4\pi^2 D^5} \quad (1)$$

where ρ is the density of paste, g is the gravitational acceleration, V is the volume of the tested material and D is the final spread.

However, Eq.(1) does not account for any inertial effects that may influence the spread of low yield stress paste in a mini-slump test. Therefore, the yield stress in their work was more likely underestimated. Moreover, these yield stresses were used to determine the Bingham viscosities by forcing agreement of flow time between the Marsh-conical test and simulations. The plastic viscosity may therefore be overestimated.

In thickened tailings disposal operations, the yield stress of the tailings in most cases ranges from 20 Pa to 50 Pa [66], for which the inertial effects caused by the mould lifting process would be non-negligible. Furthermore, the mould used for the mini-slump test in

the tailings industry is typically cylindrical. However, from previous work, little effort has been made to simulate the mini-slump test with the cylindrical mould lifting process taken into account. Given the lack of information in this regard, an investigation of the influence of mould lifting velocity on the mini-slump test was considered crucial.

In the present work, our focus was to assess the influence of lifting velocity of mini-cylindrical mould on the slump, spread, and flow time of paste with a relatively low yield stress (from about 20 Pa to 60 Pa) in a mini-slump test.

The following section describes the experimental work, followed by a description and validation of the numerical model used in the simulation. Thereafter a series of simulations were conducted to investigate the influence of lifting velocity of the mould, yield stress and plastic viscosity on the mini-slump test.

3.2 Experimental procedure

3.2.1 Materials and sample preparation

Paste materials of different moisture content were prepared by mixing kaolin clay with fresh water at a constant rotational speed for 20 minutes, resulting in a smooth, homogeneous mixture.

3.2.2 Measurement techniques

The yield stresses of paste materials were measured using a Viscotester 550 from Thermo HAAKE. This viscometer has a six-bladed vane attached to its torsion head, allowing measurement of yield stress below 1 kPa at a controlled rotational speed. The vane employed throughout this work had a height of 16 mm and a diameter of 22 mm, denoted by H_v and D_v, respectively. A plastic beaker with an inner diameter of 105 mm (donated by D_c) was used as the container in the rheological tests. The depth of immersion of the vane is described by Z_1 and Z_2, which represent the distance between the free surface and the top end of vane, and the distance between the bottom of the beaker and the low end of vane. Care was taken to assure that $Z_1 \geq 30$ mm and $Z_2 \geq 40$ mm. Therefore: $\frac{H_v}{D_v} = 0.73 < 3.5$, $\frac{D_c}{D_v} = 4.77 > 2.0$, $\frac{Z_1}{D_v} = 1.36 > 1.0$, and $\frac{Z_2}{D_v} = 1.82 > 0.5$, which indicates that the setup for vane shear tests in the present work strictly fulfilled the criteria established for satisfactory measurements with the vane method[62, 98].

The cylindrical mould used in the mini-slump test in the present work was made from PVC pipe with a wall thickness of 5 mm. The inner diameter and height of the mould were both 79 mm and the inside walls were smooth.

3.2.3 Experimental procedure

The yield stress measurement was carried out at a constant rotational speed of 0.1 rpm

[62]. The largest value recorded within 100 s was reported as the yield stress of the tested material. Previous work by Nguyen and Boger [62, 99] has suggested that this method is capable of measuring accurately and directly the true yield stress of concentrated suspensions.

It is noted that the indirect method, i.e. extrapolation using flow models based on the flow curves obtained from the viscometer tests was not considered for yield stress measurement in the work due to several reasons. First, the yield stress obtained by fitting the flow curves with rheological models (e.g. Bingham plastic, Herschel-Bulkley model) is not unique and it depends on the model assumed and the range and reliability of the experimental data available[58]. In addition, more than one model can be used to describe a given fluid with equal goodness of fit and thereby producing different yield values for the same fluid [99-101]. Consequently the yield stress from the flow models is only a relative value rather than a unique material property. Considering the final profile of the viscoplastic fluid is mostly influenced by the yield stress, it is not advisable to employ the flow models method for yield stress determination as it may increase uncertainties of the yield values.

The plastic viscosity was given by the slope of the steady state flow curve which was obtained by the CR mode (Controlled Rate) in RheoWin software from Thermo HAAKE. Each steady state flow curve was composed of 100 data points, linearly distributed within

a shear rate range from 0 to 40 s^{-1}. More precisely, the range of shear rate (from 0 to 40 s^{-1}) was evenly divided with 100 points. Then the shear rate of the vane increased from 0 to 40 s^{-1} stepwise and fixed at each shear rate point long enough that the measured shear stress remained unchanged, and then recorded. The 100 shear rate points and their corresponding unchanged shear stress composed the steady state flow curve. Since the data point in the steady state flow curve was measured at its equilibrium, the result has no time effect. Hence the steady state measurement has the highest reproducibility.

There is no standard experimental procedure for the mini-slump test using a cylindrical mould. In the present case, paste samples were poured into the cylindrical mould to overfill it. Then a spatula was used to smooth the top surface, and care was taken to lift the mould vertically, slowly and evenly. As the top surface of slumped material was usually not even, the middle point of the top surface was taken as the reference point to measure the slump. The slump height of each sample was measured four times and the mean value was reported as the final slump. The diameter of the slumped sample was measured twice in two perpendicular directions and the mean value was reported as the spread. Both slump and spread were measured to the nearest 0.02 mm with a vernier calliper. Density and moisture content were also measured at the time of testing.

To reduce the time effect, yield stress measurement and mini-slump test were conducted at virtually the same time.

3.3 Simulation

3.3.1 Numerical model

The computational fluid dynamics (CFD) software package - ANSYS FLUENT- was used to perform the simulations in this work. It is a commercially available CFD code and uses the Finite-volume method (FVM) to solve the governing equations for a fluid.

3.3.1.1 Continuity and momentum equations for incompressible flow

For the mini-slump test, the fluid (paste in this work) is assumed to be incompressible. Thus the continuity and momentum equations can be simplified as:

$$\nabla \cdot \vec{v} = 0 \tag{2}$$

$$\rho \frac{\partial \vec{v}}{\partial t} + \rho \nabla \cdot (\vec{v} \cdot \vec{v}) = -\nabla p + \nabla \cdot \bar{\bar{\tau}} + \rho \vec{g} \tag{3}$$

where $\vec{v}$ is the velocity field, p is the static pressure, ρ is the density of fluid. $\vec{g}$ is the gravitational acceleration and $\bar{\bar{\tau}}$ is the stress tensor, which is given by:

$$\bar{\bar{\tau}} = \mu(\nabla \vec{v} + \nabla \vec{v}^T) \tag{4}$$

where μ is the local viscosity of fluid.

3.3.1.2 Volume of Fluid model in ANSYSF LUENT

The volume of fluid (VOF) model is a free surface tracking technique applied to a fixed Eulerian mesh [77]. In the VOF model in ANSYS FLUENT, a single set of momentum equations is shared by two or more immiscible fluids, and the volume fraction of each of

the fluids is tracked throughout the domain [102]. If the volume fraction of the q^{th} fluid in a cell is donated as α_q, three conditions are then possible:

- $\alpha_q = 0$: The cell is empty with respect to the q^{th} fluid.
- $0 < \alpha_q < 1$: Interface between the q^{th} fluid and one or more other fluids exists in the cell
- $\alpha_q = 1$: The cell is full of the q^{th} fluid.

To track the interface(s) between the phases, the transport equation for the volume fraction of one (or more) of the phases needs to be solved. For the q^{th} phase, without mass transfer and assuming that the fluid is incompressible, this volume fraction equation can be simplified as follows:

$$\frac{\partial \alpha_q}{\partial t} + \nabla \cdot \left(\alpha_q \boldsymbol{v_q}\right) = 0 \tag{5}$$

where $\boldsymbol{v_q}$ is the velocity vector field for the q^{th} phase.

The fields for all properties in a cell are volume-averaged based on the volume fraction of each phase. For instance, in a two-phase system, if phase 1 is the primary phase, the density in each cell is given by:

$$\rho = \alpha_2 \rho_2 + (1 - \alpha_2)\rho_1 \tag{6}$$

where α_2 is the volume fraction of phase 2, ρ_1 and ρ_2 are the densities for phase 1 and phase 2 respectively.

The viscosity in this case is computed in this manner as well.

An explicit formulation with a geometric reconstruction interpolation scheme was used to solve the volume fraction equation in this work. A detailed discussion of the geometric reconstruction scheme can be found elsewhere [103]. The Pressure-Implicit with Splitting of Operators (PISO) pressure-velocity coupling scheme was employed for the transient flow simulations.

3.3.1.3 Mesh layering technique in ANSYS FLUENT

The dynamic layering technique in ANSYS FLUENT is used to add or remove layers of cells adjacent to a moving boundary in specific mesh zones (hexahedra or wedges in 3D, or quadrilaterals in 2D) [104]. A schematic of this dynamic layering is shown in **Figure 1**.

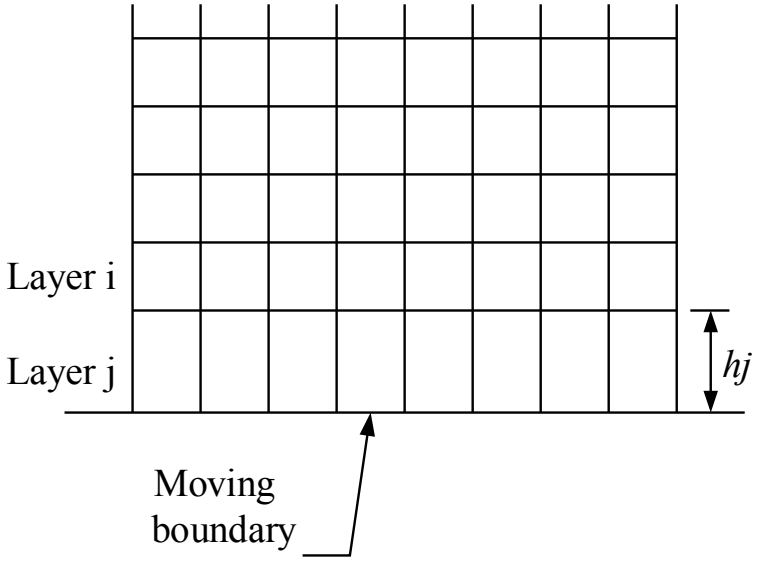

Figure 1 Dynamic layering in ANSYS FLUENT.

If the height of layer j (h_j) is increasing, layer j will not be split until

$$h_j > (1 + f_s)h_{ideal} \quad (7)$$

where f_s is the layer split factor, h_{ideal} is the ideal cell height specified for the moving boundary.

If the condition in Eq.(7) is met, layer j will be split into two layers: one is of constant height h_{ideal} adjacent to layer i and the other has a height of $(h_j - h_{ideal})$, adjoining to the moving boundary.

If the height of layer j (h_j) is reducing, layer j will be merged with layer i when the following inequality is satisfied:

$$h_j < f_c h_{ideal} \quad (8)$$

where f_c is the layer collapse factor.

A DEFINE macro in ANSYS FLUENT- DEFINE_CG_MOTION - was used to realize the movement of the mould. More detailed information can be found elsewhere [105].

3.3.1.4 Bingham model implemented in ANSYS FLUENT

The paste made up of kaolin clay and water was treated as a Bingham fluid. A Bingham fluid is defined as a viscoplastic material that behaves as a rigid body when the shear stress is lower than a threshold value, but flows as a viscous fluid when the shear stress exceeds the threshold, which is typically referred to as yield stress [18].

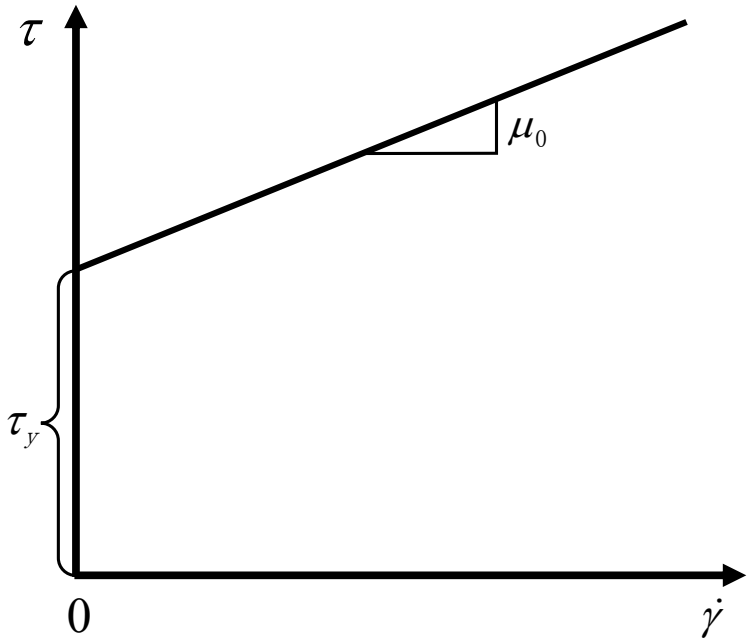

Figure 2 Shear stress as a function of shear rate for ideal Bingham model.

For the ideal Bingham model (**Figure 2**), the viscosity is given by:

$$\mu = \begin{cases} \mu_0 + \frac{\tau_y}{\dot{\gamma}}, & \tau \geq \tau_y \\ \infty, & \tau < \tau_y \end{cases} \tag{9}$$

where μ_0 is the plastic viscosity, τ_y is the yield stress of Bingham fluid, and $\dot{\gamma}$ is the shear rate.

Numerically it is impossible to model Eq.(9) rigorously due to the discontinuity of viscosity at $\dot{\gamma} = 0$. Successful efforts have been made to overcome this problem [106-108]. In ANSYS FLUENT, to guarantee appropriate continuity properties in the viscosity curve, the Bingham law for viscosity is implemented with the following form [104]:

$$\mu = \begin{cases} \mu_0 + \frac{\tau_y}{\dot{\gamma}}, & \dot{\gamma} \geq \dot{\gamma}_c \\ \mu_0 + \frac{\tau_y(2-\dot{\gamma}/\dot{\gamma}_c)}{\dot{\gamma}_c}, & \dot{\gamma} < \dot{\gamma}_c \end{cases} \tag{10}$$

where $\dot{\gamma}_c$ is the critical shear rate, beyond which the fluid flows with a plastic viscosity

of μ_0 while if the shear rates are less than $\dot{\gamma}_c$, the fluid acts like a rigid material as the viscosity is very high. The variation of shear stress (τ) with shear rate ($\dot{\gamma}$) according to the Bingham model implemented in ANSYS FLUENT is demonstrated in **Figure 3**.

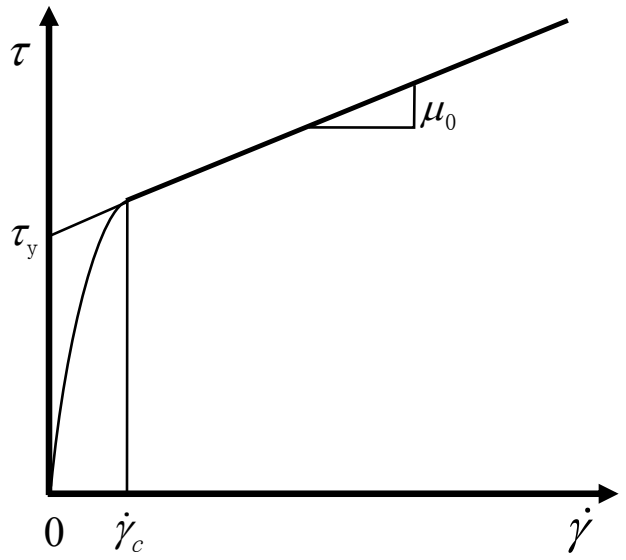

Figure 3 Shear stress as a function of shear rate for numerical Bingham model implemented in ANSYS FLUENT.

To replicate the behaviour of an ideal Bingham fluid, the critical shear rate ($\dot{\gamma}_c$) should be as small as possible, as shown in **Figure 3**. However, an extremely small $\dot{\gamma}_c$ will result in an excessively rapid increase of viscosity in the region where $\dot{\gamma} < \dot{\gamma}_c$, thereby leading to numerical instability. It is found that the appropriate critical shear rate ($\dot{\gamma}_c$) depends crucially on the yield stress τ_y. For pastes with yield stresses ranging from approximately 18 Pa to 60 Pa, it was ascertained that a value of 0.005 s^{-1} for $\dot{\gamma}_c$, which is employed throughout the present work, is small enough to reproduce the flow behaviour of ideal Bingham fluid, but sufficiently large to guarantee numerical stability of the simulation.

3.3.2 Validation

To test the validity of the Bingham model implemented in ANSYS FLUENT and the appropriateness of the critical shear rate used in this work, the velocity profiles of Bingham fluid in a horizontal circular pipe from both an analytical solution and numerical simulation were compared.

3.3.2.1 Analytical solution for Bingham fluid flow in a horizontal circular pipe

Figure 4 shows the schematic of Bingham fluid flow in a horizontal circular pipe of diameter R and infinite length. Assume that the fluid is incompressible and the flow is laminar. The analytical solution for the velocity distribution of the fully developed Bingham fluid flow can be described by a piecewise function [109, 110]:

$$u(r) = \begin{cases} -\frac{1}{\mu_0}\left[\frac{\triangle p}{4l}\left(r - \frac{2l\tau_y}{\triangle p}\right)^2 + \tau_y R - \frac{\triangle p R^2}{4l} - \frac{l{\tau_y}^2}{\triangle p}\right], & r \in [S, R] \\ -\frac{1}{\mu_0}\left(\tau_y R - \frac{\triangle p R^2}{4l} - \frac{l{\tau_y}^2}{\triangle p}\right), & r \in [0, S] \end{cases} \quad (11)$$

where $u(r)$ is the axial velocity of fluid in pipe, Δp is the axial pressure difference between cross sections AB and CD of the fluid with a length of l in the pipe, r is the radial coordinate, S is the radius of the fluid "plug" inside which the fluid flows as a whole.

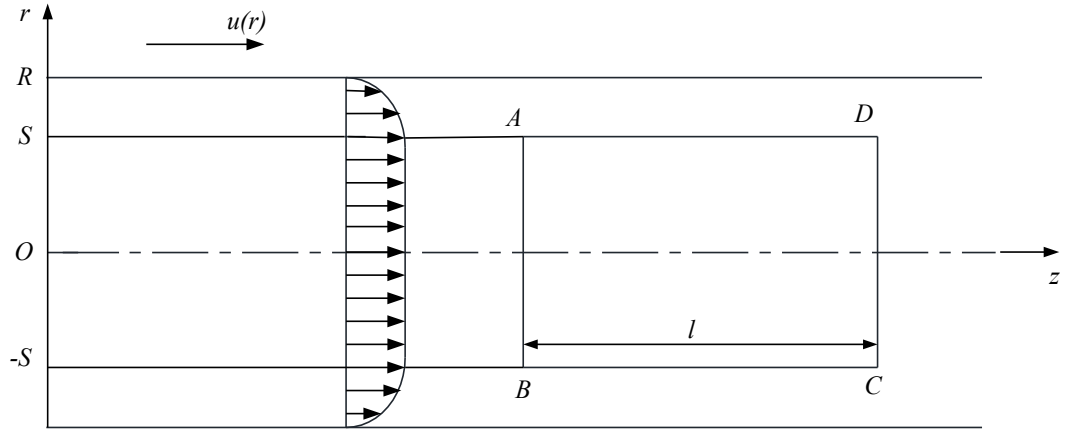

Figure 4 Fully developed flow of Bingham fluid in a horizontal circular pipe.

With the postulate that inlet velocity is u_0 and $k = \frac{\Delta p}{l}$, an altered form of the Buckingham-Reiner equation can be yielded:

$$3R^4k^4 - 8R^3\tau_y k^3 - 24\mu_0 u_0 R^2 k^3 + 16{\tau_y}^4 = 0 \qquad (12)$$

If all parameters other than k are given, k can be obtained from Eq.(12). Then the velocity distribution for a specified Bingham fluid can be obtained from Eq.(11).

3.3.2.2 Comparison of velocity profiles of Bingham fluid flow in pipe between analytical solution and numerical result

To obtain the numerical solution of velocity distribution using ANSYS FLUENT, a two-dimensional pipe with a length of 2 m and a diameter of 0.1 m was used. Since the pipe flow is axisymmetric, only half of the pipe was considered in the simulation. Quadrangles were used to discretize the computational domain to form a mesh of 400×50 (length × radius). No-slip wall and axis boundary conditions were applied to the pipe wall and centreline of the pipe respectively. The Bingham fluid flowed into the inlet of the pipe at

a constant velocity of 0.1 m/s, and past the entrance region the flow was fully developed. Finally, the fluid exited into the ambient atmosphere which was at a pressure of 1 atm. Physical properties of Sample 6 in **Table 1** were used in this simulation. **Figure 5** shows the geometry and boundary conditions in the simulation for the two-dimensional pipe flow.

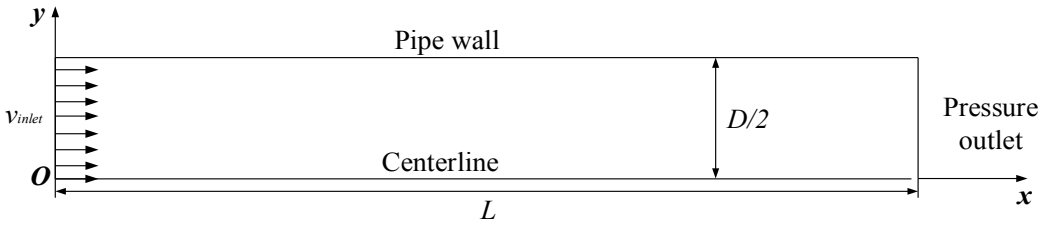

Figure 5 Geometry and boundary sets for 2D pipe flow.

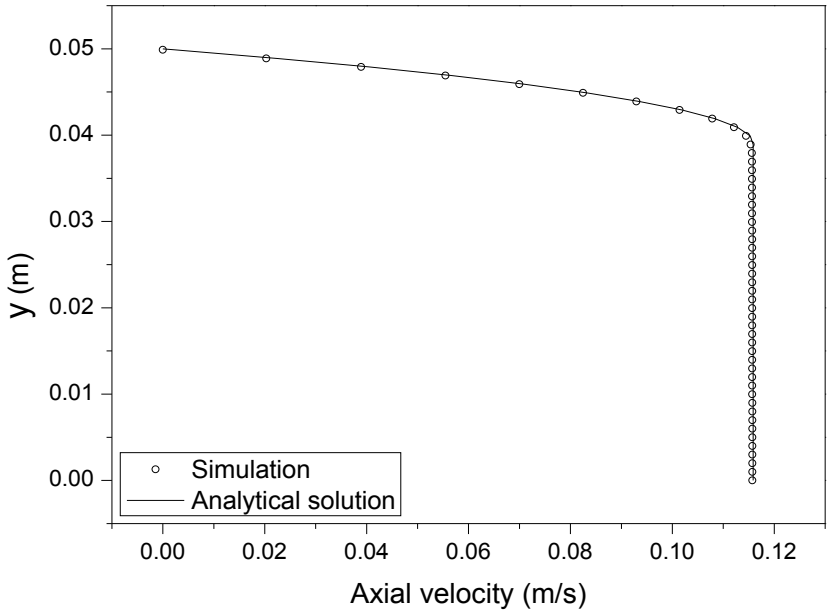

Figure 6 Velocity profiles from pipe wall to centreline.

Figure 6 shows the fully-developed velocity profile from analytical solution and the velocity profile at the outlet of the pipe from numerical simulation. The excellent coincidence indicates that the numerical model for Bingham fluid in ANSYS FLUENT

is implemented correctly. Furthermore, it suggests that the critical shear rate value of 0.005 s^{-1} utilized in this case is reasonable.

3.3.3 Numerical simulation of mini-slump test

The mini-slump test simulation considers the transient tracking of a paste-air interface in the geometry shown in **Figure 7**. A 2D geometry can be used on account of the axial symmetry of the problem. The computational mesh consists of $0.5\text{mm} \times 0.5\text{mm}$ quadrangular cells. As shown in **Figure 7**, the domain comprises three regions: paste region, mould region and air region. The dimensions of each region and boundary conditions are also displayed in **Figure 7**.

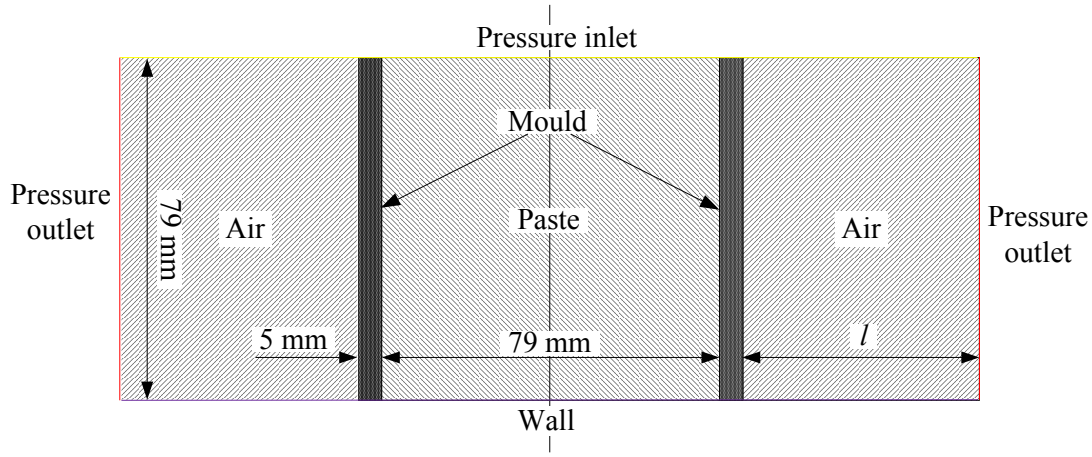

Figure 7 Geometry and boundary sets for mini-slump test. l varies according to the spreads of different samples to reduce the 'useless' computational domain.

For the laboratory mini-slump test, the paste material will stop deforming completely if we allow enough time (at least we cannot observe movement in a practical amount of time). However, in the numerical simulation the fluid will not completely stop because

the flow curve of the numerical Bingham model implemented in ANSYS FLUENT passes through the origin of coordinates, as shown in **Figure 3**. More precisely, the Bingham fluid in this simulation will keep flowing, although at a very low speed, as long as the driving force, i.e. gravity in this case, exists. Therefore it is critical to determine when to stop the simulation of the mini-slump test.

In the present work, the termination criterion was based on both the slumping speed and the spreading speed of the paste. The slumping speed is the sinking speed of the middle point of the top surface of slumped material and the spreading speed is the radial speed of the paste. Tregger et al. [91] reported that a human observer detected no more movement from the spread if the spreading speed was less than 0.3mm/s. In the present work it was found that the slumping and spread speeds became relatively stable when they were less than 0.1 mm/s. Accordingly, the calculation was not ceased until both the slumping and the spreading speeds were less than 0.1 mm/s.

The following is the chronology of events modelled in this simulation:

- At time zero, the paste region was full of paste and surrounded by the mould, while the rest of the domain was filled with air. Both fluids and mould were assumed to be at rest. To model the lifting process of the mould, the dynamic layering technique was applied in this simulation. When the simulation started, the lifting velocity of the mould was suddenly increased from 0 to a designated value. After

the separation of the mould from the paste, the mould lifting velocity returned to 0.

- Only once both the slumping and spreading speeds of the paste were below 0.1 mm/s was the iteration stopped.

The mini-slump test simulation was carried out with six paste samples and the physical properties used in the simulation are summarized in **Table 1**.

Table 1 Physical properties of the paste samples from corresponding laboratory tests.

Sample	Yield stress(τ_y, Pa)	Viscosity(μ_0, Pa·s)	Density(ρ, kg/m^3)
1	18.61	0.32	1315.0
2	23.12	0.36	1321.3
3	33.28	0.40	1342.6
4	41.10	0.44	1353.6
5	50.10	0.64	1367.4
6	56.10	0.73	1377.2

3.4 Results and discussion

3.4.1 The influence of mould lifting velocity on mini-slump test results

In order to analyse the inertial effects[1] in the mini-slump test, we used the inertial stress[2] – yield stress ratio as an indicator to evaluate the relative importance of inertial effects and yield stress in mini-slump test [95]. The typical inertial stress (I_{av}) is given by:

$$I_{av} = \max(ISL_{av}, ISP_{av}) \tag{13}$$

$$ISL_{av} = \rho(\frac{SL_f}{T_f})^2 \tag{14}$$

$$ISP_{av} = \rho(\frac{SP_f - D_0}{2T_f})^2 \tag{15}$$

where ISL_{av} and ISP_{av} (Pa) are the typical inertial stresses with respect to the vertical and radial directions respectively; SL_f and SP_f (m) are the final slump and spread respectively; D_0 (m) is the diameter of the cylindrical mould; T_f (s) is the flow time required to reach the final equilibrium state, and ρ (kg/m^3) is the density of the paste used in the mini-slump test. The typical inertial stress – yield stress ratio R_{IY} is defined as:

$$R_{IY} = \frac{I_{av}}{\tau_y} \tag{16}$$

Figure 8 summarizes the spreads versus time in mini-slump tests with different lifting velocities while the flow time (T_f) and R_{IY} of each lifting velocity are displayed in **Figure 9**. As shown in **Figure 8**, the final spread increases from (a) to (d) with the increase of mould lifting velocity. An increased mould lifting velocity introduces stronger inertial effects to the mini-slump test (see R_{IY} in **Figure 9**), increasing the extent of spread.

[1] The term "inertial effects" used in the present work is not identical to the inertia of an object which is solely quantified by its mass. Inertial effects here are the resultant effects caused by inertia. For instance, if the kinetic energy (per unit volume) of the fluid is higher, then it will be harder to stop the fluid (i.e. more negative work by resistance is required to stop the fluid) due to its inertia, which means that the inertial effects are more significant. Therefore, inertial effects are positively correlated to both mass and the magnitude of velocity.

[2] Typically "$\rho v^2/l_0$" (l_0 is the characteristic length) which is referred to as the inertial force (per unit volume) is used to get the rough orders of magnitude of the inertial term in momentum equations [111]. As "ρv^2" has a similar expression to inertial force and the same unit of stress (Pa), it is named as inertial stress, which can be construed as the kinetic energy per unit volume of a flow in terms of energy.

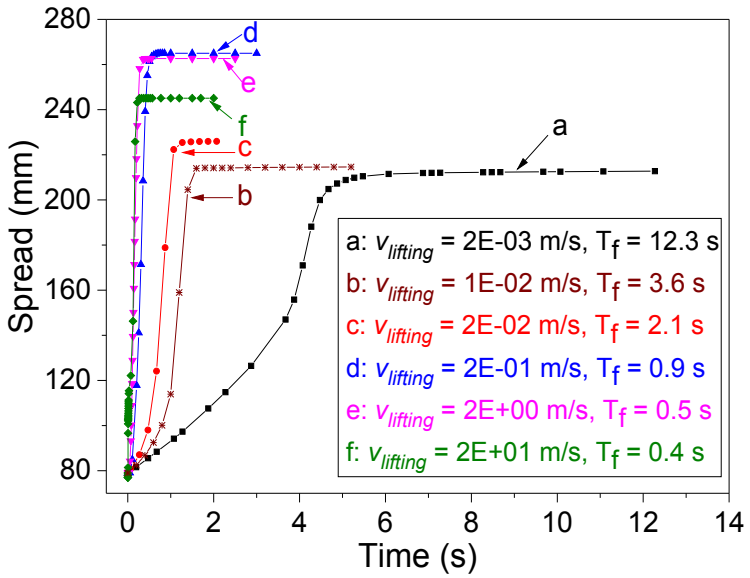

Figure 8 Evolution of spread over time for Sample 1 in the simulations with different lifting velocity of mould. Sample 1: τ_y = 18.61 Pa, μ_0 = 0.32 Pa·s, ρ = 1315.0 kg/m^3.

However, when the lifting velocity of the mould exceeded a certain value, the final spread decreased with an increase of mould lifting velocity (see (d), (e) and (f) in **Figure 8**). To understand this behaviour, a series of pictures from two simulations with mould lifting velocities of 20 m/s and 0.01 m/s are displayed in **Figure 10** to offer a contrast. As shown in **Figure 10**, the entire slumping process of the paste in the mini-slump test simulation with higher mould lifting velocity (a) differs significantly from that with lower lifting velocity (b) due to different "end effects" [111]. The slumping process of paste in **Figure 10** (b) is relatively smooth as the "end effects" are not significant. From **Figure 10** (a) it can be seen that the paste close to the inside wall of the mould lifted together with the mould due to adhesive effects. After that the lifted paste fell from a relatively higher position and "cut" the paste into two parts: an annulus and a disc. It is obvious that the

"cut" phenomenon induced by significant end effects that occur with the higher lifting velocity of the mould hindered the paste from flowing smoothly.

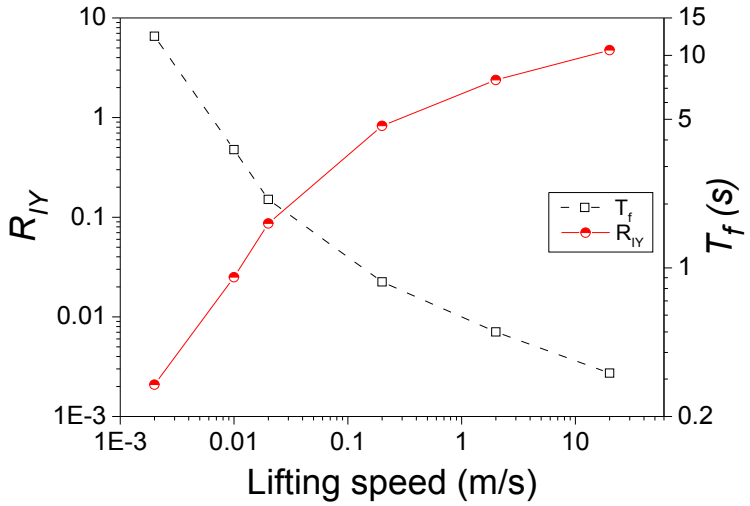

Figure 9 Inertial stress-yield stress ratio R_{IY}* and flow time (T_f, s) vs lifting velocity of mould from simulations for Sample 1. Sample 1: τ_y = 18.61 Pa, μ_0 = 0.32 Pa·s, ρ = 1315.0 kg/m^3. *Please note that the top surface of slumped paste would be "destroyed" by splashes at high mould lifting velocities as shown in **Figure 10**. Therefore, it is impossible to obtain the slump in this situation. To calculate and compare R_{IY} of simulations with the range of lifting velocities listed in **Figure 8**, the typical inertial stress (I_{av}) for the calculation of R_{IY} in **Figure 9** was evaluated by $I_{av} = ISP_{av}$.

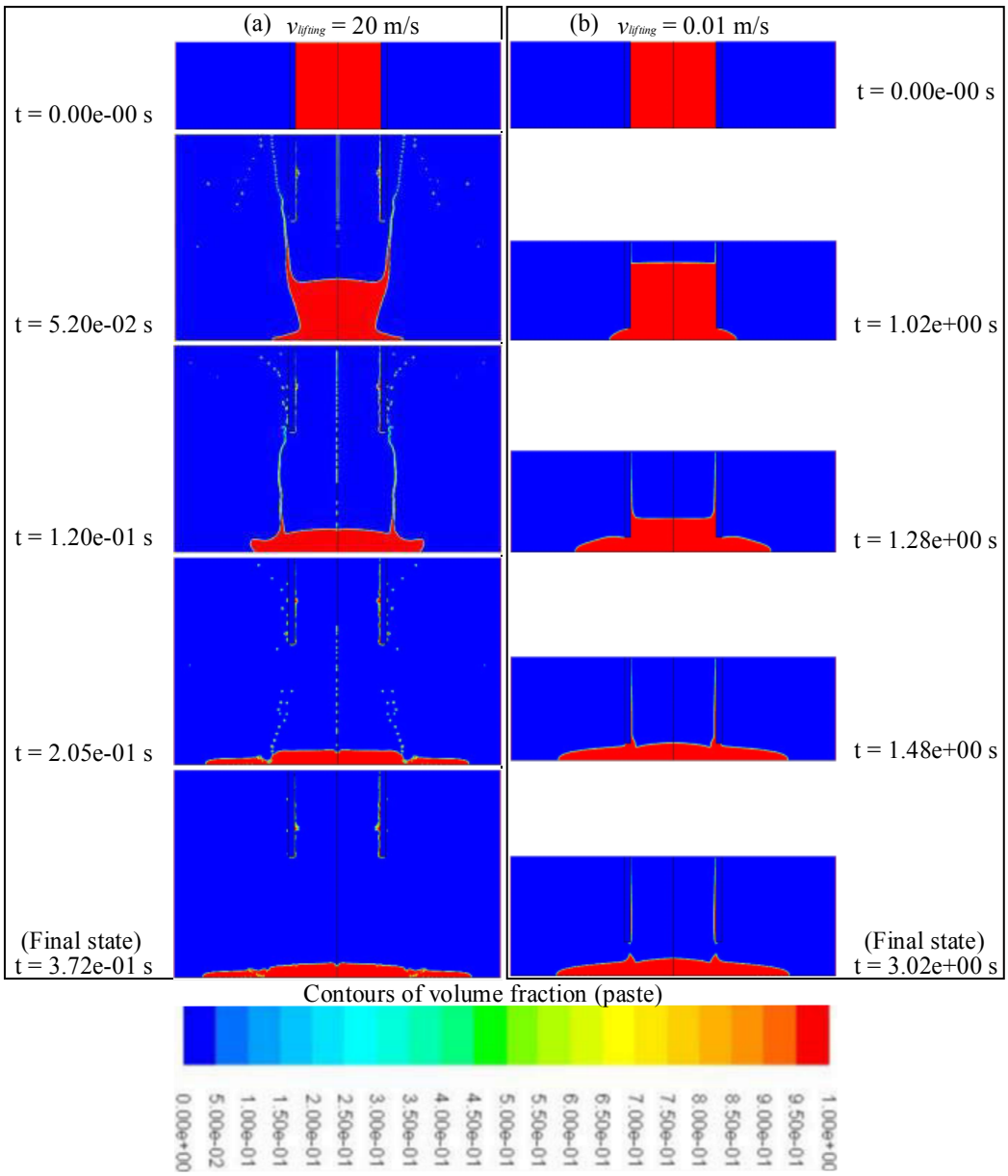

Figure 10 Comparison between simulations with different mould lifting velocities. The physical properties of Sample 1 listed in **Table 1** were used in simulation (a) and (b). Sample 1: τ_y = 18.61 Pa, μ_0 = 0.32 Pa·s, ρ = 1315.0 kg/m^3.

As an indication of the influence of inertial effects on the mini-slump test, R_{IY} decreases dramatically while the slope of R_{IY} versus lifting velocity curve increases with the reduction of mould lifting velocity, as can be seen from **Figure 9**. This indicates that

decreasing the lifting velocity can significantly reduce the influence of inertia. Furthermore, slight changes of lifting velocity at the lower velocity range results in striking variations of the inertial effects. Consequently, to reduce the influence of inertial effects to a negligible level in the mini-slump test, the mould should be lifted slowly. Moreover, to enable the results from the same series of mini-slump tests to be comparable, efforts should be made to ensure the mould lifting speed is as similar as possible.

Additionally, it is clear from **Figure 9** that the flow time (T_f) to the final equilibrium state decreases dramatically while the inertial stress-yield stress ratio (R_{IY}) increases substantially with increasing mould lifting velocity. Since R_{IY} is an indicator of the influence of inertial effects, it can be concluded that generally the smaller flow time (T_f) signifies stronger inertial effects for the mini-slump test.

Evolution of spread, rather than evolution of slump height, was chosen for presentation here because for the case of rapid lifting velocity the top surface of the slumped material was significantly distorted by 'splashing' material and it was thus impossible to discern the final height accurately.

3.4.2 The influence of yield stress and viscosity on mini-slump test

To investigate the influence of yield stress and viscosity on the mini-slump test, simulations in two scenarios, i.e. with mould lifting velocity at 0.01 m/s (case 1-3) and

instantly disappearing (designated as 'no mould') (case 1'-3'), in which the yield stress and viscosity were varied were conducted. The final profiles for the simulations are shown in **Figure 11**. **Figure 12** summarises the variation from the base cases (Case 1 and Case 1' for simulations with mould lifting process and 'no mould', respectively) of spread, slump, flow time and R_{IY}. The values of R_{IY} are presented in **Figure 13**. The evolution of slump and spread over time for the six cases in the two scenarios are demonstrated in **Figure 14** in which the flow time for each case is indicated as well by the dashed line.

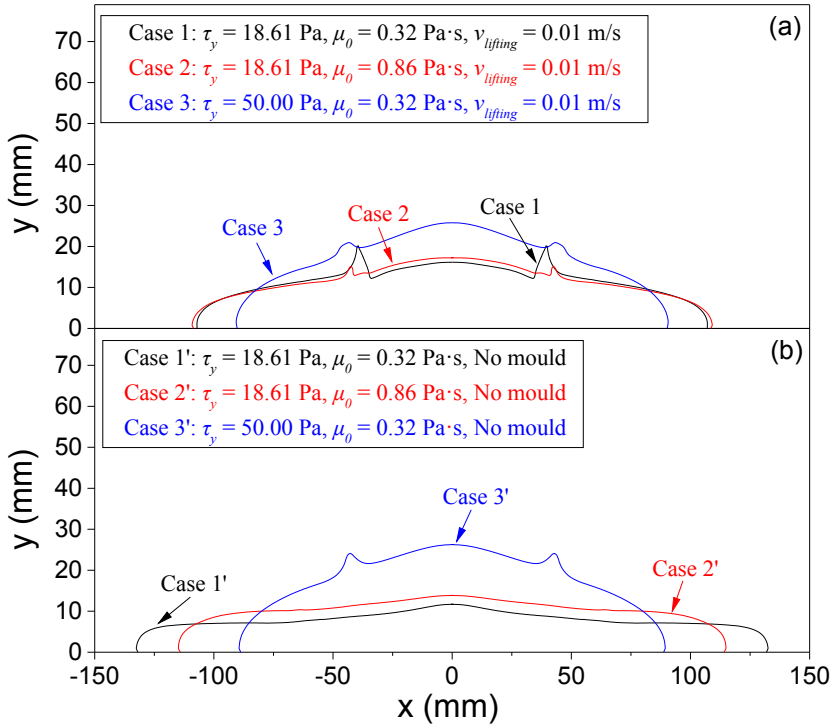

Figure 11 Final profiles from simulations with mould lifting velocity at 0.01m/s (a) and 'no mould' simulations (b). The input parameters employed in the six cases are listed in **Table 2**.

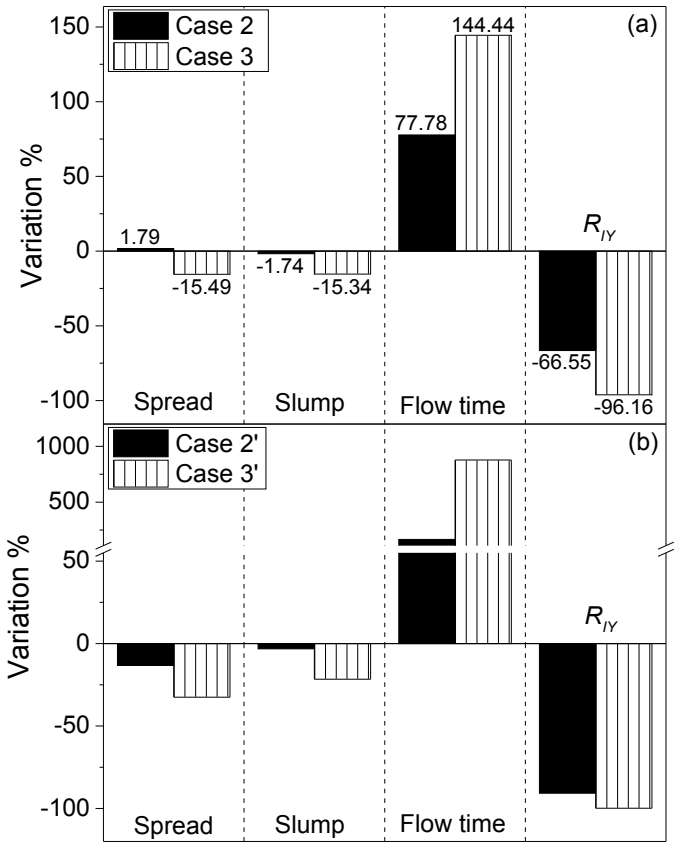

Figure 12 Variations of results from mini-slump test simulations with the increase of yield stress and viscosity in two scenarios: the mould lifting velocity is 0.01 m/s (a) and the mould disappears instantly (also referred to as 'no mould') (b). The input parameters employed in the six cases are listed in **Table 2**.

It can be concluded from the comparison between Case 1 and Case 2, Case 1' and Case 2' that generally higher viscosity leads to less spread and slump, as shown in **Figure 11**. With the increase of viscosity from 0.32 Pa·s to 0.86 Pa·s, the flow time increases as shown in **Figure 14**, and the inertial stress – yield stress ratio R_{IY} reduces as shown in **Figure 12**, leading to less slump and spread.

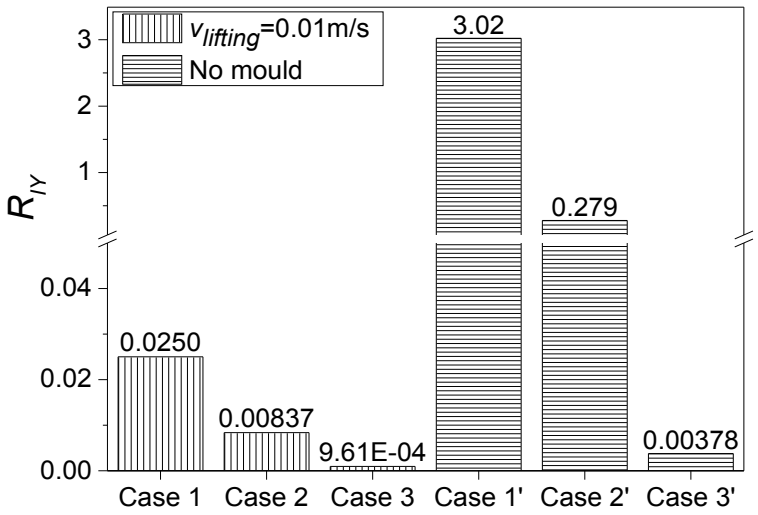

Figure 13 The values of R_{IY} for Case 1-3 and Case 1'-3' in two scenarios: mould lifting velocity $v_{lifting}$= 0.01 m/s and 'no mould'. The input parameters employed in the six cases are listed in **Table 2**.

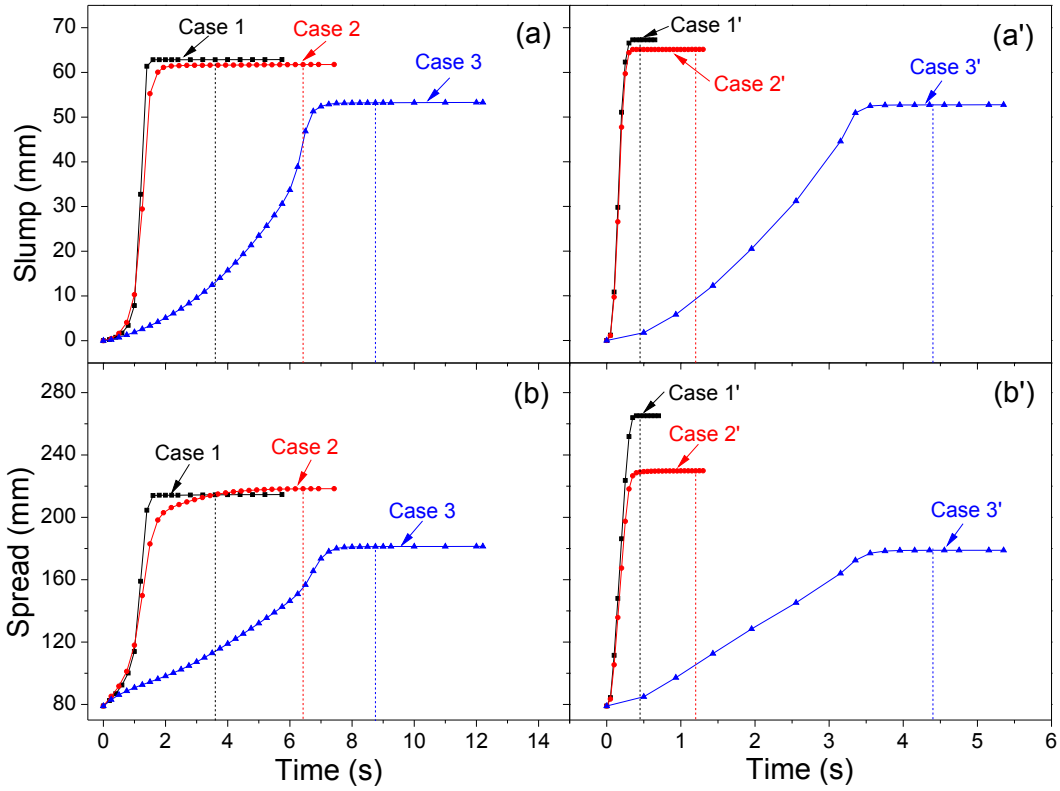

Figure 14 Evolution of slump and spread over time for six different cases (Case 1-3 and Case 1'-3') listed in **Table 2**.

Table 2 Parameters used in mini-slump test simulations for Case 1-3 and Case 1'-3'.

Cases	Yield stress (τ_y, Pa)	Viscosity (μ_0, Pa·s)	Density (ρ, kg/m^3)	Scenarios
Case 1	18.61	0.32	1315.0	$v_{lifting}$ =0.01 m/s
Case 2	18.61	0.86	1315.0	$v_{lifting}$ =0.01 m/s
Case 3	50.00	0.32	1315.0	$v_{lifting}$ =0.01 m/s
Case 1'	18.61	0.32	1315.0	'No mould'
Case 2'	18.61	0.86	1315.0	'No mould'
Case 3'	50.00	0.32	1315.0	'No mould'

Although the viscosity increases by 169% (from 0.32 Pa·s to 0.86 Pa·s), the difference in final profiles between Case 1 and Case 2 is not significant as shown in **Figure 11** (a). However, from **Figure 11** (b) the difference in final profiles between Case 1' and Case 2' is very distinct, i.e. the spread decreases by 13.31% and the slump reduces by 3.20%, as shown in **Figure 12** (b). In other words, the difference in the final profiles caused by the same variation of viscosity can be different in varied scenarios. As shown in **Figure 13**, values of R_{IY}, which indicate the importance of inertial effects for mini-slump tests with mould lifting velocity at 0.01 m/s (Cases 1-2) are much lower than those for the tests in which the mould disappeared instantly (Cases 1'-2'). Therefore it can be inferred that the same variation of viscosity tends to yield a greater difference in the slumps and spreads in the scenarios where the inertial effects are more significant.

As can be seen in **Figure 11**, the final profiles between Case 1 and Case 3, Case 1' and Case 3' are very different. A decrease of more than 15% for both spread and slump is caused by the increase in yield stress from 18.61 Pa (Case1) to 50.00 Pa (Case 3), as

shown in **Figure 12** (a). The decrease of spread and slump between Case 1' and Case 3' are even more dramatic, with a reduction of 32.53% and 21.63% for spread and slump respectively as shown in **Figure 12** (b). With the increase of yield stress, the slopes of evolution curves (spread and slump) of Case 3 and Case 3' are more gentle than the other curves in **Figure 14**, which means the average flow speed in Case 3 and Case 3' are relatively lower than the other simulations, and hence more flow time is required as shown in **Figure 14**. It is apparent that spread, slump, flow time and R_{IY} are much more affected by the yield stress of the paste, compared to viscosity. Flow time is strongly influenced by both yield stress and viscosity. Consequently, it indicates that it is irrational to determine the viscosity of the paste only by the flow time in the mini-slump test. This may be one of the reasons accounting for the poor correlations of T300 and T350 (which are the flow time required to reach the spread of 300 mm and 350 mm respectively) with plastic viscosity reported by [91, 112].

3.4.3 The influence of mould lifting velocity on mini-slump test with materials of different viscosity and yield stress

The results discussed in this section address the effect of mould lifting velocity on the resulting slumped geometry for materials with different rheological properties (yield stress and viscosity). Simulations were conducted on two materials from **Table 1**, i.e. Sample 1 and Sample 5. Two different lifting velocities were used, 0.002 m/s and 0.01

m/s; in addition, a simulation was done for the case where the mould was assumed to instantly disappear (also referred to as 'no mould'). The results are summarised in **Figure 15**, which shows that the final profiles of A1, A2 and A3 (all using Sample 1) are quite distinct, whereas the differences in final profiles of B1, B2 and B3 (all using Sample 5) are rather subtle. This indicates that the influence of the mould lifting velocity on the spread and slump is more important for paste with a lower yield stress and viscosity (Sample 1) than a higher yield stress and viscosity (Sample 5). The 'no mould' condition (A3) is very different from the others, giving an increase in spread of 24.6% compared with the slower lifting rate (A1).

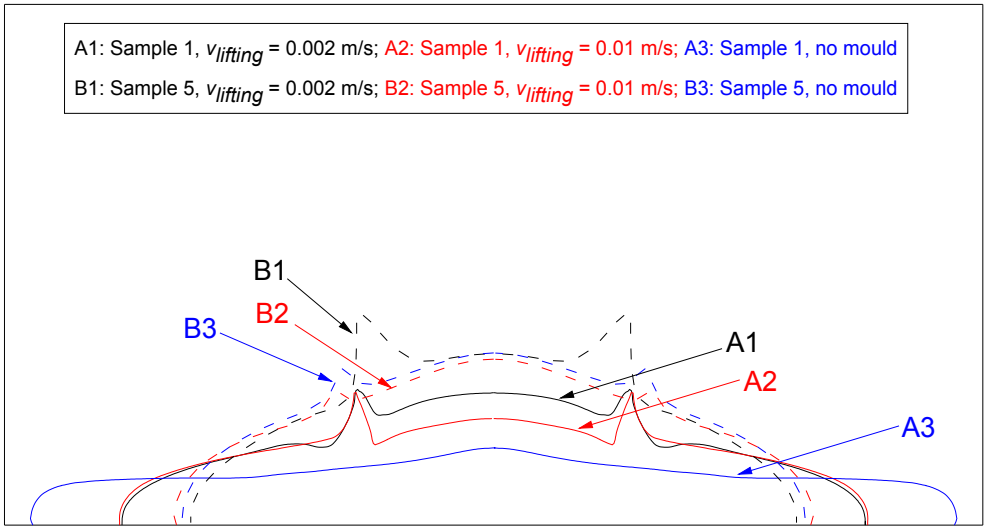

Figure 15 Final profiles for Sample 1 (A1, A2, A3) and 5 (B1, B2, B3) from simulations of three different scenarios: $v_{lifting}$ = 0.002 m/s, $v_{lifting}$ = 0.01 m/s, and 'no mould'. Sample 1: τ_y = 18.61 Pa, μ_0 = 0.32 Pa·s, ρ = 1315.0 kg/m^3; Sample 5: τ_y = 50.10 Pa, μ_0 = 0.64 Pa·s, ρ = 1367.4 kg/m^3.

Figure 16 summarises the variation of slump and spread with time for Samples 1 and 5.

It can be seen that the variations of flow time for Sample 1 are large (A1:12.2 s; A2: 3.6 s; A3:0.45 s). Moreover, compared to the flow times for Sample 5 (B1:12.4 s; B2: 10.0 s; B3:4.9 s), the flow times from corresponding simulations for Sample 1 are smaller. Furthermore, the values of R_{IY} for A1, A2 and A3 (Sample 1) and their variation are both larger than those for Sample 5 (**Figure 17**). This means that the inertial effects of paste with a lower yield stress and viscosity on the mini-slump test are more significant than for higher yield stress and viscosity. This explains the more pronounced differences of final profiles for simulations A1, A2 and A3 compared with the equivalent simulations for Sample 5.

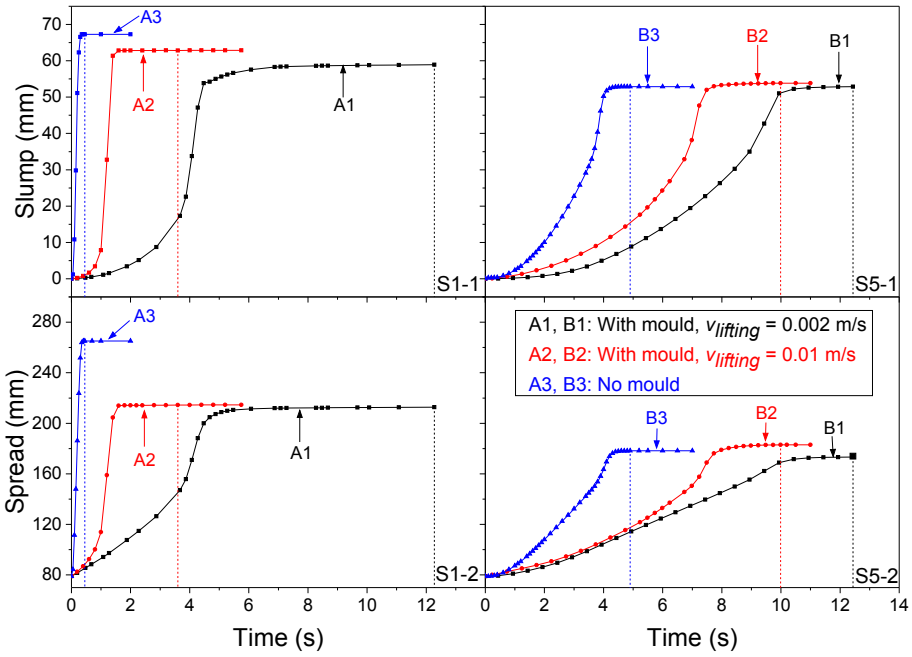

Figure 16 Evolution of slump height and radius over time for Sample 1 (panel S1-1 and S1-2) and 5 (panel S5-1 and S5-2) in different cases. Sample 1: τ_y = 18.61 Pa, μ_0 = 0.32 Pa·s, ρ = 1315.0 kg/m^3; Sample 5: τ_y = 50.10 Pa, μ_0 = 0.64 Pa·s, ρ = 1367.4 kg/m^3.

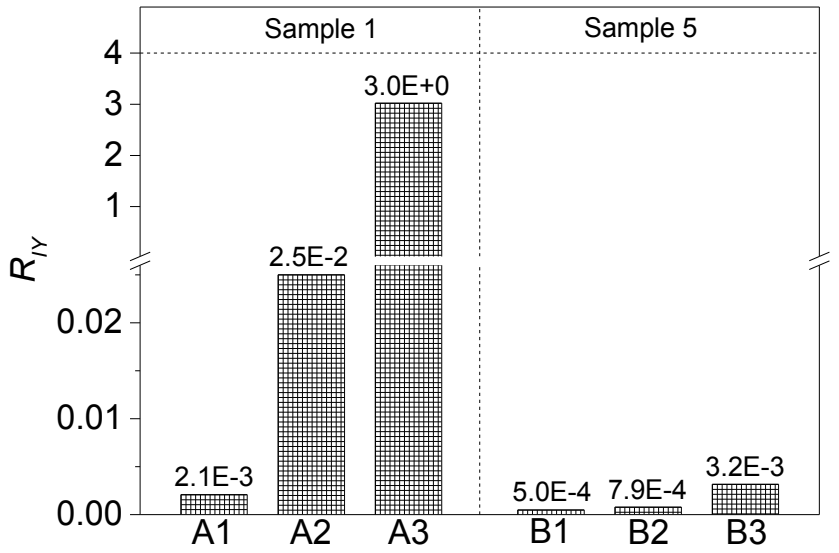

Figure 17 R_{IY} for simulations of three different scenarios ($v_{lifting}$ = 0.002 m/s for A1 and B1, $v_{lifting}$ = 0.01 m/s for A2 and B2, 'no mould' for A3 and B3) for Sample 1 and Sample 5. Sample 1: τ_y = 18.61 Pa, μ_0 = 0.32 Pa·s, ρ = 1315.0 kg/m^3; Sample 5: τ_y = 50.10 Pa, μ_0 = 0.64 Pa·s, ρ = 1367.4 kg/m^3.

It is especially notable that the final profiles from simulations with mould lifting velocities of 0.002 and 0.01 m/s for Sample 1(A1 and A2) have more or less the same spread, but their slump heights are distinctly different (**Figure 15**). This implies that measuring spread rather than slump is advisable when using the results to estimate material yield stress, particularly for materials with low yield stress and low viscosity. It deserves a mention that although the initial volume of paste is same for both A1 and A2, more paste was left on the wall of the mould of A2 than A1 due to the different mould lifting velocities as shown in **Figure 18**, which may be another reason besides the different final profiles accounting for the similarity of spreads but distinct difference in slumps between A1 and A2.

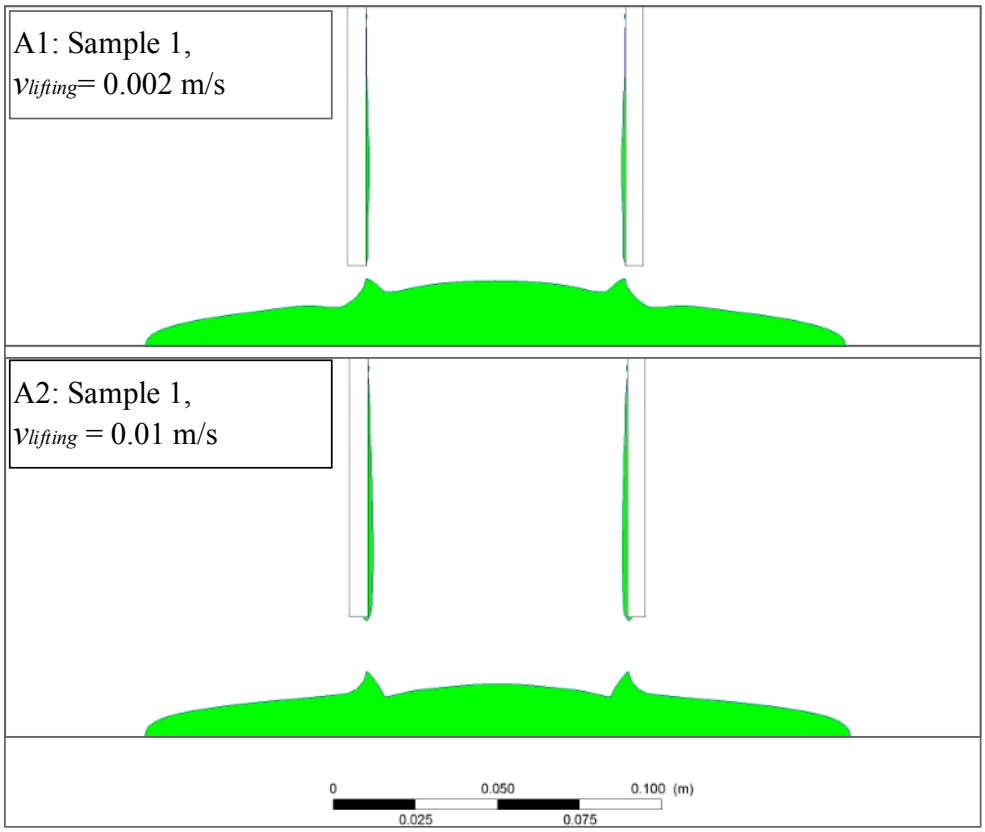

Figure 18 Results for simulations A1 ($v_{lifting}$ = 0.002 m/s) and A2 ($v_{lifting}$ = 0.01 m/s). Sample 1: τ_y = 18.61 Pa, μ_0 = 0.32 Pa·s, ρ = 1315.0 kg/m^3.

In **Figure 15**, the final profile of Sample 1 in the simulation without the mould lifting process (A3) is quite different from A1 and A2, which emphasises that the mini-slump test simulation where the mould disappears instantaneously at the beginning of the simulation is inappropriate for paste of lower yield stress and viscosity. The sudden disappearance of the mould results in a very short flow time and strong inertial effects for paste of lower yield stress and viscosity (A3 in **Figure 16** and **Figure 17**), thereby leading to larger spread and slump.

Although both simulations A3 and B3 neglected the mould lifting process, the flow time

and inertial effects for A3 and B3 differ significantly for paste with different yield stress and viscosity. As shown in **Figure 16**, the higher yield stress and viscosity enable the flow time of B3 (4.9 s) to be much longer than that of A3 (0.45 s). Moreover, the R_{IY} of B3 is much smaller than that of A3 according to **Figure 17**, which means the influence of inertial effects of the simulation for B3 without the mould lifting process is minimal. Thus the final profile of B3 is nearly the same as B1 and B2, as shown in **Figure 15**. This explains why good agreement between the results from simulation and experiment was obtained by some researchers [95, 96, 113] even though they did the simulation without the mould lifting process taken into account because they artificially increased the viscosity significantly in their simulations.

Although much less pronounced, the effect of assuming instantaneous disappearance of the mould is still evident for the higher yield stress and viscosity material. As evident from **Figure 17**, the R_{IY} of B3 is approximately 4 times as large as B2. From considerations of the inertial effects, the final slump and spread of B2 should be smaller than those of B3. However, as evident from **Figure 15**, the final slump and spread of B2 are slightly larger than those of B3. Thus we can infer that correctly accounting for the mould lifting process has some (albeit slight) potential to increase the slump and spread, which should be taken into account in the simulation.

3.4.4 Comparison between slump and spread from laboratory experiment and CFD simulation

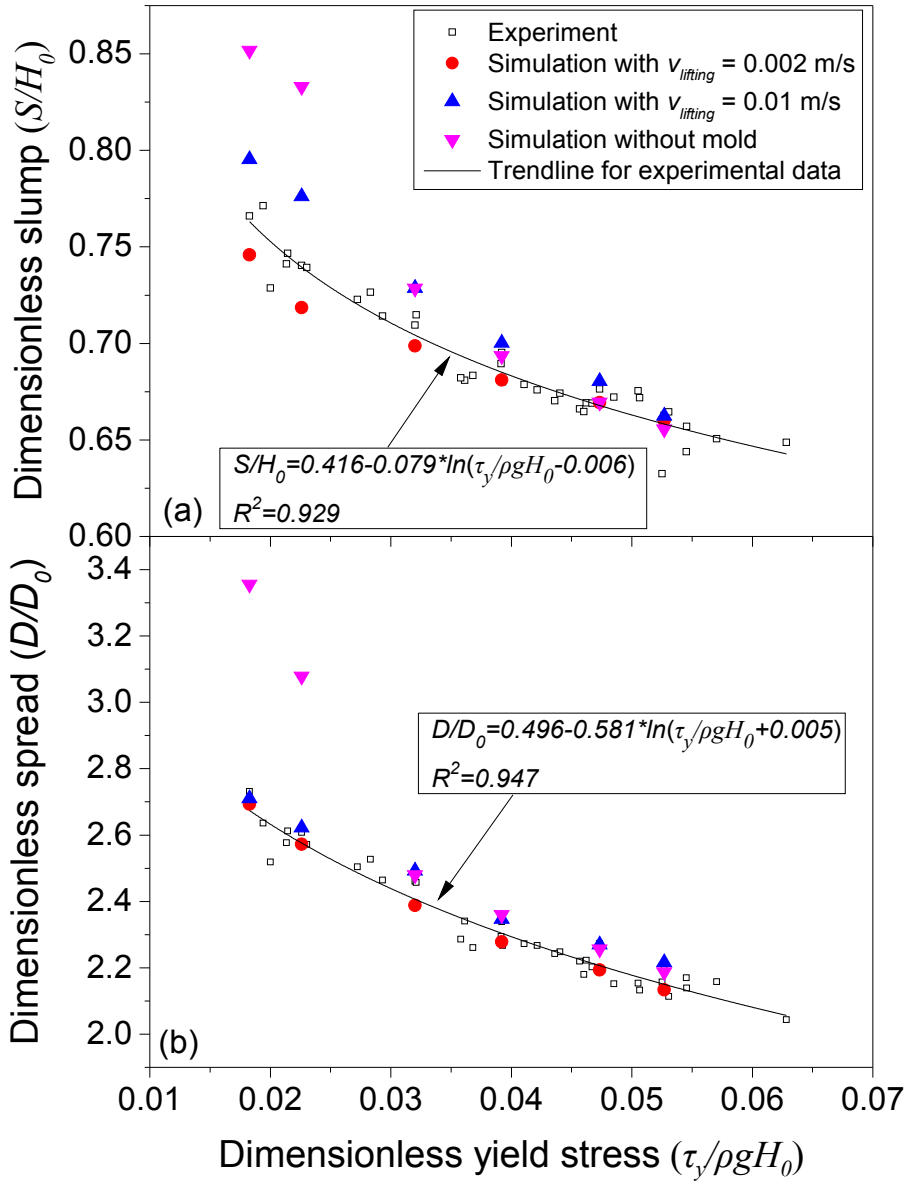

Figure 19 Comparison of slump and spread from laboratory experiment and simulations of three different scenarios: 'no mould' simulations and simulations with mould lifting velocity at 0.002 m/s and 0.01 m/s, respectively. The input parameters for simulations of Sample 1-6 are listed in **Table 1**.

Figure 19 compares the dimensionless slump (S/H_0) and dimensionless spread (D/D_0) from the experimental data with simulations using two different lifting velocities (0.002 m/s and 0.01 m/s), as well as the 'no mould' case. For $\tau_y/\rho g H_0 < 0.03$, the dimensionless slumps and spreads from simulations with instantaneous disappearance of the mould are substantially larger than those from laboratory experiments, as well as the results from the other simulations. It indicates that the 'no mould' simulation results in much stronger inertial effects for materials of lower yield stress, thus increasing the slump and spread dramatically. These results clearly indicate it is unreasonable to make the mould disappear at the initial time of the simulation for paste with low yield stress and viscosity.

To reduce the non-negligible inertial effects, some researchers increased the viscosity of paste in their simulations where the mould simply disappeared at the beginning [95, 96, 113]. This increase of viscosity can indeed enable the slump or spread to match the experimental results. However, this artificially higher viscosity used in simulation brings about at least two problems:

(1) Higher viscosity significantly increases the flow time of paste in the mini-slump test simulation (see Section 3.4.2), thereby leading to much increased computing time.

(2) Although the increased viscosity may yield good simulation results in terms of

slump and spread, it renders some other useful results from the simulation, such as flow time, completely irrelevant and certainly not comparable to those from experimental results.

Figure 20 Pictures of Sample 1 at stoppage in mini-slump test in laboratory experiment. The lifting velocity of the mould in this slump test is controlled around 0.002 m/s with special carefulness. As shown in **Table 1**, the yield stress, viscosity and density of Sample 1 are 18.61 Pa, 0.32 Pa·s and 1315.0 kg/m^3 which were derived from corresponding rheology tests.

Figure 20 shows plan and elevation views of the mini-slump test on material with a yield stress of 18.61 Pa and viscosity of 0.32 Pa·s, and **Figure 21**(b) the equivalent result from the CFD simulation; **Figure 21**(a) shows the result for a 'no mould' simulation. From **Figure 20** and **Figure 21**(b), it is apparent that the final profile from the mini-slump test simulation with a mould lifting velocity of 0.002 mm/s has a much stronger resemblance to that from laboratory experiment compared with that from the 'no mould'. This demonstrates once again that accounting for the process of lifting the mould, rather than assuming it disappears instantaneously, is critical if trying to compare experimental and

numerical results, particularly for material with relatively low yield stress values such as are typical for most thickened paste operations. Additionally, the parameters used in the simulation, if possible, should be determined by laboratory experiments.

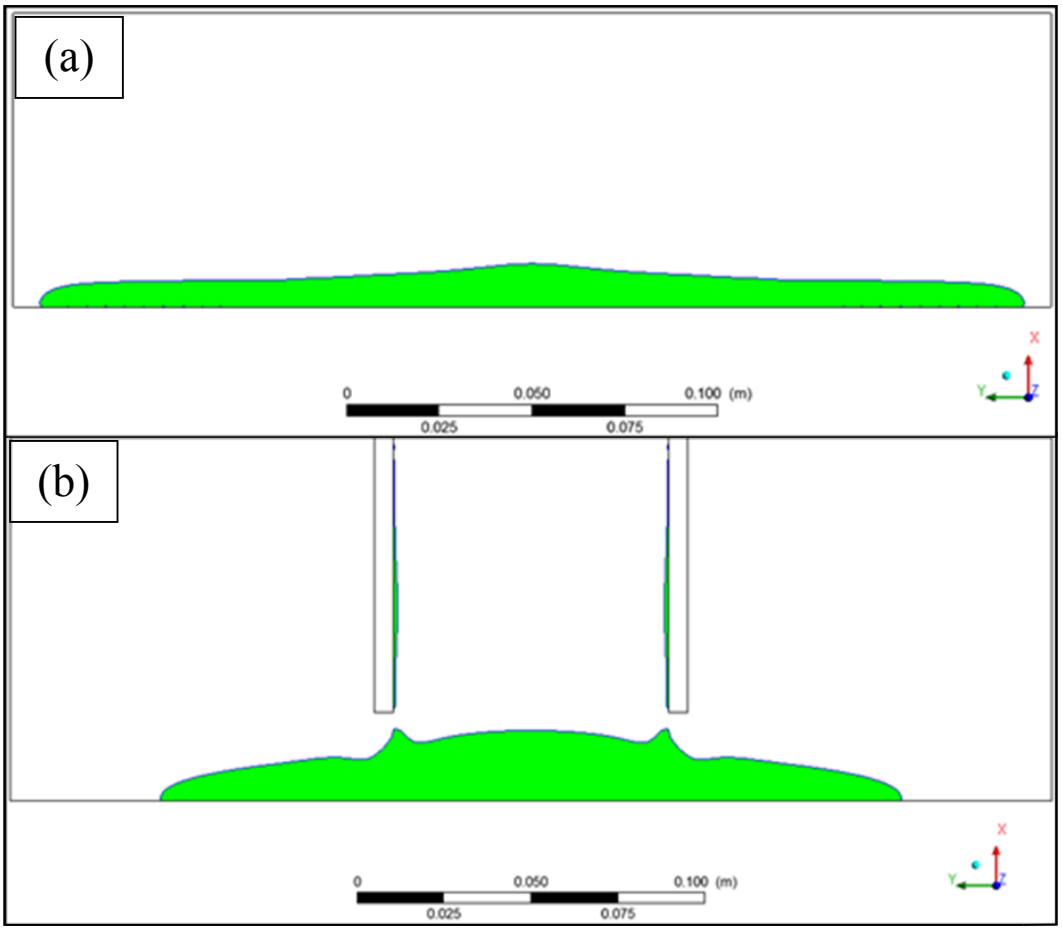

Figure 21 Final profile of Sample 1 from the slump test simulation without mould lifting process (a) and with mould lifting velocity at 0.002 m/s (b). The parameters of the physical properties of the paste used in the two simulations are: τ_y = 18.61 Pa, μ_0 = 0.32 Pa·s, ρ = 1315.0 kg/m^3 which are exactly the same as the tested values from laboratory experiment.

Typically, the lifting velocity of the mould in the laboratory experiment is between 0.002 m/s and 0.01 m/s. From **Figure 19** it is evident that the slump and spread from the laboratory experiment are generally between the results from simulations with mould lifting velocities of 0.002 m/s and 0.01 m/s. This once again indicates that a higher lifting velocity of the mould in mini-slump test may increase the slump height. This influence is particularly strong for paste with lower yield stress and viscosity, as discussed in Sections 3.4.1 and 3.4.3.

According to **Figure 19**(a), the difference in slump between the three simulations studied are very distinct when the dimensionless yield stress is lower than 0.03. However, the slumps from the three simulations gradually converge with the experimental value with increasing dimensionless yield stress. As discussed in 4.3, the inertial effects can influence the slump, and moreover, the inertial effects of paste with a lower yield stress and viscosity in the mini-slump test are more significant than for higher yield stress and viscosity.

The differences in predicted spread between simulations with a mould lifting velocity of 0.01 m/s and 0.002 m/s in **Figure 19**(b) are not as significant as the differences of slump in **Figure 19**(a) when the dimensionless yield stress is less than 0.03. It suggests that the lifting velocity of the mould influences the slump more than spread in the mini-slump test for paste of lower dimensionless yield stress. This further confirms the conclusion obtained in Section 3.4.3 that spread is more appropriate than slump as the

measure for mini-slump test when the dimensionless yield stress of tested paste is relatively low.

3.5 Conclusions

All of the discussions and conclusions in the present work are based on paste of relatively low yield stress (from approximately 18 Pa to 60 Pa) and viscosity (from around 0.3 Pa·s to 0.9 Pa·s). Specific conclusions drawn from this work include:

1. Simulation results show that spread is superior to slump as the preferred measurement in the mini-slump test for paste with relatively low yield stress and viscosity when the lifting velocity is not very high because spread is less sensitive to the variation of lifting velocity of the mould than slump. Moreover the spread is easier to measure for material of relatively low yield stress in practice. The yield stress can be estimated using Eq. (1) based on spread.
2. The varying trend of R_{IY}, which takes flow time to reach the stoppage, slump, spread, density and yield stress of paste into account, is a useful indicator for describing the variation of inertial effects in the mini-slump test. However if the value of R_{IY} can be the criterion to determine whether the inertial effects can be neglected or not in the mini-slump test still needs more thorough investigations.
3. The lifting velocity of the mould has a significant influence on the spread and

slump of the mini-slump test for paste of lower yield stress and viscosity. A higher lifting velocity may introduce stronger inertial effects, leading to larger spread and slump. It is thus crucial to keep the lifting velocity of the mould as slow as possible (within reason) in the mini-slump test for paste of lower yield stress and viscosity. However, it is worth noting that when the lifting velocity of the mould is higher than a certain value, the final spread declines with an increasing mould lifting velocity as a result of end effects.

4. Generally, an increase in viscosity can reduce the inertial effects and hence both slump and spread. Moreover, the variation of viscosity has more significant influence on the slump and spread of the mini-slump test where the inertial effects are stronger. Therefore it is not reasonable to artificially change the viscosity in simulations merely to obtain better agreement between experimental and numerical results, as is sometimes done.
5. The yield stress of the paste has a stronger influence than viscosity on spread, slump, flow time and R_{IY}. In addition the flow time in the mini-slump test is strongly influenced by both yield stress and viscosity, which may be one of the reasons why the correlations between times to certain spread values and the plastic viscosity previously reported in the literature tend to be poor.
6. The influence of mould lifting velocity on the slump and spread of mini-slump tests for lower viscosity and yield stress materials is more significant than higher viscosity and yield stress materials. Additionally it is realized that there

is some potential for the mould lifting process to increase the slump and spread in mini-slump test, indicating that the lifting process of the mould should not be neglected in simulations of the mini-slump test.

7. The increase of viscosity in a mini-slump test simulation wherein the mould is assumed to instantaneously disappear will increase the flow time, thereby resulting in a dramatic computing time increase. Additionally the 'no mould' simulation neglecting some important factors, such as the paste left on the wall, the wall friction and the constraint of the mould on the paste during flowing, cannot replicate the real flow behaviour of paste in a laboratory mini-slump test. The simulation with mould lifting process, using the parameters obtained from corresponding rheology tests, on the other hand, yields results in good agreement with mini-slump test experiments.

Acknowledgements

The first author gratefully acknowledges the China Scholarship Council (CSC) and The University of Western Australia for financial support.

Appendix 3A Experimental data of rheological tests and mini-slump tests

This appendix includes experimental data in Chapter 3. There are a total of 29 samples and for each sample, the steady state flow curve, stress growth curve, as well as the experimental results of mini-slump tests were recorded and summarised **Figure 3A** and **Table 3A**, respectively.

Figure 3A Steady state flow curves (a) and stress growth curves (b) for Sample 1-29 in Chapter 3.

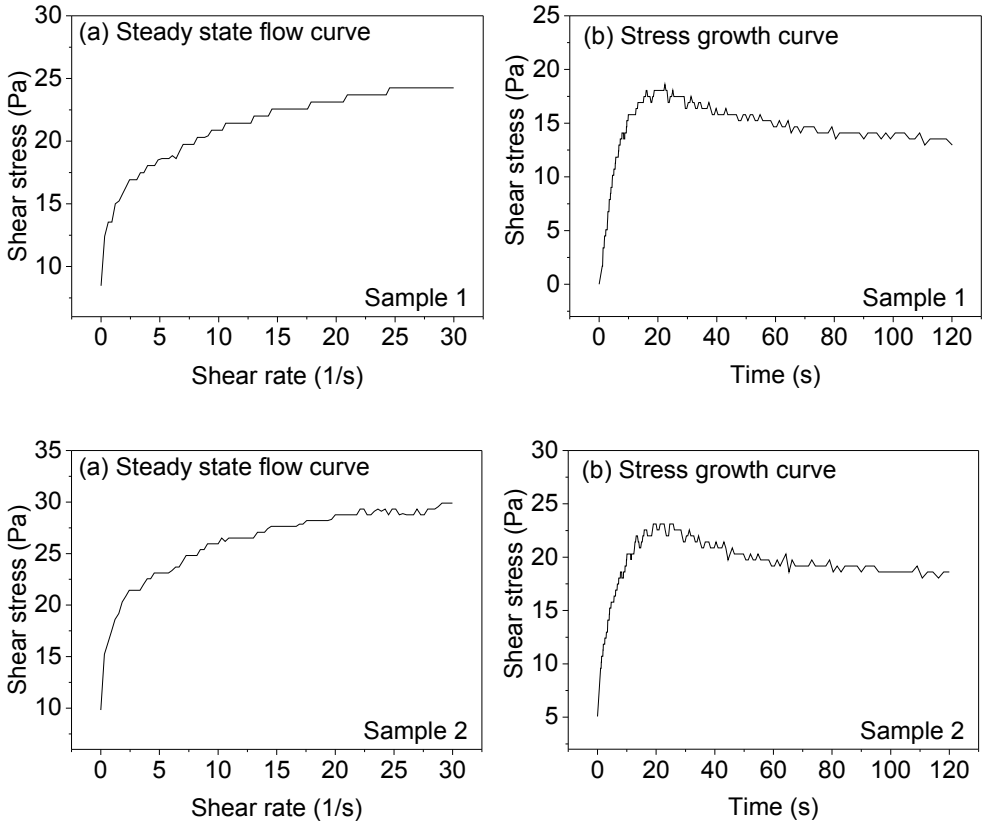

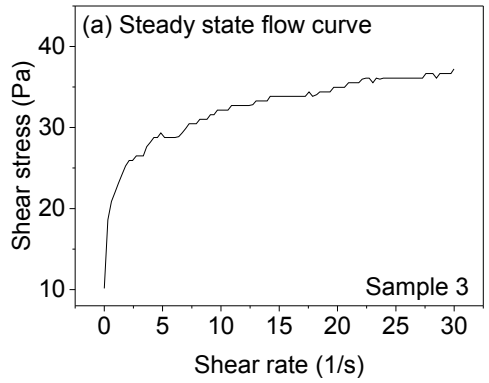
(a) Steady state flow curve
Shear stress (Pa)
Shear rate (1/s)
Sample 3

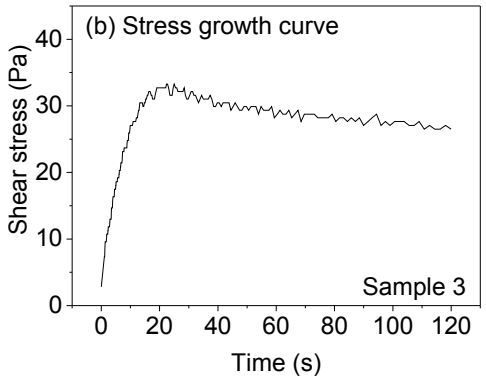
(b) Stress growth curve
Shear stress (Pa)
Time (s)
Sample 3

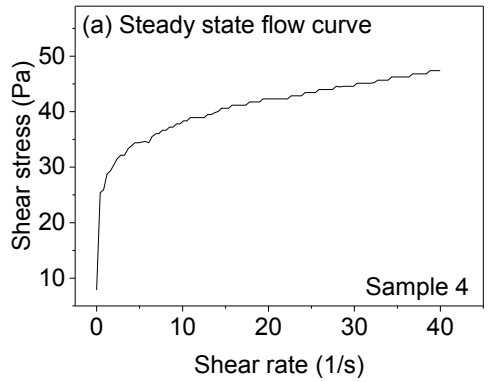
(a) Steady state flow curve
Shear stress (Pa)
Shear rate (1/s)
Sample 4

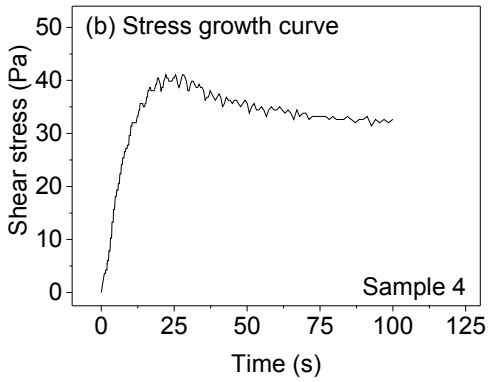
(b) Stress growth curve
Shear stress (Pa)
Time (s)
Sample 4

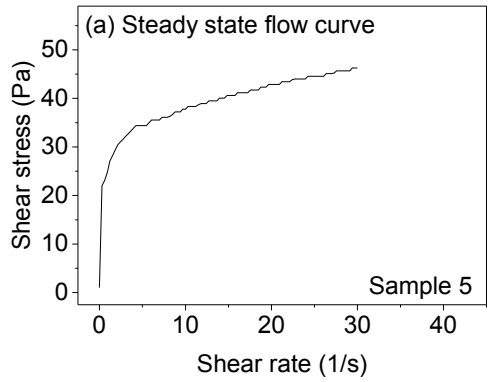
(a) Steady state flow curve
Shear stress (Pa)
Shear rate (1/s)
Sample 5

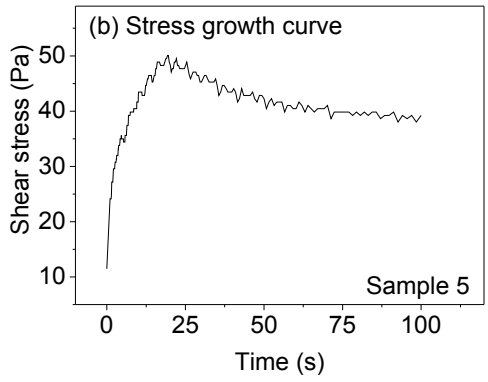
(b) Stress growth curve
Shear stress (Pa)
Time (s)
Sample 5

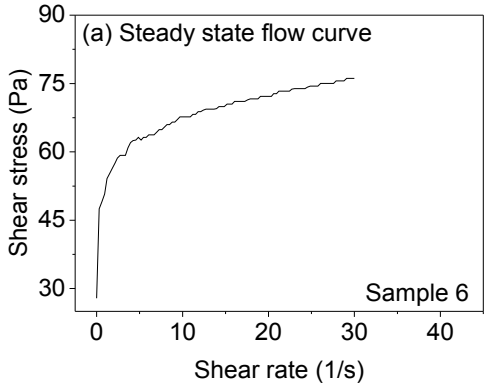
(a) Steady state flow curve
Shear stress (Pa)
Shear rate (1/s)
Sample 6

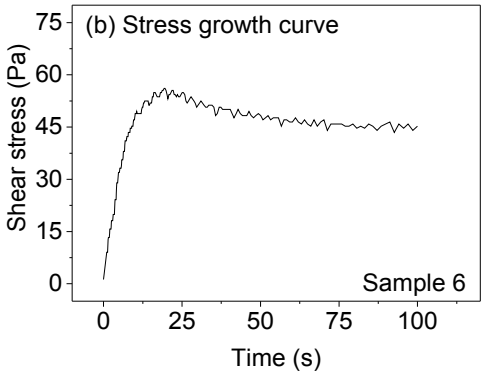
(b) Stress growth curve
Shear stress (Pa)
Time (s)
Sample 6

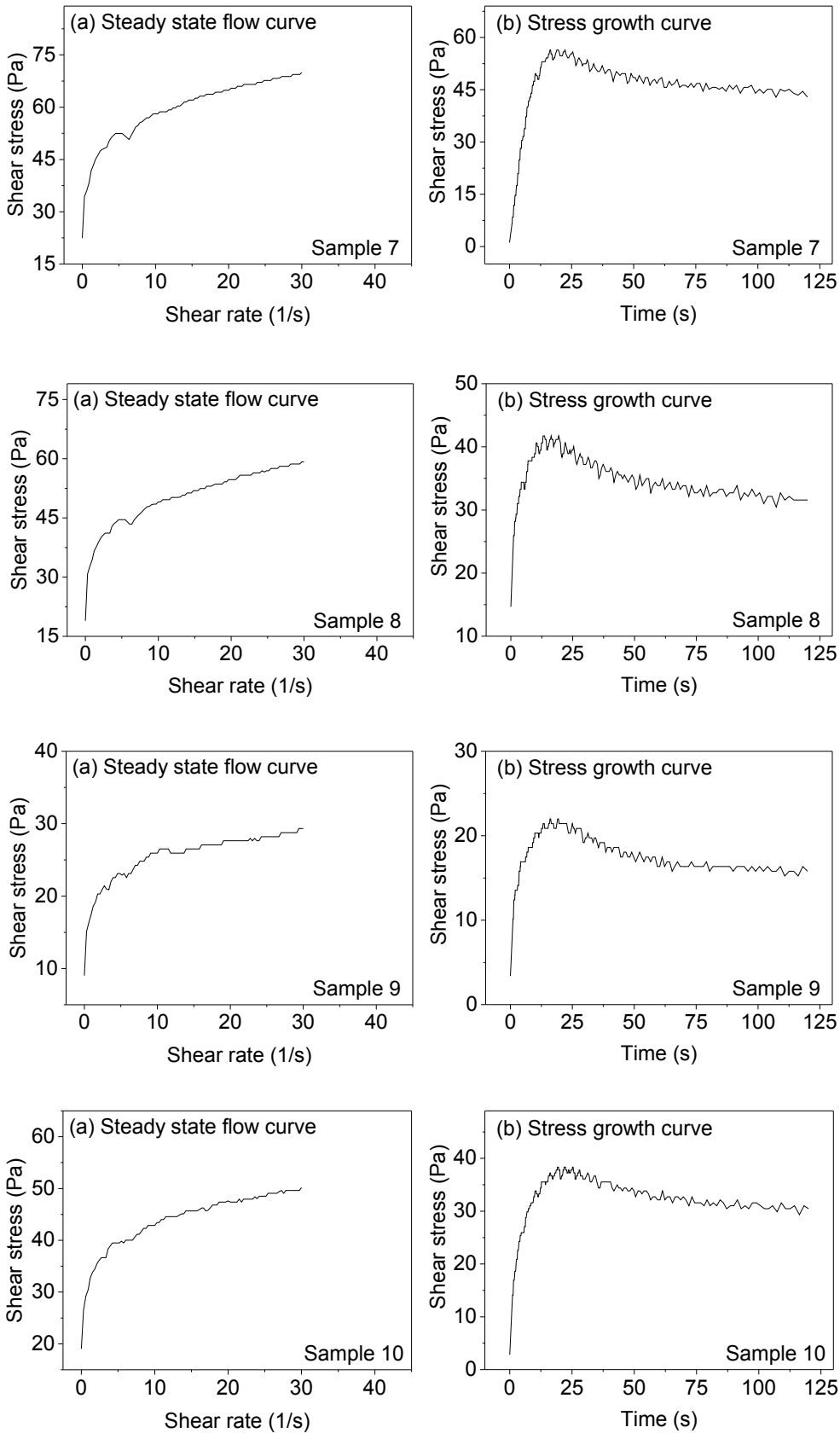
(a) Steady state flow curve
Shear stress (Pa)
Shear rate (1/s)
Sample 7
(b) Stress growth curve
Shear stress (Pa)
Time (s)
Sample 7
(a) Steady state flow curve
Shear stress (Pa)
Shear rate (1/s)
Sample 8
(b) Stress growth curve
Shear stress (Pa)
Time (s)
Sample 8
(a) Steady state flow curve
Shear stress (Pa)
Shear rate (1/s)
Sample 9
(b) Stress growth curve
Shear stress (Pa)
Time (s)
Sample 9
(a) Steady state flow curve
Shear stress (Pa)
Shear rate (1/s)
Sample 10
(b) Stress growth curve
Shear stress (Pa)
Time (s)
Sample 10

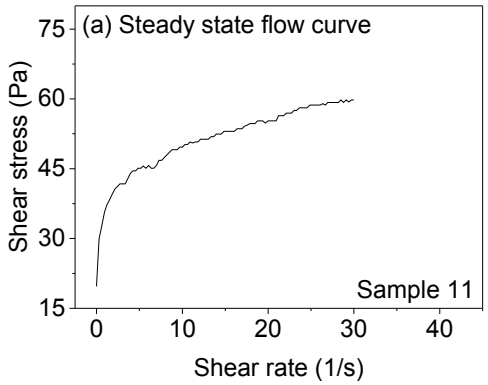
(a) Steady state flow curve
Shear stress (Pa)
Shear rate (1/s)
Sample 11

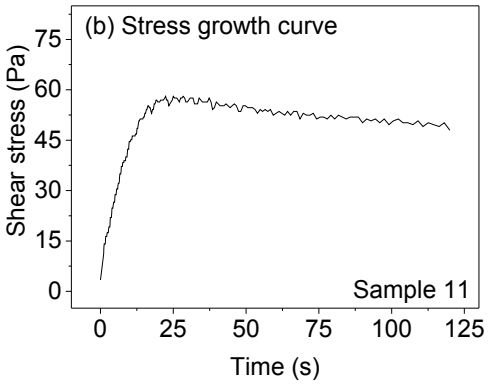
(b) Stress growth curve
Shear stress (Pa)
Time (s)
Sample 11

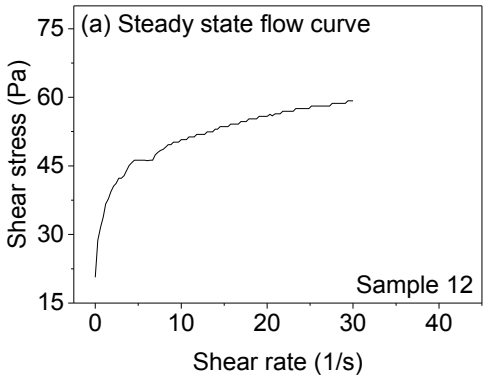
(a) Steady state flow curve
Shear stress (Pa)
Shear rate (1/s)
Sample 12

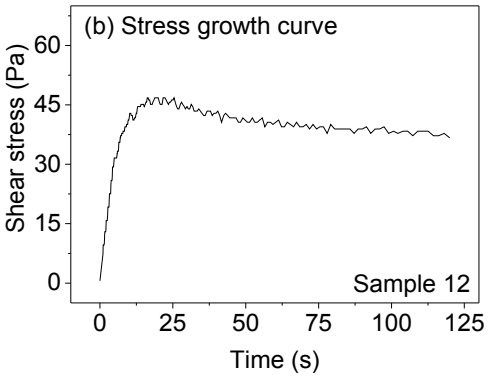
(b) Stress growth curve
Shear stress (Pa)
Time (s)
Sample 12

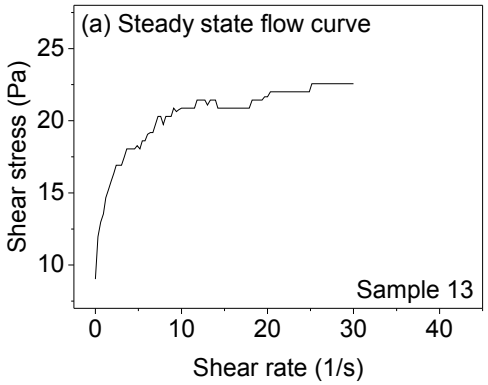
(a) Steady state flow curve
Shear stress (Pa)
Shear rate (1/s)
Sample 13

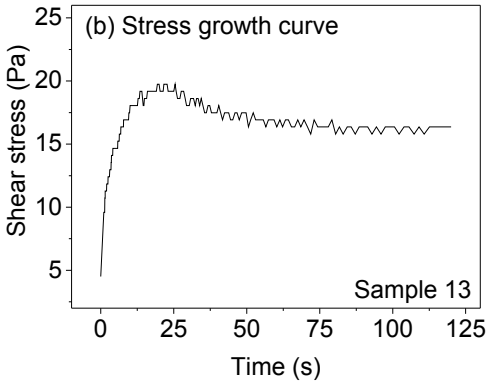
(b) Stress growth curve
Shear stress (Pa)
Time (s)
Sample 13

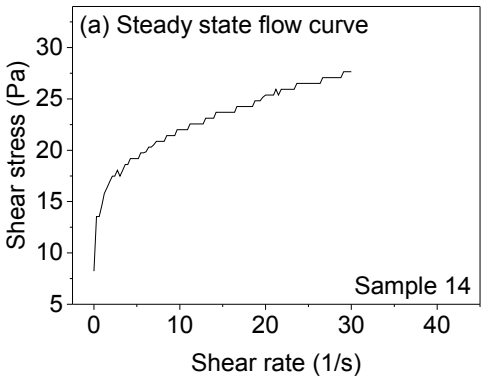
(a) Steady state flow curve
Shear stress (Pa)
Shear rate (1/s)
Sample 14

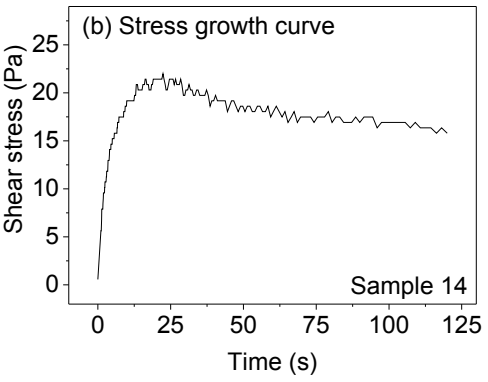
(b) Stress growth curve
Shear stress (Pa)
Time (s)
Sample 14

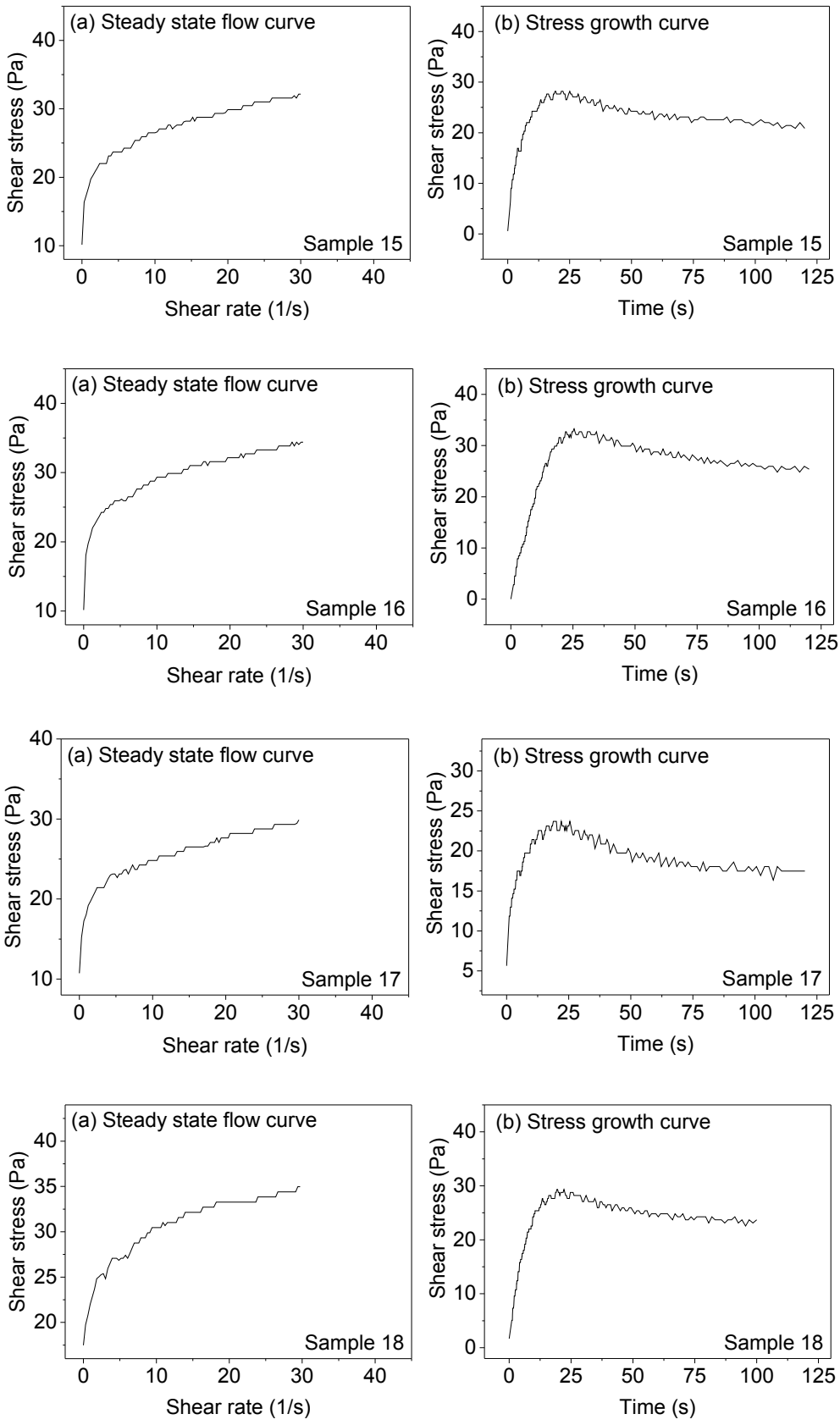
(a) Steady state flow curve
Shear stress (Pa)
Shear rate (1/s)
Sample 15
(b) Stress growth curve
Shear stress (Pa)
Time (s)
Sample 15
(a) Steady state flow curve
Shear stress (Pa)
Shear rate (1/s)
Sample 16
(b) Stress growth curve
Shear stress (Pa)
Time (s)
Sample 16
(a) Steady state flow curve
Shear stress (Pa)
Shear rate (1/s)
Sample 17
(b) Stress growth curve
Shear stress (Pa)
Time (s)
Sample 17
(a) Steady state flow curve
Shear stress (Pa)
Shear rate (1/s)
Sample 18
(b) Stress growth curve
Shear stress (Pa)
Time (s)
Sample 18

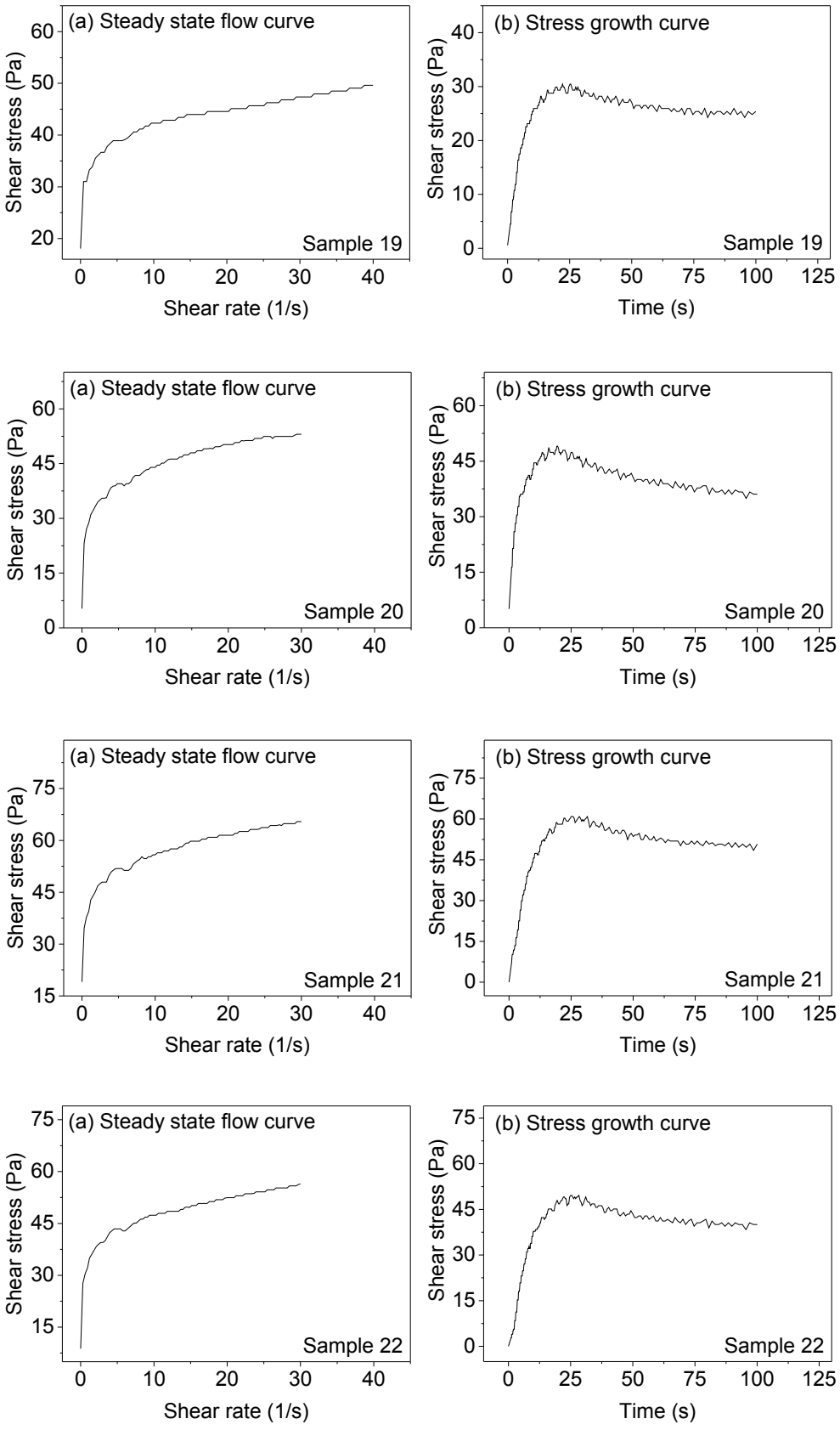
(a) Steady state flow curve
Shear stress (Pa)
Shear rate (1/s)
Sample 19
(b) Stress growth curve
Shear stress (Pa)
Time (s)
Sample 19
(a) Steady state flow curve
Shear stress (Pa)
Shear rate (1/s)
Sample 20
(b) Stress growth curve
Shear stress (Pa)
Time (s)
Sample 20
(a) Steady state flow curve
Shear stress (Pa)
Shear rate (1/s)
Sample 21
(b) Stress growth curve
Shear stress (Pa)
Time (s)
Sample 21
(a) Steady state flow curve
Shear stress (Pa)
Shear rate (1/s)
Sample 22
(b) Stress growth curve
Shear stress (Pa)
Time (s)
Sample 22

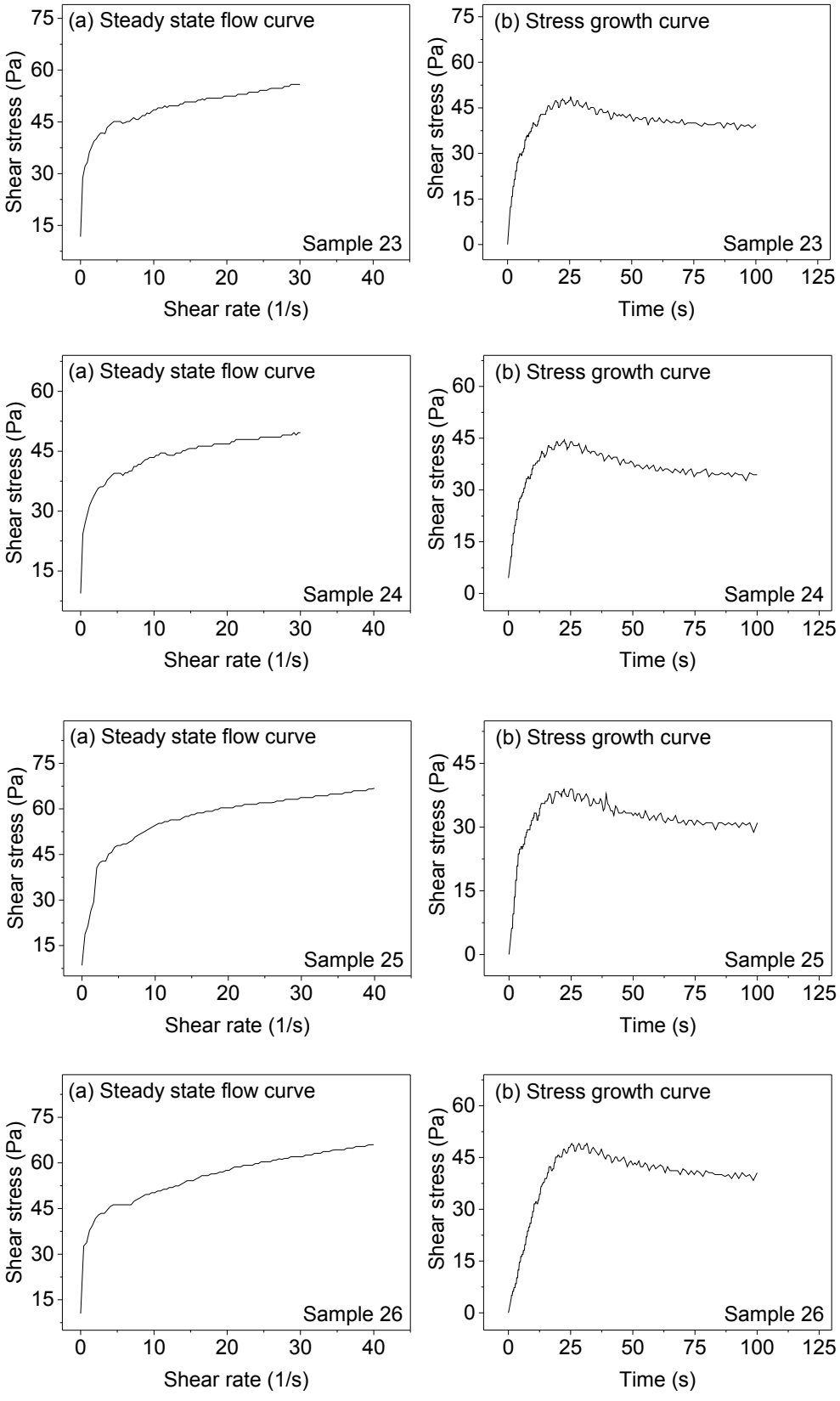
(a) Steady state flow curve
Shear stress (Pa)
Shear rate (1/s)
Sample 23
(b) Stress growth curve
Shear stress (Pa)
Time (s)
Sample 23
(a) Steady state flow curve
Shear stress (Pa)
Shear rate (1/s)
Sample 24
(b) Stress growth curve
Shear stress (Pa)
Time (s)
Sample 24
(a) Steady state flow curve
Shear stress (Pa)
Shear rate (1/s)
Sample 25
(b) Stress growth curve
Shear stress (Pa)
Time (s)
Sample 25
(a) Steady state flow curve
Shear stress (Pa)
Shear rate (1/s)
Sample 26
(b) Stress growth curve
Shear stress (Pa)
Time (s)
Sample 26

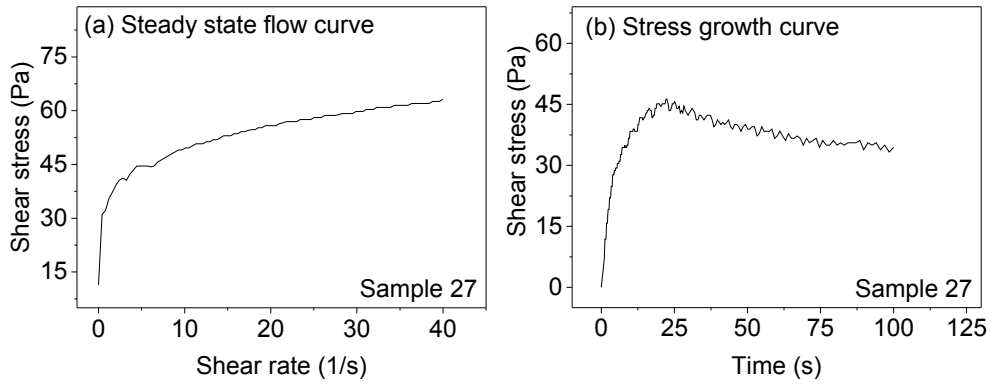
(a) Steady state flow curve
Shear stress (Pa)
Shear rate (1/s)
Sample 27
(b) Stress growth curve
Shear stress (Pa)
Time (s)
Sample 27

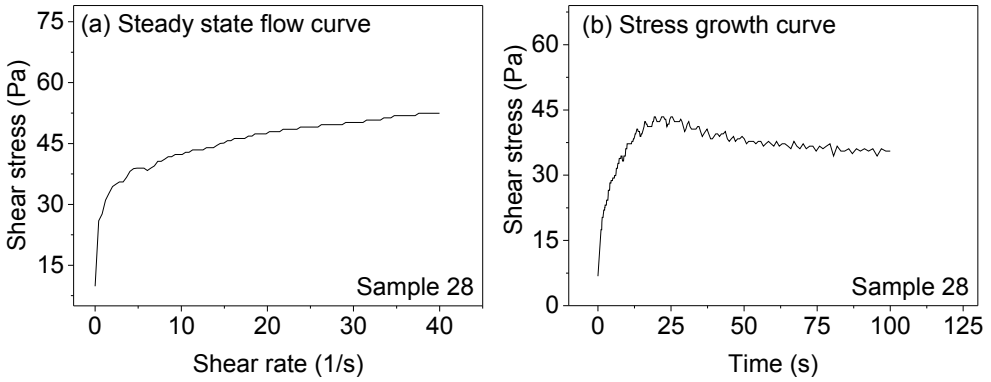
(a) Steady state flow curve
Shear stress (Pa)
Shear rate (1/s)
Sample 28
(b) Stress growth curve
Shear stress (Pa)
Time (s)
Sample 28

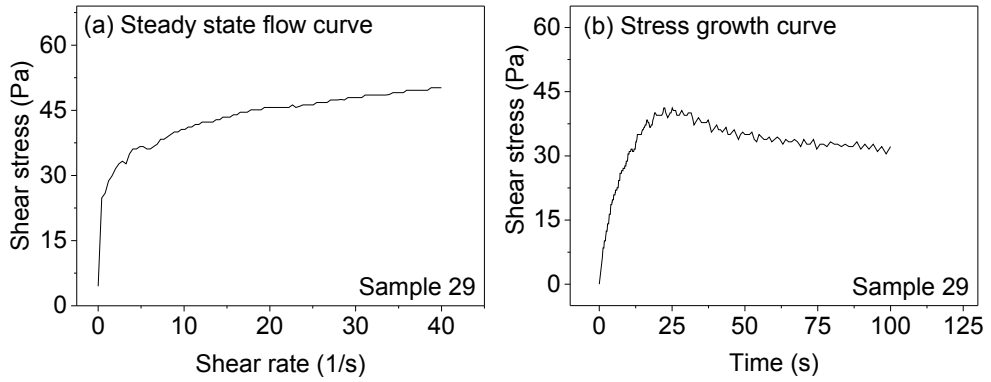
(a) Steady state flow curve
Shear stress (Pa)
Shear rate (1/s)
Sample 29
(b) Stress growth curve
Shear stress (Pa)
Time (s)
Sample 29

Table 3A Experimental data of mini-slump tests on kaolin suspensions with different water content (The yield stress and viscosity were obtained from **Figure 3A**).

Sample No.	Yield stress (Pa)	Viscosity (Pa·s)	Slump (mm)	Spread (mm)	Density (kg/m3)	Water content (%)
1	18.61	0.32	60.51	213.75	1315.0	156.36
2	23.12	0.36	58.49	204.02	1321.3	147.51
3	33.28	0.40	56.05	192.40	1342.6	136.18
4	41.40	0.44	54.92	182.76	1353.6	127.96
5	50.10	0.64	53.43	177.60	1367.4	126.68
6	56.10	0.73	52.36	171.35	1377.2	122.94
7	56.4	0.93	49.96	168.4	1386.91	118.66
8	41.74	0.76	53.72	177.12	1372.4	126.89
9	22	0.33	58.56	201.58	1331.3	146.90
10	38.35	0.57	53.79	182.9	1370.3	127.96
11	58.09	0.77	50.86	169.40	1376.3	119.99
12	46.81	0.73	53.26	175.62	1372.8	124.51
13	19.74	0.24	60.94	206.25	1314.5	154.91
14	22	0.40	58.99	204.38	1325.6	146.81
15	28.2	0.42	57.10	195.80	1337.9	139.91
16	33.28	0.42	56.46	192.10	1338.7	137.29
17	23.69	0.35	58.40	201.18	1328.3	144.88
18	29.33	0.43	57.39	197.62	1337.5	140.93
19	30.46	0.37	56.42	192.70	1342.3	137.35
20	49.07	0.77	52.87	173.55	1370.9	124.74
21	60.91	0.76	51.40	168.50	1379.2	121.38
22	49.63	0.71	52.85	171.97	1372.7	123.86
23	48.50	0.63	52.62	173.35	1371.8	125.34
24	44.56	0.59	53.40	177.12	1365.3	127.77
25	38.92	0.73	53.99	176.61	1365.12	128.14
26	49.07	0.70	52.51	170.24	1376.99	123.62
27	46.25	0.65	52.96	175.19	1370.19	126.04
28	43.43	0.51	53.62	177.52	1366.12	128.24
29	41.17	0.50	54.47	179.28	1358.13	-

4. USING THE FLUME TEST FOR YIELD STRESS MEASUREMENT OF THICKENED TAILINGS

Abstract

In thickened tailings disposal operations, the yield stress, which is a unique physical property of thickened tailings, is a key design parameter as it has a controlling influence on the final slope of deposited tailings. A quick but rough estimate of the yield stress is typically obtained using a mini-slump test in industry. This paper explores the feasibility of using a laboratory flume test to measure the yield stress of thickened tailings.

The model of slow sheet flow (SSF) which has previously been used to model flume tests and the Fourie and Gawu (FG) model, which was developed for interpretation of flume tests on thickened tailings, are compared. The SSF model, derived within the framework of long-wave approximation, is shown to only hold for flumes with frictionless sidewalls (or very wide flumes), whereas the FG model is valid for flumes of finite width and nonslip sidewalls. These findings were confirmed using CFD simulations of laboratory flume tests with nonslip and free-slip sidewalls on materials with yield stresses ranging from 20 to 60 Pa. Simulations to investigate the sensitivity of the final beach profile in the flume test to variations of yield stress and viscosity were performed. The results suggest that the final profile is very sensitive to yield stress variation but relatively insensitive to viscosity variation. This relative insensitivity to viscosity further justifies

the use of the FG model for evaluation of yield stress from flume test data, as this model ignores the effect of viscosity.

Simulations of mini-slump tests were conducted to demonstrate that different mould lifting velocities may introduce different inertial effects, thereby impacting the final profile and hence the yield stress extrapolated from slump tests. Moreover, comparison between the profiles predicted by several theoretical models for slump tests and CFD simulation results revealed that the existing models are not capable of capturing the final shape of the slumped material, which is invariably distorted by the mould friction to some extent. Consequently, the accuracy of the yield stress extrapolated from mini-slump tests is not high. The small errors in yield stresses calculated from the CFD simulation results using the FG model suggest that yield stresses may be determined from flume tests with very high accuracy using the FG model.

Keywords: Thickened tailings; Yield stress; Flume test; CFD modelling; Wall friction.

4.1 Introduction

Yield stress, which is defined as the minimum stress that must be applied in order to induce flow, is a key design parameter in the industrial application of surface disposal of thickened tailings (sometimes termed paste). The yield stress of thickened tailings must be low enough that the energy required to transport the tailings by pipeline to the tailings storage facility is minimised, but must be high enough to ensure that the designed beach

slope can be achieved in the field, i.e. two often essentially conflicting requirements. Additionally, as is now evident from numerous case studies, the yield stress of tailings increases exponentially with increasing solids concentration [1, 54, 55, 63, 114], which indicates that in some circumstances a small variation in tailings concentration may result in a significant change in yield stress. Therefore it is crucial to monitor and control the yield stress of thickened tailings when used for surface disposal. Although there are a number of techniques for measuring the yield stress of thickened tailings [1, 15, 58, 99], the slump test has become a preferred option in resource industries (such as minerals, coal, and the oil sands) to obtain a quick and easy on-site measurement of yield stress [50, 55, 95].

However, the accuracy of this method is comparatively low as a result of its inherent disadvantages. For example, the lifting velocity of the mould in a mini-slump test may influence the final spread and slump, especially for material of relatively low yield stress and viscosity as reported by several researchers [72, 97]. Considering the mould is normally lifted manually, the accuracy of the slump test is likely to be operator dependent.

This paper investigates the feasibility of using a laboratory flume to measure the yield stress of thickened tailings. In the laboratory flume test, which has been used to predict the beach slope of conventional tailings deposits, a quantity of tailings slurry is discharged from an elevated storage tank into a flume, producing a sloped profile once deposition ceases. This profile is usually concave-up, as a consequence of the segregating nature of

conventional (low solids content) tailings. The profile achieved in the flume is used to predict the beach slope developed in the field [36]. This method is questionable for thickened tailings, since unrealistically steeper slopes have been achieved in the flume compared with those in the field [4, 24]. Unlike conventional tailings which do not show a yield point, thickened tailings are more likely to behave as yield stress fluids which are typically described by the Bingham plastic model. The apparent viscosity for an ideal Bingham fluid is given by:

$$\eta = \begin{cases} \mu_0 + \frac{\tau_y}{\dot{\gamma}}, & \tau \geq \tau_y \\ \infty, & \tau < \tau_y \end{cases} \quad (1)$$

where μ_0 is the plastic viscosity which is also referred to as viscosity in this work, $\dot{\gamma}$ is the shear rate and τ_y is the yield stress of Bingham fluid. It can be seen from Eq.(1) that an ideal Bingham fluid is a visco-plastic material that will behave as a rigid body if the shear stress is lower than the yield stress, but will flow as a viscous fluid if the shear stress exceeds the yield stress. It is noted that the term “ideal Bingham model” is used to distinguish it from the Bingham model numerically implemented in ANSYS FLUENT, which is discussed in Section 4.3.

To explain the disparity in beach slopes of thickened tailings achieved in flume tests and the field, Simms [37] first used the theoretical solution for slow sheet flow (SSF) of a Bingham fluid that had previously been derived by Liu and Mei [82] within the framework of long-wave approximation. He found that the overall slope of the deposit was significantly influenced by both the scale of flow and the underlying topography.

Henriquez et al. [38] pursued the method in Simms [37] to study the dynamic flow behaviour and multilayer deposition of gold paste tailings using laboratory flume tests. They suggested that the yield stress obtained by fitting the SSF model to laboratory flume tests with a flume width of 150 mm is characteristic of the behaviour during deposition of thickened tailings. Mizani et al. [69] carried out laboratory flume tests on high density gold tailings to investigate the likely stack geometry of thickened tailings. The flume used was 2430 mm long and 152 mm wide. The SSF equations were used to provide a best fit to the measured profile by varying the yield stress of the thickened tailings to verify the capability of the SSF model to simulate the flume test. The SSF model employed in their work will potentially not hold if the long-wave approximation is not fulfilled [82]. For the final profiles achieved in their laboratory flume tests on thickened tailings, the fluid depth around the deposition point was typically comparable with the flume width. The wall friction can play an important role in the equilibrium state of thickened tailings in a flume test as suggested by Fourie and Gawu [26]. All of these may render the application of the SSF model to laboratory flume tests inappropriate.

The L-box test, which is used to assess the ability of fresh self-compacting concrete (SCC) to flow through tight obstructions without segregating or blocking is widely used in the concrete industry. Nguyen et al. [115] proposed a theoretical analysis to relate the yield stress to the final profile of fluids in an L-box. They reported that given the yield stress of tested material, the model can be used to predict the final profile of the material achieved in an L-box if the gate is lifted slowly enough during the test.

Fourie and Gawu (FG) [26] developed a very similar model but taking the base angle into account to illustrate the importance of wall friction in flume tests, thus explaining the unrealistically steeper slopes yielded by flume tests compared with those achieved in the field for thickened tailings. It was found that the beach slope decreases with an increasing flume width. Moreover, the profiles measured in flume tests using thickened tailings agreed well with the theoretical predictions using the yield stresses independently determined by the vane method. However, the inertial effects which may impact the profiles in flume tests were not discussed.

In view of the uncertain application of the SSF model to laboratory flume tests, and desirability to obtain the yield stress of thickened tailings accurately without resorting to use of expensive and delicate instruments, such as the vane rheometer, the present work uses computational fluid dynamics (CFD) to explore the feasibility of using a laboratory flume test to obtain the yield stress of thickened tailings. Firstly, the SSF and FG models are described to facilitate the analysis of the differences and relations between the two models. Thereafter the numerical model (CFD) and settings used in simulations are described. A detailed comparison between the SSF and FG models is subsequently made using 3D simulations to determine the superior model for yield stress measurement using a flume test. Moreover, the sensitivity of the final profile in a flume test to variations in yield stress and viscosity is investigated using CFD simulations. Additionally, the flume test is compared with the mini-slump test in terms of accuracy of yield stress measurement. Finally, several comments on the application of laboratory flume test data

to yield stress measurement are made. It is noted that thickened tailings, which are treated as Bingham fluids in the present work, refer to fluids where suspended solids are fine enough to not settle or segregate during the flume deposition process, so that they can be modelled using the homogeneous fluid approach [116].

4.2 Description of models used

Two mathematical models (SSF and FG), which were used to predict the final profiles achieved in flume tests, are described in this section, examining their differences and applicable conditions.

4.2.1 Theoretical analysis for the slow sheet flow (SSF) of yield stress fluid

The analytical solution for the slow sheet flow of a yield stress fluid which has been derived by several authors [82, 117, 118] within the framework of the long-wave approximation was used to model laboratory flume tests using thickened tailings previously presented by other researchers [34, 37, 69]. **Figure 1** shows the schematic of a thin layer of a yield stress fluid on a horizontal plane. Within the framework of the long-wave approximation [82, 117, 119], the momentum equations in x and z directions for a slow moving free surface flow (2D) on a flat base are therefore:

$$0 = -\frac{\partial p}{\partial x} + \frac{\partial \tau}{\partial z} \tag{2}$$

$$0 = -\rho g - \frac{\partial p}{\partial z} \tag{3}$$

where ρ is the fluid density, g is the gravitational acceleration, p is the pressure and

τ is the shear stress.

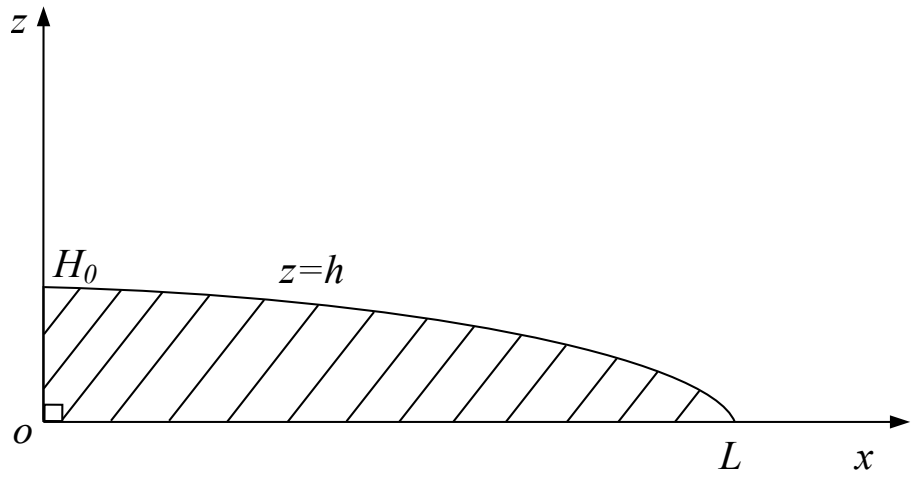

Figure 1 A sheet of Bingham fluid on a flat plane

The expression for pressure p can be obtained by integrating Eq.(3) from z to the free surface of the fluid with atmospheric pressure being the reference:

$$p = \rho g(h - z) \tag{4}$$

where $h = h(x)$ is the distance between the free surface and the plane bed.

Integrating Eq.(2) from z to the free surface by taking account of Eq.(4) and boundary conditions ($\tau = 0$ at $z = h$) yields:

$$\tau = -\rho g(h - z)\frac{\partial h}{\partial x} \tag{5}$$

At the threshold of flow the shear stress at the bottom of the material equals the yield stress of the fluid:

$$\tau_y = -\rho g h \frac{dh}{dx} \tag{6}$$

Then the final (equilibrium) profile of a sheet of yield stress fluid on a flat plane can be described by integrating Eq.(6):

$$x = L - \frac{\rho g h(x)^2}{2\tau_y} \tag{7}$$

where L is the length of the final profile.

The volume of the fluid (per unit width along y) may be given by:

$$A = \int_0^{H_0} L - \frac{\rho g}{2\tau_y} z^2 \, dz = LH_0 - \frac{\rho g}{6\tau_y} {H_0}^3 \tag{8}$$

where H_0 is the maximum thickness of the final profile (at $x = 0$).

As the point (0, H_0) is on the profile (see **Figure 1**), therefore:

$$L = \frac{\rho g}{2\tau_y} {H_0}^2 \tag{9}$$

Combining Eqs. (8) and (9) yields:

$$A = \frac{\rho g}{3\tau_y} {H_0}^3 \tag{10}$$

Given the volume of the fluid per unit width along y, the yield stress and density, the fluid thickness at the deposition point can be obtained from Eq.(10). Then the length of the final profile can be computed by Eq.(9). Finally, the final profile of the yield stress fluid on a flat plane may be yielded by Eq.(7), as long as the inertial effects can be neglected during the fluid deposition.

4.2.2 Fourie and Gawu's (FG) model for flume tests on yield stress fluids

The analytical solution for the profile of yield stress fluid at a threshold static equilibrium in a rectangular flume has been derived by Fourie and Gawu [26] with a similar approach used previously to predict the flow of slurry from a breached tailings dam [7, 120], with a view to quantifying the errors of using slopes of thickened tailings achieved in flume tests for direct extrapolation to field applications. Only the situation where the base is

horizontal is analysed in the present work.

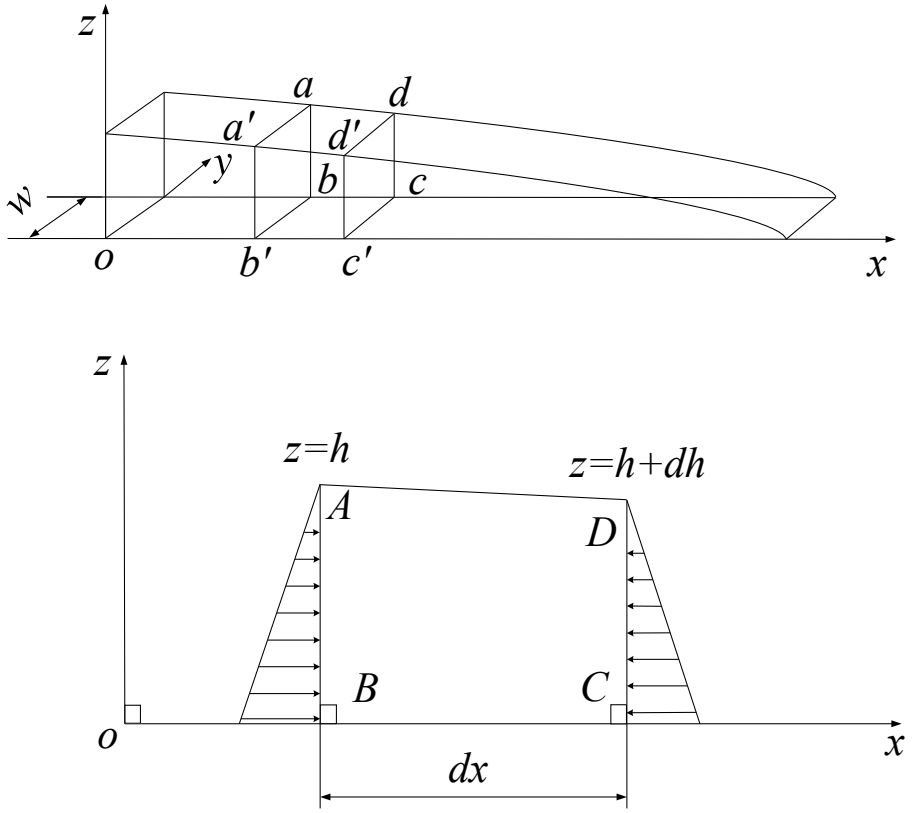

Figure 2 Sketch of a control volume for flow in a rectangular flume with a flat base.

With a number of simplifying assumptions a differential equation can be established by equating the driving and resisting forces acting on the control volume in the x direction as shown in

Figure 2. The forces acting on the control volume ($abcda'b'c'd'$) at the threshold of motion in x direction are:

1. The resultant force F_1 in x direction caused by hydrostatic pressure acting on $abb'a'$ and $dcc'd'$:

$$F_1 = \frac{1}{2}\rho g h^2 w - \frac{1}{2}\rho g (h+dh)^2 w \tag{11}$$

2. The shearing force F_2 on bottom:

$$F_2 = -\tau_y w dx \tag{12}$$

3. The shearing force F_3 on the sidewalls of flume:

$$F_3 = -\tau_y (2h + dh) dx \tag{13}$$

where w is the flume width. The negative signs of F_2 and F_3 indicate that these two forces are in $-x$ direction.

Considering that the resultant force in x direction of the control volume should be null (i.e. $\sum_{i=1}^{3} F_i = 0$) at the threshold static equilibrium (i.e. once flow stops) and assuming that $dxdy \approx dydy \approx 0$, the following equation can be obtained by combining Eqs.(11) to (13):

$$dx = \frac{\rho g w h}{-\tau_y (2h+w)} dh \tag{14}$$

The final profile of the yield stress fluid along the longitudinal direction (x direction) in a rectangular flume with a horizontal base can be described by:

$$x = L - \frac{\rho g w}{2\tau_y} [h(x) + \frac{w}{2} \ln \frac{w}{2h(x)+w}] \tag{15}$$

As (0, H_0) is on the free surface it follows from Eq.(15) that:

$$L = \frac{\rho g w}{2\tau_y} \cdot (H_0 + \frac{w}{2} ln \frac{w}{2H_0+w}) \tag{16}$$

where H_0 is the thickness of the yield stress fluid at the deposition point.

With the assumption that the fluid thickness is constant in the y direction (perpendicular to the sidewalls of the flume, see **Figure 2**) the volume of fluid (V) can be calculated by:

$$V = w \int_0^{H_0} L - \frac{\rho g w}{2\tau_y} [h(x) + \frac{w}{2} ln \frac{w}{2h(x)+w}] dh \tag{17}$$

Eq.(17) can be solved with Eq.(16) taken into account:

$$V = \frac{\rho g w^2}{4\tau_y}\left(H_0^2 - wH_0 + \frac{w^2}{2} ln \frac{2H_0+w}{w}\right) \quad (18)$$

Given the volume (V) of fluid used in the flume test, the yield stress (τ_y), density (ρ) and the flume width (w), the height (H_0) at the discharge point (assuming there is no scour hole caused by dropping fluid) and the flow distance (L) may be obtained from Eqs.(18) and (16). Then the predicted final profile of the yield stress fluid in the flume ignoring inertial effects can be attained from Eq.(15).

4.2.3 Evaluation of the two models (SSF and FG)

If the flume width is infinite ($w \to \infty$) Eq.(14), which is for a rectangular flume with finite width, will reduce to:

$$dx = \frac{\rho g h}{-\tau_y} dh \quad (19)$$

which is identical to Eq.(6) derived within the framework of long-wave approximation.

It seems that the difference in the analytical solutions between SSF (Eq.(7)) and FG model (Eq.(15)) are caused by flume width.

On the other hand, if it is assumed that the sidewalls of the flume are frictionless (i.e. $F_3 = 0$), the combination of Eqs.(11) to (13) reads:

$$dx = \frac{\rho g h}{-\tau_y} dh \quad (20)$$

which is exactly the same as Eq.(19) obtained by assuming that the flume width is infinite.

Consequently an infinite flume width is equivalent to the sidewalls of the flume being

frictionless in terms of the influence on the final profile in a flume test. This is a very important and useful conclusion because it indicates that it is not appropriate to use the SSF equation to model a laboratory flume test unless frictionless sidewalls (or a wide enough flume) and no-slip bottom condition can be achieved simultaneously. It is worth noting that neither the SSF equation nor FG holds for the scenario where inertial effects of flow are significant.

4.3 Numerical model

ANSYS FLUENT, a commercially available CFD code was used to perform the simulations. To track the interface between Bingham fluid and air, the volume of fluid method (VOF), a free surface tracking technique for immiscible phases [77] was used. The governing equations for the incompressible flow problem of two phases includes the conservation equations for mass, momentum and the volume fraction advection equation, which can be found elsewhere [72].

The coupled level-set and VOF model that overcomes the deficiency of the level-set method in preserving volume conservation and discontinuity of VOF equation was activated [121]. Since gravity, which plays an important role in a flume test, was involved in the simulations, the implicit body force treatment was enabled to take the partial equilibrium of pressure gradient and body forces into account to improve solution convergence. An explicit geometric reconstruction scheme with the volume fraction cut-off and Courant number at 1e-06 and 0.25 was specified as the volume fraction

formulation for the VOF model. A detailed discussion of the geometric reconstruction scheme can be found elsewhere [103]. The pressure-based coupled solver solving the momentum and continuity equations in a coupled fashion was employed to obtain a rapid and monotonic convergence rate and hence fast solution times [122]. The gradients were computed at the cell centre from the values of the scalars at the cell face centroids using the Least Squares Cell Based method. The PREssure Staggering Option (PRESTO!) scheme which is the default for VOF multiphase simulations in ANSYS FLUENT was used for the pressure interpolation. The discretization scheme of Second Order Upwind was employed for both momentum and level-set equations [74]. First order implicit time discretization which is the only available transient formulation for the explicit VOF simulations was applied [71].

Thickened tailings were treated as Bingham fluids that only start to flow when the stress exceeds a certain value (known as the 'yield stress') [17] in the present work. The Bingham relation which is normalized in ANSYS FLEUNT to guarantee the continuity of the viscosity curve at the null shear rate was used to model the flow of thickened tailings [71]:

$$\eta = \begin{cases} \mu_0 + \frac{\tau_y}{\dot{\gamma}}, & \dot{\gamma} \geq \dot{\gamma}_c \\ \mu_0 + \frac{\tau_y(2-\dot{\gamma}/\dot{\gamma}_c)}{\dot{\gamma}_c}, & \dot{\gamma} < \dot{\gamma}_c \end{cases} \tag{21}$$

where $\dot{\gamma}_c$ is the critical shear rate.

It is noted that if the critical shear rate ($\dot{\gamma}_c$) reduces to zero, Eq.(21) will represent the

ideal Bingham fluid which behaviours as solid if the shear stress is less than the yield stress, as indicated by Eq.(1). Therefore the critical shear rate should be as small as possible to reproduce the ideal Bingham fluid behaviour. However, numerical instability issues tend to be induced with an unduly small value of $\dot{\gamma}_c$. An appropriate critical shear rate should be capable of satisfying the requirements for both the reproducibility of the ideal Bingham fluid behaviour and numerical stability. Gao and Fourie [72] reported that the critical shear rate was mainly dependent on the yield stress of Bingham fluid and 0.005 s^{-1} for $\dot{\gamma}_c$ was appropriate for the yield stress between 18 Pa to 60 Pa. Considering that the yield stress of the Bingham fluid in this work is within this range, 0.005 s^{-1} for critical shear rate was employed.

A detailed discussion on the validation of the numerical model in ANSYS FLUENT for the flow of thickened tailings can be found elsewhere [72].

In the computational domain the place where the volume fraction of fluid was 0.5 was deemed the interface between Bingham fluid and air. The final profile in the flume test was the interface at the centreline of the flume.

4.4 Results and discussion

All the simulations of laboratory flume tests performed are three-dimensional (3D). Two dimensional (2D) axisymmetric simulations were conducted for the mini-slump test. **Figure 3** shows a sketch of the flume test employed throughout the work. The reason the

geometry appears 'stepped' is to minimise the CFD grid size and is based on the observation that the tailings profile thins with distance from the deposition point (i.e. the inlet). The inlet is a small square pipe of $21\ \text{mm} \times 21\ \text{mm}$ which is equivalent to a circular pipe with a diameter of $21\ \text{mm}$ in terms of the hydraulic diameter. The flume test with a small inlet and narrow flume width ($150\ \text{mm}$) in the work is very representative of a typical laboratory flume test [26, 34]. To reduce the inertial effects caused by the flume height, the distance from the inlet to the flume base is relatively small ($200\ \text{mm}$ for materials with yield stress of 56.1 Pa and $100\ \text{mm}$ for 18.6 Pa and for 1.5×18.6 Pa).

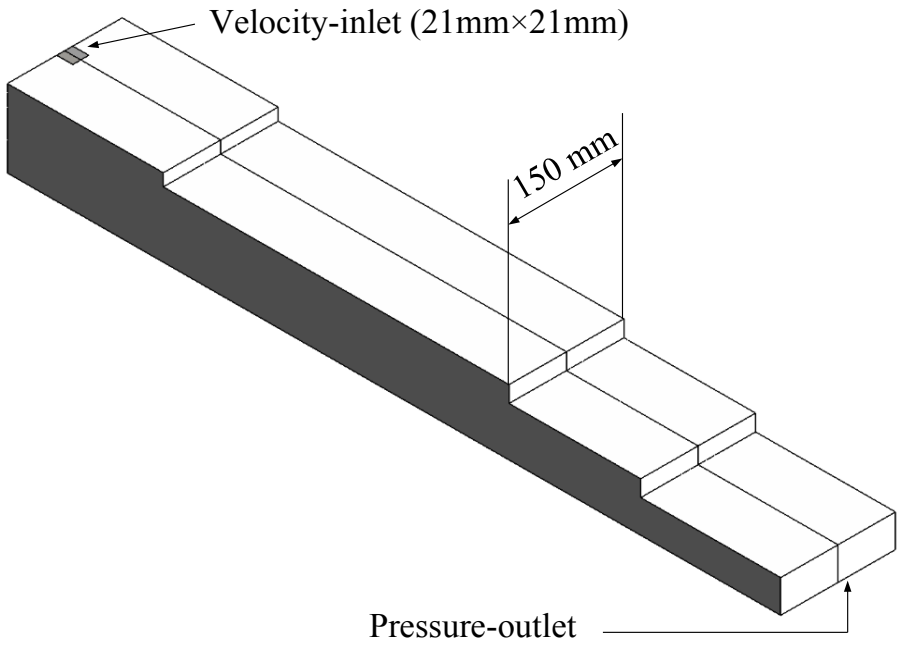

Figure 3 Geometry of the 3D simulations of the laboratory flume test with a small square inlet used in the work.

In the laboratory flume test the Bingham fluid will stop flowing completely given enough time. However, complete stoppage of flow cannot be reached in the numerical simulations

as the flow curve of the Bingham model implemented in ANSYS FLUENT passes through the origin. In other words, the Bingham fluid in the simulation will not stop completely as long as the simulation is running. To determine an acceptable stoppage time in the simulations, the spreading speed of the front toe was monitored. It was found that the rate of decrease of spreading speed of the front in flume tests declined very slowly once it was less than 0.3 mm/s. Consequently, the simulations were stopped when the spreading speeds were slower than 0.3 mm/s.

Regular hexahedra were used to discretise the 3D geometries of flumes and care was taken to reduce the difference in sides of the elements in order to increase the accuracy of the simulations. Square cells were used to discretise the 2D computational domain of mini-slump test simulations. Mesh independence was verified for all simulation results in the present work and is discussed later in Section 4.4.1.1.

4.4.1 Yield stress measurement with laboratory flume test

This section investigates the potential for using the laboratory flume test for measuring yield stress. Firstly, simulations of flume tests using relatively low yield stress (18.6Pa) material with frictionless and nonslip sidewalls were conducted to find out the difference between the SSF model and FG model predictions and to suggest which model is more appropriate for simulating laboratory flume tests. The influence of yield stress and viscosity variations on final profiles in the flume test was studied and the applicability of flume tests interpreted using the FG model for relatively high yield stress (56.1 Pa)

material was investigated. It is worth noting that the focused range of yield stress values in the present work is roughly from 20 Pa to 60 Pa which covers the majority of cases of actual thickened tailings disposal operations [66]. The materials with yield stresses of 18.6 and 56.1 Pa employed in this work were mixtures of kaolin clay and water.

4.4.1.1 Comparison between SSF and FG models for yield stress measurement using laboratory flume tests.

To determine the preferred model for simulating laboratory flume tests, simulations of four cases of flume tests on material of 18.6 Pa were performed. Information on the four cases is listed in **Table 1**. As shown in **Table 1**, nonslip-wall conditions were enforced on the sidewalls in Cases 1 and 2 and free-slip conditions were applied to the sidewalls in Cases 3 and 4. The flume bases in all four cases used nonslip-wall conditions. Two inlet velocities (0.2 m/s and 1 m/s) were used to evaluate the influence of flow rate on the final profiles achieved in the laboratory flume tests.

Table 1 Detailed information of the 3D simulations of flume tests for the investigation of sidewall friction and inflow rate (The material properties are: 18.6 Pa, 0.32 Pa·s and 1315.0 kg/m^3)

Cases	v_{inlet}(m/s)	Flow rate(litre per minute)	Sidewalls	Flume bottom	Discharge time(s)
Case 1	1	26.46	Nonslip	Nonslip	12
Case 2	0.2	5.292	Nonslip	Nonslip	60
Case 3	1	26.46	Free-slip	Nonslip	12
Case 4	0.2	5.292	Free-slip	Nonslip	60

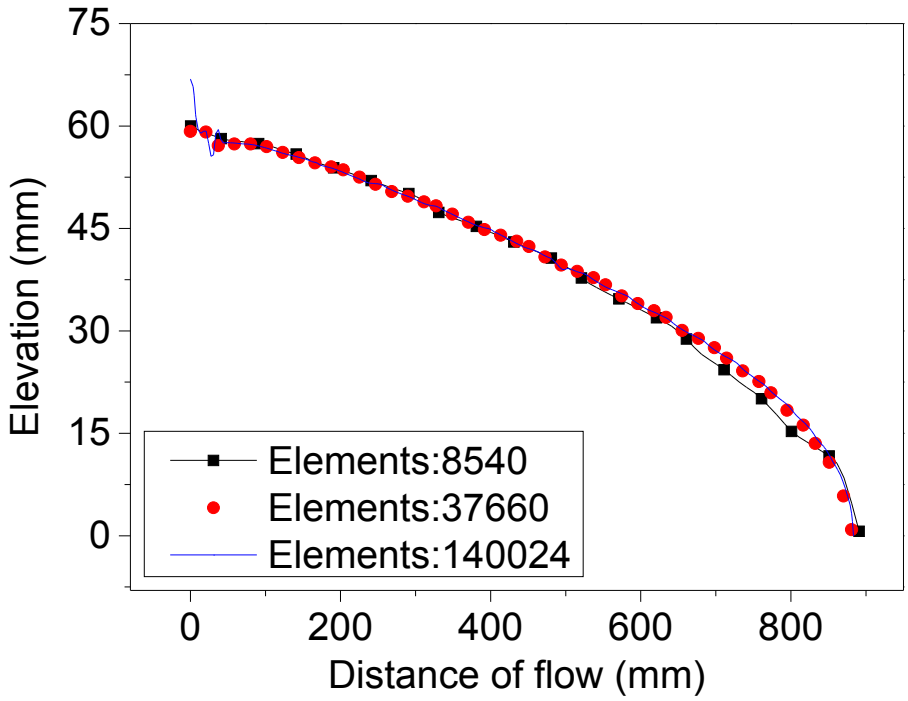

Figure 4 Final profiles from flume test simulations of different elements for mesh-independence study for Case 1 listed in **Table 1**.

An evaluation of mesh-independence was performed for all the simulations in the present work but only that for Case 1 listed in **Table 1** is presented as an example. **Figure 4** illustrates the final profiles from the flume test simulations of Case 1 in **Table 1** with three different numbers of elements: 8540, 37660 and 140024. It is evident that the final profile from the simulation with 8540 elements is slightly different from the other two as a result of the coarser mesh. The final profiles of the simulations with 37660 and 140024 elements virtually coincide, except for a minor difference close to the discharge point. Accordingly, the profiles of these two simulations are mesh-independent and the final profile of the simulation with 140024 elements was utilised in the work.

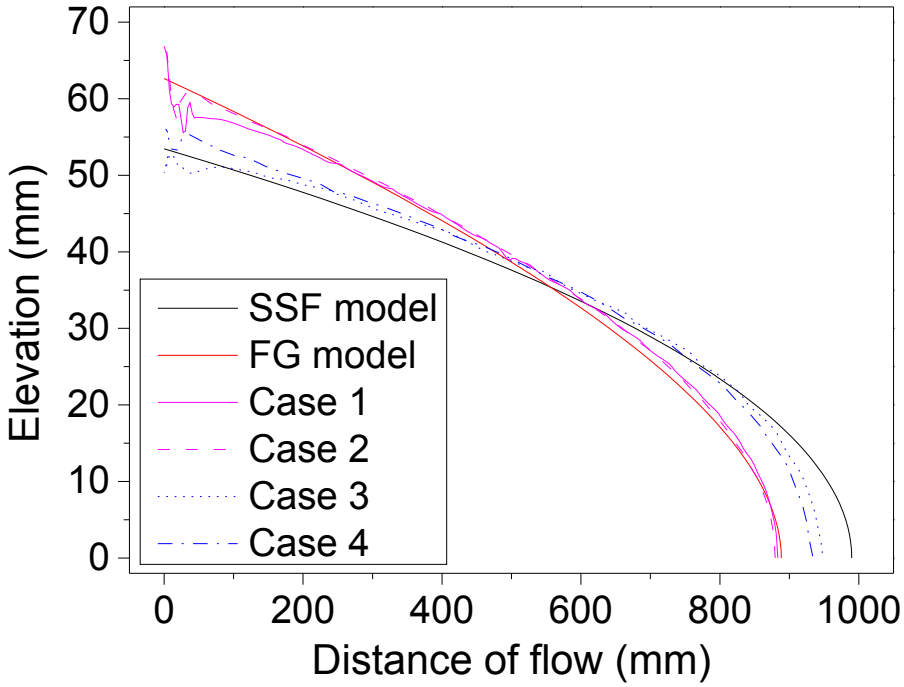

Figure 5 Final profiles of the four cases listed in **Table 1** and the predictions from SSF and FG models. The material properties are: 18.6 Pa, 0.32 Pa·s and 1315.0 kg/m^3.

Figure 5 summarises the final profiles of the four cases listed in **Table 1** and the predictions from the SSF and FG models. It is noted that the material properties used for the model predictions are the same as those used in the numerical simulations. The predicted profiles are not a best-fit curve obtained by varying the yield stress of the material, as is usually done. It can be seen from **Figure 5** that the profiles from simulations with free-slip sidewalls (Cases 3 and 4) agree well with the SSF prediction despite the fact that the flow distances from simulations are slightly shorter than the predicted distance of flow. The FG model yields very good prediction for the simulations with nonslip boundary conditions enforced on the sidewalls of the flume (Cases 1 and 2). It indicates that the difference between the SSF and FG models results from the friction along flume sidewalls as discussed in Section 4.2.3. Moreover, the differences in the final

profiles between Cases 1 and 2, and Cases 3 and 4 are most pronounced for the area near the deposition point. The inlet velocity has relatively little effect on the equilibrium profile, and is certainly insignificant compared to the effect of slip vs non-slip wall conditions. The inertial effects during the flume tests with different inlet velocities (1 and 0.2 m/s) were thus relatively modest. In addition it is clear that the slopes from the cases with nonslip sidewalls (Cases 1 and 2) are steeper than those with free-slip sidewalls (Cases 3 and 4), indicating that nonslip flume sidewalls tend to increase the slopes achieved in flume tests. This is one reason why slopes from flume tests on thickened tailings tend to overestimate the beach slopes achieved in the field.

Figure 6 shows the iso-surfaces of volume fraction of 0.5 from Cases 1 and 3 to demonstrate the relative influence of nonslip sidewalls and free-slip sidewalls. As can be clearly seen from **Figure 6** (a), the profile from a simulation with nonslip sidewalls has a tongue-shaped front, whereas the profile from a simulation with free-slip sidewalls has a linear front (**Figure 6**(b)). **Figure 7** shows the profile of thickened tailings in a laboratory flume test with sidewalls made of glass. The tongue-shaped front and the little ripples on the surface of the tailings suggest that sidewall friction did exist in the laboratory flume test (despite glass being used) and should not be neglected. It is widely accepted that a no-slip boundary condition at the wall is valid for viscous fluid within the framework of a continuum hypothesis where the fluid is considered to be homogeneous and of uniform properties [123-125]. Coussot [126] carried out open channel experiments on natural clay-water mixtures at different solid concentrations. Both rough (expanded metal with

an equivalent roughness of 6 mm) and smooth (plywood) channel walls (bottom and sides) were utilised and no slip along channel sides and bottom was observed. Fourie and Gawu [26] conducted tests in a 150 mm wide flume on flocculated gold tailings at 59% solids content. The flume was made of Perspex to enable observation and measurement of the deposit profile. Very good agreement was achieved between the measured profile in the flume test and the profile predicted by the FG model using a fully sheared yield stress value independently determined by a vane method. Consequently, the FG model which takes the friction of sidewalls into account is considered more relevant for laboratory flume tests unless a zero-friction sidewall condition can be guaranteed, (which is very difficult).

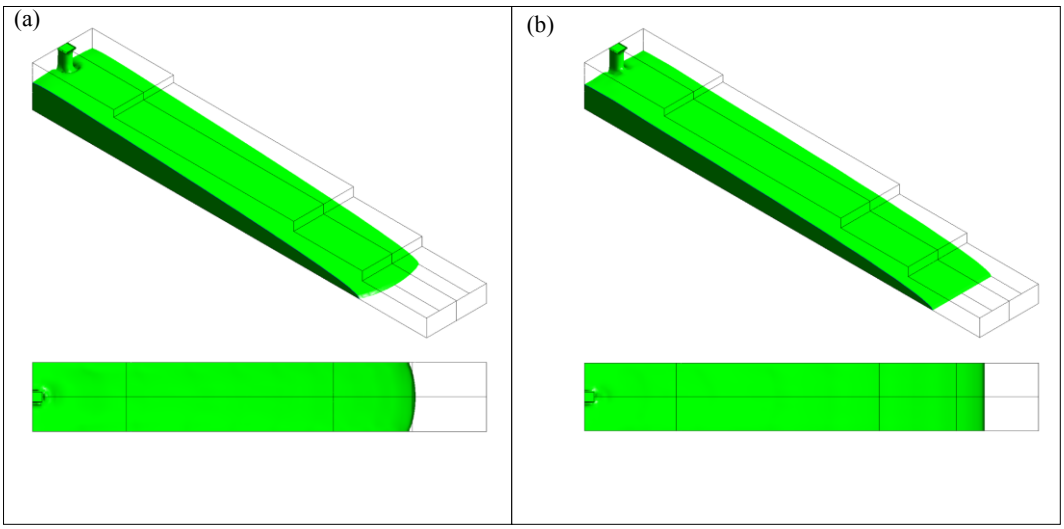

Figure 6 Comparison between isosurfaces of volume friction of 0.5 from flume test simulations (Case 1 and Case 3 in **Table 1**) with nonslip sidewalls (a) and free-slip sidewalls (b). The material properties are: 18.6 Pa, 0.32 Pa·s and 1315.0 kg/m^3.

Figure 7 A laboratory flume test with glass sidewalls on thickened tailings. The photo is provided by Paterson & Cooke Chile.

Does the SSF model (free-slip condition) hold if the sidewalls of the flume are greased? An interesting experiment was conducted by Coulomb, which was referred to by Stokes [127]. Coulomb oscillated a metallic disk in water, initially very slowly. Then the disc was smeared with grease. Finally the grease was even covered with powdered sandstone. To Coulomb's surprise the resistance was hardly increased in the two latter cases. Recently Henriquez and Simms [34] carried out laboratory flume tests to investigate the multilayer deposition of gold paste tailings. The flume was made of transparent acrylic with a width of 150 mm. They reported that there was no significant effect on the final profile achieved in the flume when a hydrophobic grease was used to lubricate the flume

walls. Apparently the ungreased flume walls were not frictionless otherwise it would be nearly impossible to stop the tailings from travelling in their horizontal flume. Since there was no noticeable difference in the profiles from greased and ungreased flume tests, we may deduce that the greased flume walls had a similar condition to the ungreased walls which were evidently not free-slip. Therefore the SSF model, which assumes the sidewalls are frictionless, does not hold for laboratory flume tests, even when the walls are greased.

According to the discussions above it is believed that the FG model, which takes sidewall friction into account, is more applicable for simulating flume tests than the SSF model, which assumes that the sidewalls are free-slip, particularly considering that the walls of nonslip or negligible-slip conditions are easier to achieve than free-slip conditions.

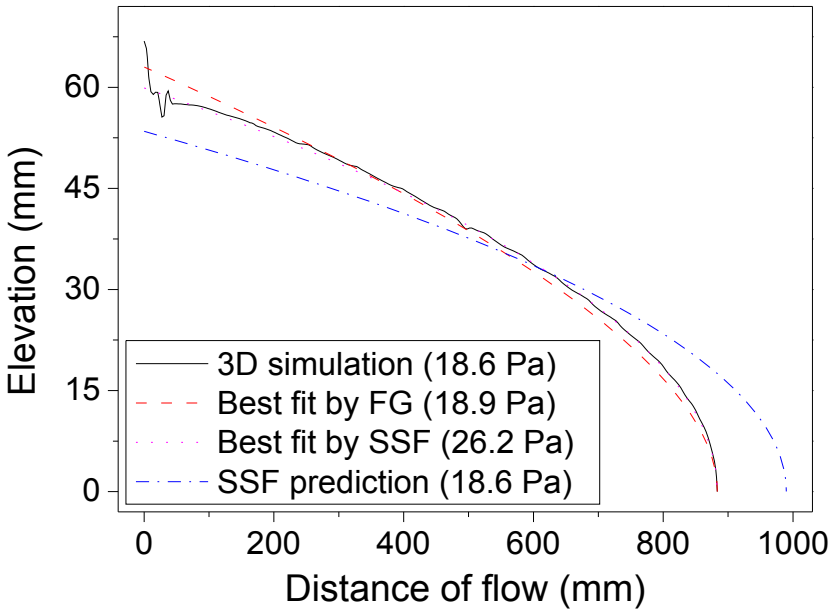

Figure 8 Comparison between the profiles from 3D simulation (Case1 in **Table 1**), best fit curves by FG and SSF models and the SSF prediction with 18.6 Pa used in simulation.

To illustrate the consequences of using the SSF model to calculate the yield stress from flume test data, the profile of Case 1 in **Table 1**, the best fit curves from the SSF and FG models as well as the SSF prediction using the yield stress (18.6 Pa) employed in the simulation are summarised in **Figure 8**. The best-fit yield stresses by the FG and SSF models were computed from the flow distance of the 3D simulation. As shown in **Figure 8** the best-fit yield stress from FG model is 18.9 Pa which is very close to 18.6 Pa, the true yield stress used in the simulation. (It is noted that the term "true yield stress" is used to designate the yield stress used in a CFD simulation, thus differentiating it from the one back-calculated using a best-fit method). However the best-fit yield stress from SSF model is 26.2 Pa which is nearly 41% higher than the true yield stress. The predicted profile by SSF model with the true yield stress (18.6 Pa) is longer and flatter than that of the simulation with non-slip sidewalls as shown in **Figure 8**. Thus the SSF model tends to overestimate the yield stress if results from a laboratory flume test are back analysed. It is noteworthy that if the inertial effects in the flume test are just strong enough such that the final profile of the simulation in **Figure 8** is "pushed" further and flatter to coincide with the SSF prediction (18.6 Pa), the yield stress from best fit using SSF model may be consistent with the true yield stress. This is because the inertial effects counteract the sidewall friction so that it appears that there is no sidewall friction. However, this coincidence should not justify the applicability of the SSF model in the laboratory flume test.

To summarise, it would be unconservative to use the SSF model to assess the yield stress

in a laboratory flume test as the preconditions of free-slip sidewalls (or small enough ratios of fluid depth to characteristic length scale of the contact surface with the plane bed) are rarely fulfilled for a laboratory flume on thickened tailings slurry as shown in **Figure 7**. Considering that the FG model taking sidewall friction into account yields excellent predictions for the profiles of 3D simulations of flume tests, it may be feasible to obtain the yield stress of a material by fitting the FG model to the final profile achieved in a laboratory flume test (as long as inertial effects are not significant).

4.4.1.2 The influence of yield stress and viscosity variations on final profiles in the flume test.

Since the FG model does not account for fluid viscosity, which may influence the inertial effects and hence the final profile to some extent, it is of interest to investigate the influence of viscosity in the flume test. Simulations of flume tests in three cases were performed to assess the "sensitivity" of the final profiles to the variations of yield stress and viscosity. Information on the three cases is listed in **Table 2**. **Figure 9** illustrates the profiles of the 3D simulations listed in **Table 2** as well as the profiles predicted by the FG model with the corresponding yield stresses employed in simulations: 18.6 Pa and 27.9 Pa. Although the viscosity of Case 2 increased by 50% over the base case (Case 0), the final profile of Case 2 is remarkably similar to Case 0 and both profiles (Case 0 and Case 2) are well predicted by the FG model with 18.6 Pa, as shown in **Figure 9**. It suggests that the influence of viscosity on the final profiles achieved in the laboratory flume test is relatively minor. As clearly illustrated in **Figure 9**, however, the same percentage

variation of yield stress resulted in a significant change in the profiles between Case 1 and Case 0. It can be concluded that the final profile in the laboratory flume test, where the inertial effects are relatively weak, is highly sensitive to the yield stress variation but virtually insensitive to the variation of viscosity, thus suggesting use of the FG equations to obtain the yield stress from a flume test even though the model does not take the viscosity of fluid into account. Also, it is noted from **Figure 9** that the final profile of Case 1 was well predicted by the FG model with the same yield stress (27.9 Pa) used in the simulation. The yield stress in thickened tailings slurry disposal operations typically ranges from 20 to 50 Pa [66]. Since we have already shown that laboratory flume tests with relatively low yield stress (18.6 Pa and 27.9 Pa) materials are amenable to interpretation using the FG model, it is desirable to confirm if this approach is also suitable for higher yield stress material.

Table 2 Cases for the investigation of yield stress and viscosity influence in flume test

Cases	v_{inlet} (m/s)	Flow rate(LPM)	Boundary conditions for sidewalls and bottom	Discharge time (s)	Yield stress (Pa)	Viscosity (Pa·s)
Case 0	1	26.46	Nonslip	12	18.6	0.32
Case 1	1	26.46	Nonslip	12	1.5×18.6	0.32
Case 2	1	26.46	Nonslip	12	18.6	1.5×0.32

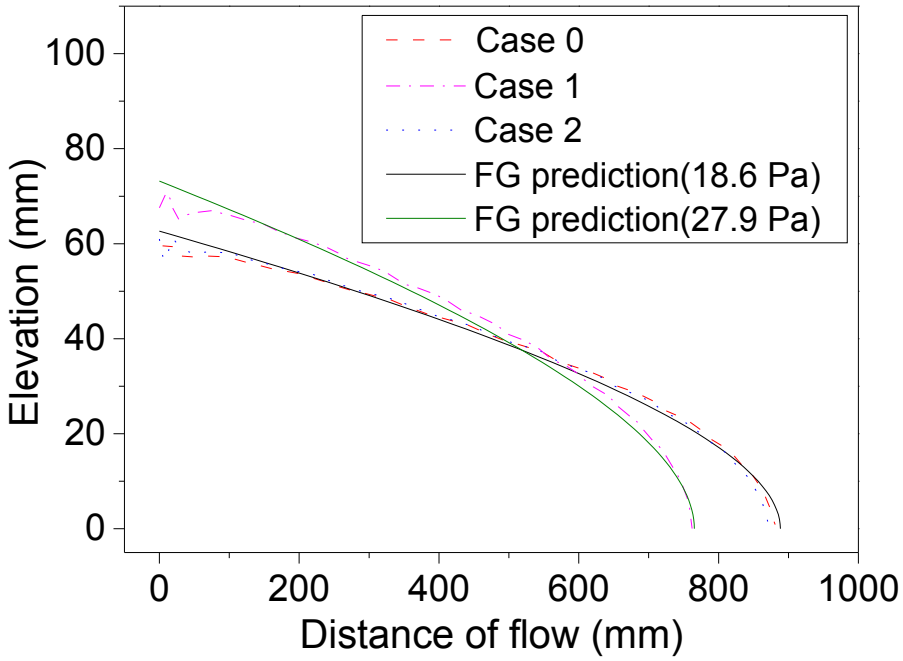

Figure 9 Comparison of profiles from simulations of the cases listed in **Table 2** and FG predictions with yield stresses of 18.6 and 27.9 Pa.

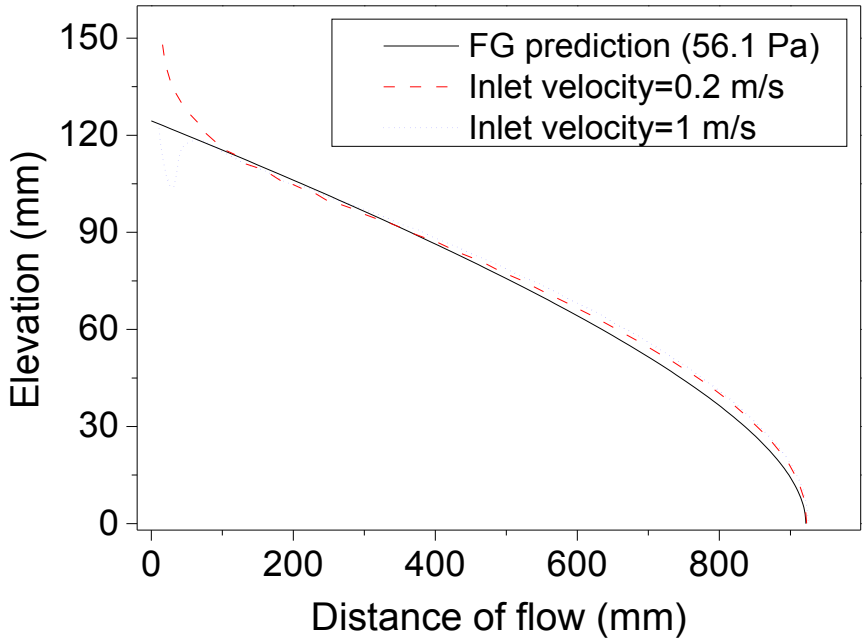

Figure 10 Final profiles from 3D simulations of flume tests with different inlet velocities on materials of relatively high yield stress and FG prediction. The material properties in the two simulations are: 56.1 Pa, 0.73 Pa·s and 1377.2 kg/m^3.

Two simulations of flume tests with the same volume of Bingham fluid at 56.1 Pa and 0.73 Pa·s were carried out. Two inlet velocities (0.2 and 1 m/s corresponding to inflow rates of 5.29 and 26.46 LPM) with corresponding discharge times of 120 s and 24 s were employed to assess the influence of inflow rate on final profiles. **Figure 10** shows the final profiles from the two simulations of flume tests with different inlet velocities and the FG prediction with 56.1 Pa which was used in the two simulations. The excellent agreement between the FG prediction and the simulation results suggests that the laboratory flume test interpreted with the FG model is relevant to both low yield stress and relatively high yield stress materials. Although the profiles around the inlet are very different for the two simulations due to the different inlet velocities, the remainder of the profiles are very similar, as shown in **Figure 10**. Moreover, the flow distances from the two simulations are initially virtually identical to the predicted value but slowly diverge when the flow distance is larger than 400 mm. Therefore it may be advisable to obtain the yield stress by using the flow distance rather than the entire profile as the different inflow rates used here have less influence on the total flow distances than they do on the shape of the profiles. In addition, it is easier to measure the flow distance than the entire profile in a flume.

4.4.2 Comparison between laboratory flume test and mini-slump test for yield stress measurement

To investigate the influence of mould lifting velocities on the final profiles in mini-slump

tests, six cases of simulations with three lifting velocities (10, 50 and 100 mm/s) for materials with yield stresses at 18.6 and 56.1 Pa were performed. A cylindrical mould with an inner diameter and a height of 79 mm was employed in the simulations. Information on the numerical model (CFD) for simulations of mini-slump tests with the mould lifting process taken into account can be found in our previous work [72]. **Figure 11** shows the final profiles of the six cases of mini-slump tests. It is evident that both slumps and spreads were influenced significantly by the variation of mould lifting velocities for lower yield stress material, as shown in **Figure 11**(a). Although the spreads did not change significantly in **Figure 11**(b), the slumps declined considerably with an increase of model lifting velocities from 10 to 100 mm/s. It reveals that the model lifting velocity has an important effect on the final profile in a mini-slump test, which has been noticed by several workers [72, 97]. Because the yield stress is extracted from the spread or slump value, the lifting velocity of the mould may thus influence the yield stress to a certain extent. Considering the mould lifting process is typically performed manually, the yield stress from a mini-slump test tends to be operator-dependent, especially for material with a relatively low yield stress.

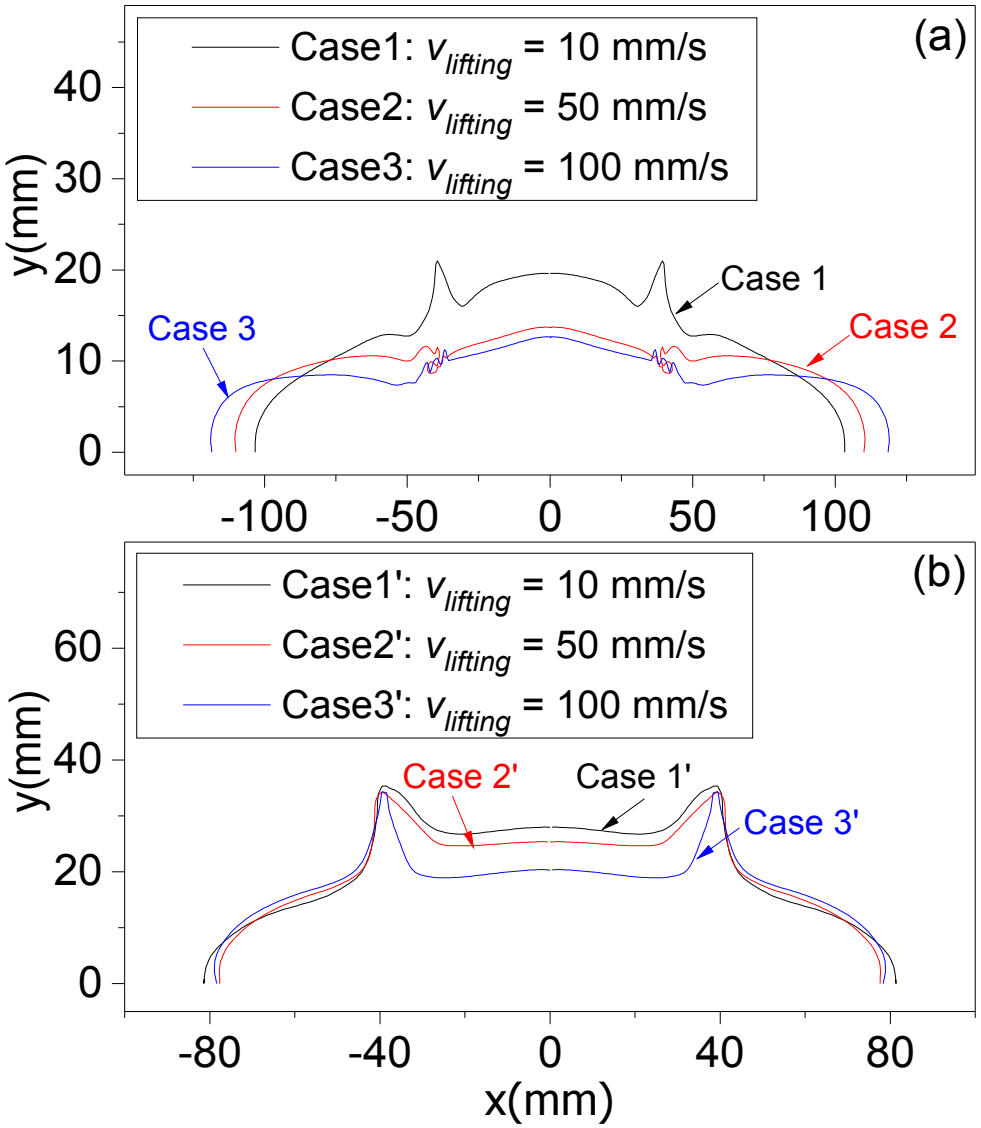

Figure 11 Final profiles from simulations of mini-slump test with different mould lifting velocities on materials (a) 18.6 Pa, 0.32 Pa·s and 1315.0 kg/m^3 and (b) 56.1 Pa, 0.73 Pa·s and 1377.2 kg/m^3.

There are several theoretical models used to evaluate the yield stress in slump test. Pashias and Boger [50] established the correlation between the slump and yield stress for a cylindrical slump test:

$$s' = 1 - 2\tau_y'\left[1 - ln\left(2\tau_y'\right)\right] \tag{22}$$

where s' and τ_y' are slump and yield stress in dimensionless form, which are given by:

$$s' = \frac{s}{H_0},\ \tau_y' = \frac{\tau_y}{\rho g H_0} \tag{23}$$

where s is the slump and H_0 is the height of the cylindrical mould.

With the Von Mises yield criterion implemented, a similar analytical solution was proposed by Roussel and Coussot [95] for the cylindrical slump test:

$$s' = 1 - \sqrt{3}\tau_y'\left[1 - ln\left(\sqrt{3}\tau_y'\right)\right] \tag{24}$$

Kokado et al. [128] derived the analytical solutions for the slump test on fluids of relatively low yield stress within the framework of long-wave approximation:

$$\tau_y = \frac{225\rho g V^2}{4\pi^2 {SP_f}^5} \tag{25}$$

where V is the volume of the tested material, SP_f is the final diameter of the collapsed material (i.e. spread).

Figure 12 illustrates the difference between the profiles predicted by the three theoretical solutions listed above and the CFD simulation results for a mould lifting velocity of 10 mm/s for mini-slump tests on materials of yield stresses of 18.6 and 56.1 Pa. Generally, the model of Kokado et al. is more relevant to the simulation results in terms of the similarity of the profiles for both materials. For a mini-slump test on the material of 18.6 Pa, the predicted slumps and spreads from the models of Pashias et al. and Roussel and Coussot (RC) are very different from the simulation results, whereas the model of Kokado et al. yields much better predictions, indicating that the first two models are not valid for the flow dominated by "pure shear flow" [95]. Even though the model of Kokado et al. is

more accurate for the 18.6 Pa material, the extrapolated yield stress with the model is around 29 Pa, 57% higher than the true yield stress (18.6 Pa). It appears that the models of Pashias et al. and RC made better predictions with respect to the slump for the material at 56.1 Pa than for 18.6 Pa as shown in **Figure 12**. However, differences between the predicted and simulated profiles are still evident.

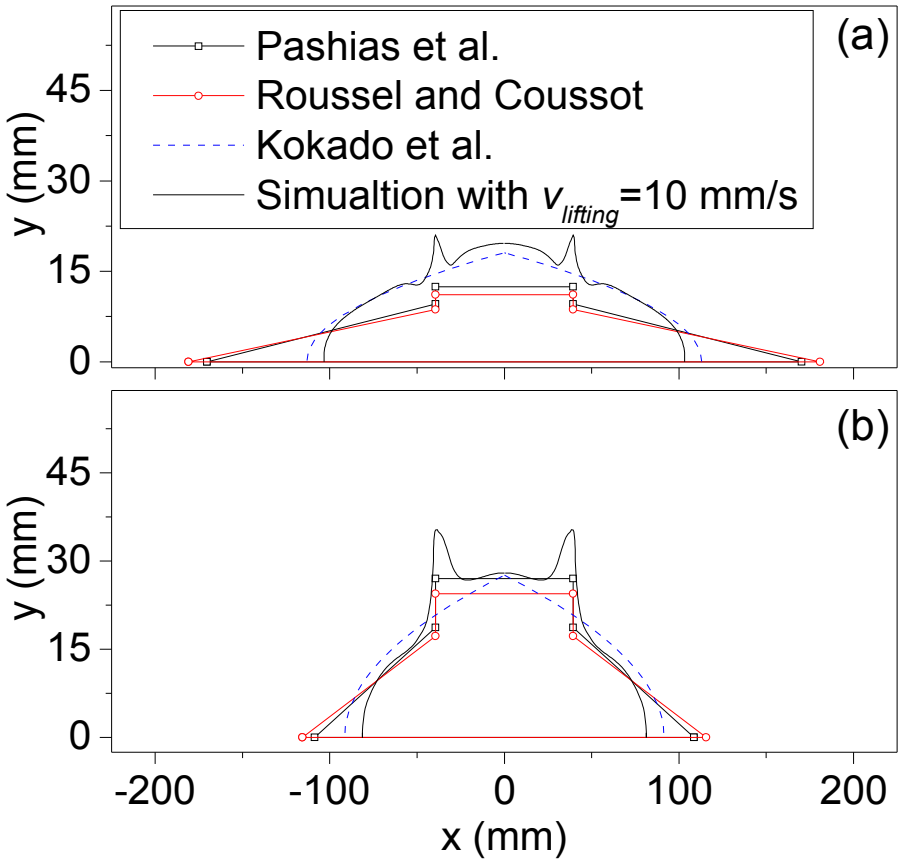

Figure 12 Profiles from the predictions using three different theoretical models and the simulation results for mini-slump tests on materials (a) 18.6 Pa , 0.32 Pa·s and 1315.0 kg/m^3 and (b) 56.1 Pa, 0.73 Pa·s and 1377.2 kg/m^3.

Table 3 summarises the yield stresses extrapolated from the results of six simulations for mini-slump tests (slump or spread values) using the three theoretical models (Eq.(22) to

Eq.(25)) as well as the corresponding percentage errors. The percentage error is given by:

$$Percentage\ error = \frac{Calculated\ value - True\ value}{True\ value} \times 100\% \quad (26)$$

Table 3 The yield stresses calculated from mini-slump test simulations with different theoretical models and the corresponding percentage errors.

Yield stress employed in simulation (Pa)	Lifting velocity of the mould (mm/s)	τ_y calculated by the model of Pashias et al.(Pa)	τ_y calculated by the model of Roussel and Coussot (Pa)	τ_y calculated by the model of Kokado et al. (Pa)
18.6	10	34.2 (+83.5%)	39.4 (+111.9%)	29.3 (+57.4%)
56.1	10	58.9 (+5.1%)	36.4 (+21.3%)	101.1 (+80.2%)
18.6	50	21.1 (+13.5%)	24.4 (+31.1%)	21.0 (+12.8%)
56.1	50	51.2 (-8.8%)	59.1 (+5.4%)	127.2 (+126.7%)
18.6	100	19.0 (+2.2%)	22.0 (+18.0%)	14.5 (-22.2%)
56.1	100	37.4 (-33.2%)	43.2 (-22.9%)	117.6 (+109.7%)

For the material with yield stress of 18.6 Pa, the errors of the yield stresses calculated using the models of Pashias et al. and RC decrease with the increase of mould lifting velocity (or inertial effects), as shown in **Table 3**. Moreover, for the material with yield stress of 18.6 Pa, the error of Kokado et al. model for lifting velocity of 50 mm/s is +12.8% which is much smaller than an error of +57.4%, which corresponds to a lifting velocity of 10mm/s. Since all the theoretical models for slump tests are established on the assumption that there are no inertial effects (at least negligible) in the slump test, the inertial effects (or lifting velocity of the mould) should be as small as possible in the tests in order to obtain accurate yield stresses using the theoretical models. However the relatively small lifting velocity of the mould at 10 mm/s yielded worse results than 50 mm/s for material of 18.6 Pa. Moreover, for the material of 56.1 Pa, the errors for both Pashias et al. and RC decrease with an increasing mould lifting velocity from 10 mm/s,

which indicates that lower lifting velocity does not always yield more accurate yield stress values, even though the theoretical models do not account for any inertial effects. One of the reasons is that the mould lifting process distorted the final profile of the slumped material, making it diverge from the final profile it should be (without mould influence). Additionally, the theoretical models are based on many assumptions and some of them may be not entirely valid in the real test. Overall, not only the variation of mould lifting velocities but also the mould lifting process itself has an influence on the final profile, thereby making the theoretical models unable to capture the final profiles of a mini-slump test accurately; accordingly, the yield stress extrapolated from a mini-slump test is likely to be only approximate. It is stressed that although the mini-slump test is not an accurate method to measure the yield stress, it is still a quick and easy way to assess the rheological properties of thickened tailings in the field, and in particular to provide a means of quality control.

Laboratory flume tests may be superior to mini-slump tests for yield stress measurement of thickened tailings in terms of accuracy. Firstly, the final profile in a mini-slump test is more likely to be influenced by inertial effects than in a laboratory flume test. For example, for the mini-slump test with a mould lifting velocity of 50 mm/s on the material of 18.6 Pa, the flow duration was approximately 0.5 s for a slump of around 65 mm according to our simulation. The typical inertial stress ($I = \rho v^2$) was $I \approx 22.2$ Pa which is even larger than the yield stress (18.6 Pa) of the tested material. However, for the laboratory flume test with an inlet velocity of 1 m/s on the same material (Case 0 in **Table 2**), the flow

duration was of the order of 15 s for a flow distance of 883 mm. Thus the typical inertial stress for the flume test was $I \approx 4.6$ Pa, which is much smaller than the yield stress of the material (18.6 Pa). The final profile of material in a mini-slump test tends to be distorted by the inertial effects, thereby influencing the accuracy of the extrapolated yield stress. For the laboratory flume test, on the other hand, the flow speed of the material in the flume is relatively low as a result of the small inlet, low inlet velocity and the extra resistance from sidewalls. Accordingly, inertial effects in the flume test are negligible, which improves the accuracy of this approach. Moreover, the volume of fluid in a mini-slump test is normally much less than that used in a laboratory flume test which may result in larger measurement error in the mini-slump test than in the flume test.

The simulations of flume tests undertaken in the work, the extrapolated yield stresses from the simulations with FG model and the corresponding percentage errors are summarised in **Table 4**. The minor deviations of the yield stresses extrapolated from the FG model from the true values used in simulations indicate that the laboratory flume test interpreted using the FG model may provide an accurate and robust method for measuring the yield stress of thickened tailings. Since the flume test has been widely used in studies of potential tailings disposal operations, being able to extract an accurate measure of yield stress from the results of a flume test using the FG model is an added bonus, requiring no additional effort. Moreover, although further investigation is required, it may be possible to downscale the laboratory flume to a desktop-flume (similar to the Bostwick Consistometer used in the food industry in terms of the flume size [129]) which may

provide a cheap and easy way for yield stress measurement of thickened tailings in both laboratory and the field without necessarily utilising costly and sophisticated equipment such as a vane rheometer.

Table 4 The yield stresses calculated from flume test simulations with FG model and detailed information of the simulations.

Simulation number	Inlet velocity (m/s)	τ_y used in simulations (Pa)	Viscosity (Pa·s)	Density (kg/m^3)	Discharging time (s)	Flow distance from simulation (mm)	τ_y calculated by FG model (Pa)	Error (%)
1	1	18.6	0.32	1315.0	12	883.35	19.0	+2.15
2	0.2	18.6	0.32	1315.0	60	879.60	19.1	+2.69
3	1	1.5×18.6	0.32	1315.0	12	762.05	28.2	+1.08
4	1	18.6	1.5×0.32	1315.0	12	872.98	19.5	+4.84
5	1	56.1	0.73	1377.2	12	598.18	56.6	+0.89
6	0.2	56.1	0.73	1377.2	60	599.69	56.2	+0.19
7	1	56.1	0.73	1377.2	24	925.13	55.6	-0.89
8	0.2	56.1	0.73	1377.2	120	922.55	55.9	-0.36

In the oil sands industry, high molecular weight polymers are widely used to flocculate mature fine tailings (MFT) before or during deposition to enhance dewatering and shear strength development. The flocs may range from several millimetres to half a decimetre in size which can be easily identified visually, and physically separated from the flowing mass [130]. The presence of floc aggregate masses results in heterogeneous fluids for which the vane technique may be inappropriate for measuring the yield stress, as the continuum assumption (density, velocity etc.) that any rheological approach relies on, for the flocculated MFT may be invalid [131]. In the stress growth technique [62], where the vane rotates at a low and constant speed with the torque (or shear stress) measured as a

function of time, the shear stress tends to fluctuate with time if the continuum assumption is invalid. This phenomenon was observed in the stress growth tests for both pulp fibre suspensions and flocculated MFT [132, 133]. For the flume test, the floc structures formed in the polymer-amended MFT are sheared and degrade during the discharge and deposition. Therefore the continuum assumption is more reasonable in flume tests. More importantly, the flocculated MFT experiences shearing as well when it is pumped and transported by pipeline and discharged to the deposition site [134]. Consequently, it is suggested that the flume test may be more appropriate than the vane test for flocculated MFT as the yield stress from a flume test may be more characteristic of the behaviour during surface deposition considering the similarity between a flume test and field deposition, as reported by Mizani et al. [133, 135].

4.4.3 The application of a laboratory flume test to measuring yield stress

Several comments on the laboratory flume test used for yield stress measurement may be made:

- The yield stress of the thickened tailings should be roughly between 20 Pa to 60 Pa. The technique may well be applicable outside this range, but was not investigated in this work. The tailings tested should be non-segregating.
- Make sure the flume is horizontal which will simplify the calculations.
- It is not necessary to lubricate the sidewalls or base since the FG model assumes that the shear stresses at walls are equal to the yield stress of the material. Do not wet the flume before testing, as the water content of the thickened tailings near the walls will

otherwise be increased, thereby reducing the shear stress on the walls and distorting the inferred yield stress value.

- A small discharge nozzle with low flow velocity should be used so that the inertial stress will be negligible compared to the yield stress of the tested material. According to our simulations, a tube with a diameter of 21 mm and discharge velocity of 0.2 m/s can guarantee negligible inertial effects.
- The height between the outlet and the flume base should be as small as possible (within reason) to reduce the inertial effects, especially for tailings of low yield stress.
- Make sure sufficient fluid is discharged into the flume to form a profile that is long enough. Firstly, the long flow distance should reduce measurement error, and secondly, with an increase of the volume of fluid discharged into the flume, the spreading speed of the fluid will reduce gradually as shown in **Figure 13**, thereby reducing the inertial effects.
- The flow distance along the centreline of the flume and the volume of the fluid deposited should be measured and used to calculate the yield stress.
- The discharge time can be recorded if feasible, which can be used to calculate the average spreading speed of the fluid in the flume, thus assessing the inertial stress in the test.
- Given the volume (V) of fluid discharged into the flume, the flow distance (L), fluid density (ρ) and the flume width (w), the yield stress (τ_y) can be calculated from Eqs.(16) and (18).

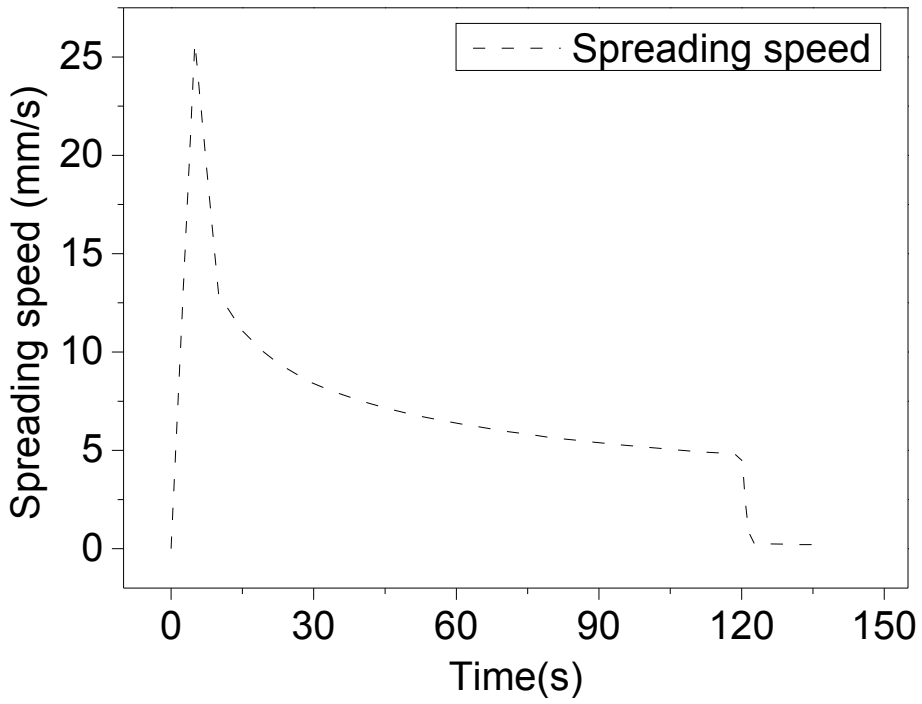

Figure 13 Spreading speed evolution of the front in the simulation of flume test with a discharging time of 120 s. The inlet velocity is 0.2 m/s and material properties are: 56.1 Pa, 0.73 Pa·s and 1377.2 kg/m^3.

4.5 Conclusions

All of the discussions and conclusions in the present work are based on fluids with yield stresses from approximately 18 to 60 Pa and viscosity from around 0.3 to 0.8 Pa·s which are homogeneous and non-segregating. The pipe discharging fluid into the flume test is relatively small (21 mm × 21 mm) with low inlet velocities (0.2 and 1 m/s).The inertial effects are thus negligible in the flume test. The flume width is not very wide (150 mm in this work). Specific conclusions include:

1. The SSF model for slow spreading of a sheet of yield stress fluid is generally not valid for laboratory flume tests of thickened tailings due to the sidewall friction of the flume.

Theoretically this model only holds if the flume width is infinite or the sidewalls of a flume are frictionless (the inertial effects certainly should be negligible).

2. The excellent agreement between the predicted profiles by the FG model and the simulation results with nonslip bottom and sidewalls shows that the FG model, which was developed for laboratory flume tests and took the sidewall friction into account, is more appropriate to model laboratory flume tests as long as the wall slip at the sidewalls and base is negligible.
3. Laboratory flume tests with low deposition rates can be used to measure the yield stress of non-segregating thickened tailings by using the FG model. Moreover, simulation results reveal that the final profile in a flume test is sensitive to yield stress variation but relatively insensitive to the variation of viscosity, which is beneficial for yield stress measurement as the FG model, which is used to obtain yield stress from the final profile, does not account for viscosity.
4. The results of mini-slump test simulations demonstrate that different mould lifting velocities may introduce different inertial effects, thereby impacting the final profiles. Moreover, comparison between the predicted profiles by several theoretical models for the slump test and CFD simulation results reveals that the existing models are not capable of capturing the final shape of slumped material accurately, not only because of the inadequacy of the theoretical models but also the final profile is distorted by the wall friction of the mould. Consequently, the degree of accuracy of the yield stress calculated from a mini-slump test is not very high. Notwithstanding, the mini-slump test provides a

quick and easy way to evaluate the rheological properties of thickened tailings to a first approximation in the field.

5. The minor errors of the yield stress calculated from the simulation results suggest that the flume test interpreted with the FG model is extremely accurate with respect to determining the yield stress of thickened tailings. Therefore, it may provide a cheap and robust way of measuring the yield stress of thickened tailings without necessarily resorting to a costly rheometer. Moreover, the flume test may be more appropriate for the yield stress measurement of heavily flocculated clay tailings (e.g. MFT) compared with the vane technique, considering the similarity (i.e. materials are sheared before and during deposition) between the flume test and field deposition, as well as the possible invalidity of the continuum assumption caused by the presence of large floc particles, which constitute a disadvantage in the vane test, given the small size of vanes typically used.
6. The opportunity exists for downscaling the laboratory flume to a desktop-flume, which may lead to a cheap, easy and accurate way for yield stress measurement of thickened tailings in both the laboratory and the field.

Acknowledgements

This work was supported by resources provided by the Pawsey Supercomputing Centre with funding from the Australian Government and the Government of Western Australia; the first author gratefully acknowledges the China Scholarship Council (CSC) and The University of Western Australia for financial support.

5. GENERAL CONCLUSIONS

5.1 The significance of the work

With the development of the thickening technique, thickened tailings disposal has seen increasing popularity in mine waste management resulting from its inherent advantages over conventional tailings disposal. The beach slope prediction is of critical importance for thickened tailings disposal, which typically involves a laboratory flume test. The laboratory flume test has been successfully used to predict the beach slope of conventional tailings for many years. However, it has been found to produce much steeper slopes for thickened tailings than the beach slopes achieved in the field. This difference is generally attributed to the presence of yield stress of thickened tailings which is a key design parameter for thickened tailings disposal. Although the mini-slump test has been widely used in industry to offer a quick estimation for the yield stress, its accuracy is relatively low due to some inherent defects. This thesis was conducted to study these problems.

Chapter 2 highlights factors that have previously been neglected when interpreting flume test data, and thus the work contributes to future work on interpretation of flume test data. Moreover, two dimensionless parameters were proposed to predict the average beach slope in 2D planar simulations of both S-R and discharge flume tests for thickened tailings. The proposed model offers some interesting possibilities for beach slope prediction of thickened tailings in the field, although further investigations are needed. Additionally

the good agreement between CFD simulation and experimental results found in literature enhances confidence in the veracity of the computational results. Therefore CFD simulations may offer a way to study the full-scale deposition of thickened tailings in future. Chapter 3 provides an in-depth computational study on the measurement of yield stress by slump testing. It focuses on the importance of mould removal speed when measuring the properties of relatively low yield stress materials. It firstly proves that the spread is superior to slump as the preferred measurement in the mini-slump test for paste with relatively low yield stress and viscosity, which provides a very useful guideline for the industrial application of the mini-slump test. To seek an alternative to the mini-slump test for accurate but cheap and easy yield stress measurement, Chapter 4 explores the feasibility of using a laboratory flume test to measure the yield stress of thickened tailings. The fundamental conclusion of this work, important for both industrial and research contexts, is that this approach can lead to a cheap, easy and accurate technique for yield stress measurement of thickened tailings in both the laboratory and the field.

5.2 The main findings of the thesis

5.2.1 Studies on thickened tailings deposition in flume tests using the CFD method

- Two dimensionless parameters were proposed to establish the relationship between the average slope and relevant parameters for a planar deposition of thickened

tailings based on both S-R and discharge flume tests, which has a potential to predict the beach slope of thickened tailings in the field, although further investigations are required.

- The slope of the final profile of a yield-stress fluid decreases with an increasing fluid volume, which indicates that the beach slope of thickened tailings is flow-scale dependent. In other words, it is not advisable to use small-scale tests for direct extrapolation to field applications;
- Higher energy results in longer and flatter final profiles of thickened tailings;
- Generally, the yield stress of thickened tailings has more influence on the slope than does viscosity. The importance of viscosity for the final profile formation of thickened tailings increases with an increase of inertial effects during the deposition process. Therefore, it is inferred that the influence of viscosity can be negligible if the inertia effects are sufficiently low in the deposition of thickened tailings;
- The flume width has a significant influence on the slope of thickened tailings in a laboratory flume test. A smaller flume width increases the slope of thickened tailings in a flume. This is an important result as it demonstrates the inadvisability of using slopes achieved in laboratory flume tests to directly extrapolate to beach slopes in field deposition;
- An increasing base angle results in the reduction of the resulting slope, which suggests that the beach slope of thickened tailings is influenced by base topography

in the field;

- The agreement between simulation results and laboratory observations in the literature gives confidence in the veracity of the computational results. Consequently, CFD simulations may provide a way to investigate the deposition of thickened tailings in a full-scale field impoundment.

5.2.2 Spread is better: An investigation of the mini-slump test

- Spread is superior to slump as the preferred measurement in the mini-slump test for paste with relatively low yield stress and viscosity when the lifting velocity is not very high (i.e. less than 1 cm/s) because spread is less sensitive to the variation of lifting velocity of the mould than slump;
- The varying trend of the ratio of inertial stress to yield stress (R_{IY}), which takes flow time to reach the stoppage, slump, spread, density and yield stress of paste into account, is a useful indicator for describing the variation of inertial effects in the mini-slump test. However if the value of R_{IY} can be the criterion to determine whether the inertial effects can be neglected or not in the mini-slump test still needs more thorough investigations;
- The lifting velocity of the mould has a significant influence on the spread and slump of the mini-slump test for paste of lower yield stress and viscosity. A higher lifting velocity may introduce stronger inertial effects, leading to larger spread and slump.

It is thus crucial to keep the lifting velocity of the mould as slow as possible (within reason) in the mini-slump test for paste of lower yield stress and viscosity. However, it is worth noting that when the lifting velocity of the mould is higher than a certain value, the final spread declines with an increasing mould lifting velocity as a result of end effects;

- Generally, an increase in viscosity can reduce the inertial effects and hence both slump and spread. Moreover, the variation of viscosity has more significant influence on the slump and spread of the mini-slump test where the inertial effects are stronger. Therefore it is not reasonable to artificially change the viscosity in simulations merely to obtain better agreement between experimental and numerical results, as is sometimes done;
- The yield stress of the paste has a stronger influence than viscosity on spread, slump, flow time and R_{IY}. In addition the flow time in the mini-slump test is strongly influenced by both yield stress and viscosity, which may be one of the reasons why the correlations between times to certain spread values and the plastic viscosity previously reported in the literature tend to be poor;
- The influence of mould lifting velocity on the slump and spread of mini-slump tests for lower viscosity and yield stress materials is more significant than higher viscosity and yield stress materials. Additionally it is realised that there is some potential for the mould lifting process to increase the slump and spread in the mini-slump test,

indicating that the lifting process of the mould should not be neglected in simulations of the mini-slump test;

- The increase of viscosity in a mini-slump test simulation wherein the mould is assumed to instantaneously disappear will increase the flow time, thereby resulting in a dramatic computing time increase. Additionally the 'no mould' simulation neglecting some important factors, such as the paste left on the wall, the wall friction and the constraint of the mould on the paste during flowing, cannot replicate the real flow behaviour of paste in a laboratory mini-slump test. The simulation with mould lifting process, using the parameters obtained from corresponding rheology tests, on the other hand, yields results in good agreement with mini-slump test experiments.

5.2.3 Using the flume test for yield stress measurement of thickened tailings

- The slow spreading flow (SSF) model for yield stress fluids is generally not valid for laboratory flume tests of thickened tailings due to the sidewall friction of the flume. Theoretically this model only holds if the flume width is infinite or the sidewalls of a flume are frictionless (the inertial effects certainly should be negligible);
- The excellent agreement between the predicted profiles by the FG model and the simulation results with nonslip bottom and sidewalls shows that the FG model, which was developed for laboratory flume tests and took the sidewall friction into

account, is more appropriate to model laboratory flume tests as long as the wall slip at the sidewalls and base is negligible;

- Laboratory flume tests with low deposition rates can be used to measure the yield stress of non-segregating thickened tailings by using the FG model. Moreover, simulation results reveal that the final profile in a flume test is sensitive to yield stress variation but relatively insensitive to the variation of viscosity, which is beneficial for yield stress measurement as the FG model, which is used to obtain yield stress from the final profile, does not account for viscosity;
- The results of the mini-slump test simulations demonstrate that different mould lifting velocities may introduce different inertial effects, thereby impacting the final profiles. Moreover, comparison between the predicted profiles by several theoretical models for the slump test and CFD simulation results reveals that the existing models are not capable of capturing the final shape of slumped material accurately, not only because of the inadequacy of the theoretical models but also the final profile is distorted by the wall friction of the mould. Consequently, the degree of accuracy of the yield stress calculated from a mini-slump test is not very high. Notwithstanding, the mini-slump test provides a quick and easy way to evaluate the rheological properties of thickened tailings to a first approximation in the field;
- The minor errors of the yield stress calculated from the simulation results suggest that the flume test interpreted with the FG model is extremely accurate with respect

to determining the yield stress of thickened tailings. Therefore, it may provide a cheap and robust way of measuring the yield stress of thickened tailings without necessarily resorting to a costly rheometer. Moreover, the flume test may be more appropriate for the yield stress measurement of heavily flocculated clay tailings (such as MFT) compared with the vane technique, considering the similarity (i.e. materials are sheared before and during deposition) between the flume test and field deposition, as well as the possible invalidity of the continuum assumption caused by the presence of large floc particles, which constitute a disadvantage in the vane test, given the small size of vanes typically used;

- The opportunity exists for downscaling the laboratory flume to a desktop flume, which may lead to a cheap, easy and accurate way for yield stress measurement of thickened tailings in both the laboratory and the field.

5.3 Future work

Based on the work conducted in this thesis, some recommendations for the future work are made as follows:

1. Investigations on thickened tailings deposition in flume tests have been performed by using CFD simulations in Chapter 2. The factors, including fluid volume, energy, yield stress, viscosity, flume width and base angle, have been considered. Further research may be extended to deposition methods, such as multilayer deposition and

multi-pipe deposition method in consideration of the fact that both deposition methods are commonly used in industry and expected to have considerable influence on the beach slope achieved in the field.

2. After the tailings are discharged from spigots into a tailings storage facility, a number of small channels of the tailings tend be formed on the beach. It is likely that these small channels gradually converge to form a large channel which influences the beach slope achieved in the field. The spreading flow of thickened tailings in flumes has been studied using CFD simulations in Chapter 2. It is desirable to carry out research on the open-channel junction flow of thickened tailings using CFD simulations in future in order to develop a good understanding of the converging phenomenon encountered in thickened tailings deposition.

3. The CFD simulations in this thesis were performed in the laminar flow regime. The laminar flow assumption for thickened tailings flow is reasonable in this thesis considering the relatively higher yield stress (approximately from 20 to 60 Pa) and viscosity (0.32-10 Pa·s) used in the simulations as well as the relatively simple geometry. However, for the open-channel junction flow discussed above, turbulent flow is possible if the yield stress and viscosity are relatively low and the flow velocity is relatively high. Although there are plenty of analytical solutions and experimental data [136-139] to validate the laminar open-channel flow of yield stress fluids in a CFD software package, the validation of a turbulent model for yield

stress fluid flow is much more challenging [140-143]. Therefore there is a strong need to carry out research on the validation of turbulent models for yield stress fluid flow. Once the turbulent model is validated, CFD simulations can be used confidently to model the turbulent flow of thickened tailings, which will enable the CFD method to obtain more industrial applications in the operations of thickened tailings disposal.

4. Although there are several methods of beach slope prediction for thickened tailings in the literature [65], the accurate prediction in design has proved difficult. Since this thesis has proved that the CFD method is capable of simulating small-scale flow of the Bingham fluid, which is typically used to model thickened tailings, it would be of great interest to seek a way to scale up a small-scale deposition test to a larger or even full scale deposition using the CFD method, considering the flexibility of simulations over experiments.

5. The simulations in this thesis are based on the homogenous fluid approach which assumes that there is no segregation and sedimentation in the flow of thickened tailings. However the segregation would occur for the thickened tailings of relatively low yield stress. Therefore the future work may take the particle settling process into account for scenarios where the sedimentation is important.

Appendix A

STUDIES ON FLUME TESTS FOR PREDICTING BEACH SLOPES OF PASTE USING THE CFD METHOD

Abstract

With the development of thickening techniques, non-segregating, thickened tailings disposal (which is referred to as paste in some cases) appears to be gaining in popularity because of its inherent advantages over conventional tailings (segregating slurry) disposal. One method of investigating the beach profile of thickened tailings is to use a laboratory flume test. Although this method has been utilised to predict the beach profile of conventional tailings successfully for many years, it tends to yield much steeper beach slopes than what is measured in the field. Both experimental and theoretical methods have been used to investigate the flume test in an effort to interpret the enormous disparity of beach slopes of thickened tailings between flume test and field. However, little work to date has been done by using the computational fluid dynamics (CFD) method. To develop a comprehensive understanding of the flume test for thickened tailings, a series of simulations of flume tests were carried out using a commercially available CFD code – ANSYS FLUENT. The influence of several factors, including flume width, initial potential energy (which is equivalent to flow rate), volume of tailings, yield stress and

viscosity, on beach slope in flume tests was investigated. The simulation results show great consistency with those of previous research, which indicates the potential application of CFD methods for beach slope prediction in thickened tailings operations.

A.1 Introduction

Laboratory flume tests have been applied successfully for many years to predict the beach slopes of conventional tailings impoundments, where particles settle out during deposition or transportation, resulting in a change in particle size distribution along the beach [36, 46].

With the development of thickening techniques, non-segregating, thickened tailings disposal is becoming increasingly popular as a result of its inherent advantages (for example, low water consumption, reduced wall-building costs, and reduction of some of the risks associated with conventional tailings disposal) over conventional tailings disposal [25, 63]. However, the flume test has been found to produce unrealistically steep beach slopes for thickened tailings compared with what is achieved in the field [4, 35].

Considerable effort has been made to interpret the enormous disparity of beach slopes of thickened tailings between flume tests and field observations. Sofra and Boger [63] carried out laboratory flume tests to identify the factors, including yield stress, viscosity, depositional flow rate and slope of the underlying base, affecting the deposition behaviour

of thickened tailings with the yield stress varying from 17 to 210 Pa. They used a flume made from clear glass with a length of 2 m and a width of 0.2 m. Through dimensional analysis for material and geometrical parameters, they found that the slope of thickened tailings with different rheology and density is a function of the dimensionless yield stress, the Reynolds and the Froude numbers.

Simms [37] used the ‘‘lubrication theory” to explore the relation between field beach slopes and those from laboratory flume tests for thickened tailings. He asserted that both the scale of flow and the underlying topography have a significant influence on the slope of the deposit. Henriquez et al. [38] pursued the method proposed in Simms [37] to study the dynamic flow behaviour and multilayer deposition of paste tailings. Besides the beach slope’s dependency on flow-scale, they reported no significant changes in the final profiles when the flume width was narrowed from 15 to 10 cm in their flume tests, which was obviously not consistent with Fourie and Gawu’s results [26]. Mizani et al. [69] modelled stack geometry of high density tailings with the lubrication theory and concluded that the equations based on this theory can describe the cyclic deposition of thickened tailings during early stages in both laboratory and field.

Fourie and Gawu [26] conducted both theoretical and experimental work to illustrate the discrepancy of the beach slopes between laboratory flume tests and field observations. The results showed that the slope decreased rapidly with the increase of flume width up

to 500 mm, but became independent of the width when it was greater than 1,600 mm. Meanwhile they developed a numerical model taking the wall friction into account, to compare the model with experimental results, and good agreement was obtained.

Compared to the large amount of experimental and theoretical studies, very little work has been conducted using computational fluid dynamics (CFD) to investigate the flume tests for thickened tailings or paste.

The work reported here uses CFD simulation to assess the influence of several factors on the beach slope achieved in flume tests for paste or thickened tailings. The generic term "paste" is used in this paper. A series of two-dimensional simulations were carried out to investigate the influence of initial potential energy, volume, yield stress and viscosity of paste on the resulting beach slope, while three-dimensional simulations were conducted to study the influence of flume width. It is stressed that the intention of this work is not to compare CFD models with experimental data from flumes. Rather, it is to highlight factors that have previously been neglected when interpreting flume test data, and thus the paper contributes to future work on interpretation of flume test data.

The following section describes the numerical model used in the present work, followed by its validation. Thereafter a series of simulations for different scenarios were described and the corresponding results discussed.

A.2 Numerical model

Simulations in this work were carried out using ANSYS FLUENT, a commercially available CFD code using Finite-Volume Method (FVM) to solve the governing equations. A Bingham model was used to simulate the flow behaviour of paste.

A.2.1 Governing equations

For incompressible flow, the mass and momentum conservation equations in an inertial reference frame (non-acceleration) can be simplified as:

$$\nabla \cdot \boldsymbol{V} = 0 \tag{1}$$

$$\rho \frac{\partial \boldsymbol{V}}{\partial t} + \rho \nabla \cdot (\boldsymbol{V} \cdot \boldsymbol{V}) = -\nabla p + \nabla \cdot \boldsymbol{\tau} + \rho \boldsymbol{g} \tag{2}$$

Where $\mathbf{V}$ is the velocity vector field, ρ is the density of fluid, p is the static pressure, $\boldsymbol{\tau}$ is the stress tensor and $\boldsymbol{g}$ is the gravitational acceleration.

The volume of fluid (VOF) model is used to track the free surface of the fluid in ANSYS FLUENT [102]. In the VOF method, the interface between two phases is characterised by the volume fraction of each fluid that is governed by the volume fraction equation:

$$\frac{\partial \alpha_q}{\partial t} + \nabla \cdot \left(\alpha_q \boldsymbol{v_q}\right) = 0 \tag{3}$$

Where α_q and $\boldsymbol{v_q}$ are the volume fraction and velocity vector field for the q^{th}phase.

For a two-phase system with phase 1 defined as the primary phase, the density in each

cell is given by:

$$\rho = \alpha_2\rho_2 + (1 - \alpha_2)\rho_1 \tag{4}$$

Where $\alpha_2$is the volume fraction of phase 2, $\rho_1$and ρ_2 are the densities for phase 1 and phase 2 respectively. The viscosity of fluid in each cell is computed with the same method.

A.2.2 Bingham model

In the present work, the Bingham model was used to describe the paste which theoretically has a non-zero shear stress when the strain rate is zero [17]. The Bingham law for viscosity implemented in ANSYS FLUENT is given by:

$$\mu = \begin{cases} \mu_0 + \frac{\tau_y}{\dot{\gamma}}, & \dot{\gamma} \geq \dot{\gamma}_c \\ \mu_0 + \frac{\tau_y(2-\dot{\gamma}/\dot{\gamma}_c)}{\dot{\gamma}_c}, & \dot{\gamma} < \dot{\gamma}_c \end{cases} \tag{5}$$

where μ_0 is the plastic viscosity of the material, τ_y is the yield stress and $\dot{\gamma}_c$ is the critical shear rate. For low strain rate ($\dot{\gamma} < \dot{\gamma}_c$), the material acts like a very viscous fluid, while Bingham's constitutive equation is applied beyond the critical shear rate $\dot{\gamma}_c$.

A.3 Validation

To validate the Bingham model implemented in ANSYS FLUENT, velocity profiles of Bingham fluid in a horizontal circular pipe from both the analytical solution and numerical simulation were compared.

For a simple case of Bingham fluid flowing in a horizontal circular pipe, the analytical

solution for velocity distribution can be described by a piecewise function [109, 110]:

$$u(y) = \begin{cases} -\frac{1}{\mu_0}\left[\frac{k}{4}\left(y - \frac{2\tau_y}{k}\right)^2 + \tau_y R - \frac{kR^2}{4} - \frac{{\tau_y}^2}{k}\right], & y \in [S, R] \\ -\frac{1}{\mu_0}\left(\tau_y R - \frac{kR^2}{4} - \frac{{\tau_y}^2}{k}\right), & y \in [0, S] \end{cases} \quad (6)$$

where $u(y)$ is the axial velocity of fluid in a pipe, μ_0 and τ_y are the plastic viscosity and yield stress for Bingham fluid respectively, k is the axial pressure difference per unit length, y is the radial coordinate, S is the radius of the "plug" core inside which there is no shearing flow. The schematic of pipe flow of Bingham fluid is illustrated in **Figure 1**.

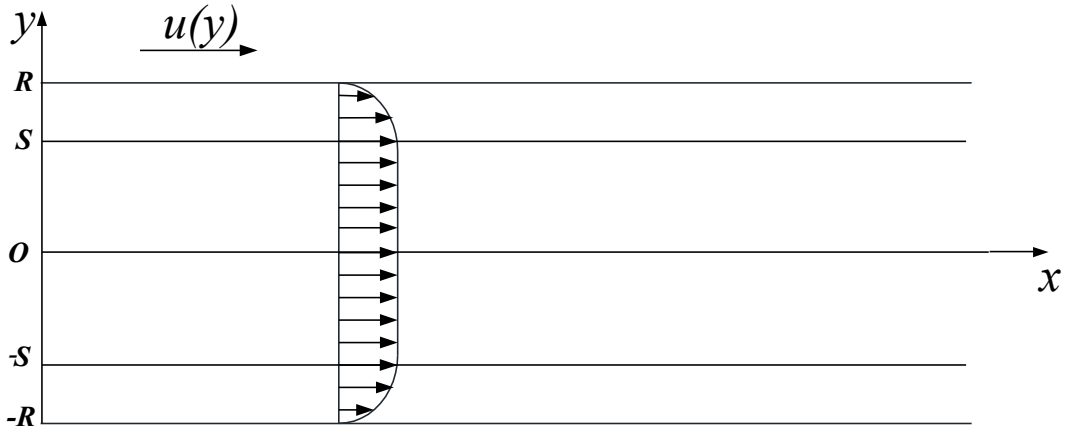

Figure 1 Schematic of Bingham fluid flow in a horizontal circular pipe.

Assume that the inlet velocity is u_0, the Buckingham-Reiner equation can be rewritten as:

$$3R^4k^4 - 8R^3\tau_y k^3 - 24\mu_0 u_0 R^2 k^3 + 16{\tau_y}^4 = 0 \quad (7)$$

Given all parameters aside from k, k can be calculated from Eq.(7), and thus the velocity distribution of the specified Bingham fluid can be obtained from Eq.(6).

For the simulation of Bingham fluid flowing in a horizontal circular pipe, a pipe with a

length of 2 m and a diameter of 0.1 m was considered. A two-dimensional (2D) axially symmetric simulation was conducted. The computational domain was discretised by quadrangles into a mesh of 400 × 50 (length by radius). No-slip wall and axis boundary conditions were used for the pipe wall and centreline of the pipe respectively. The inlet velocity was 0.1 m/s and a pressure-outlet boundary with a zero gauge pressure was specified for the outlet of the pipe. **Figure 2** shows the setup for the 2D simulations of axisymmetric Bingham fluid flow in the circular pipe.

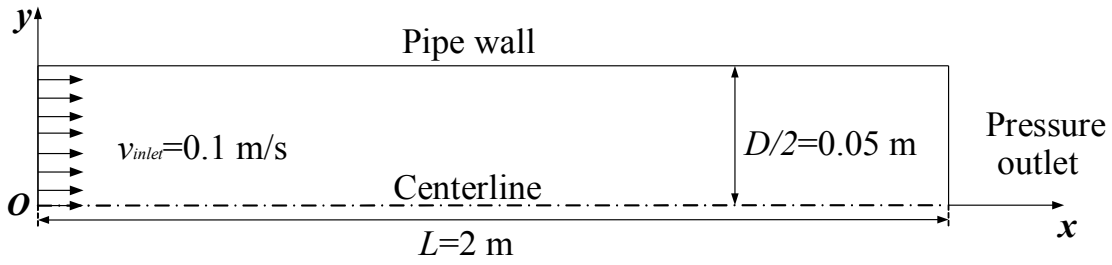

Figure 2 2D axisymmetric setup for the simulation of Bingham fluid flow in a circular pipe.

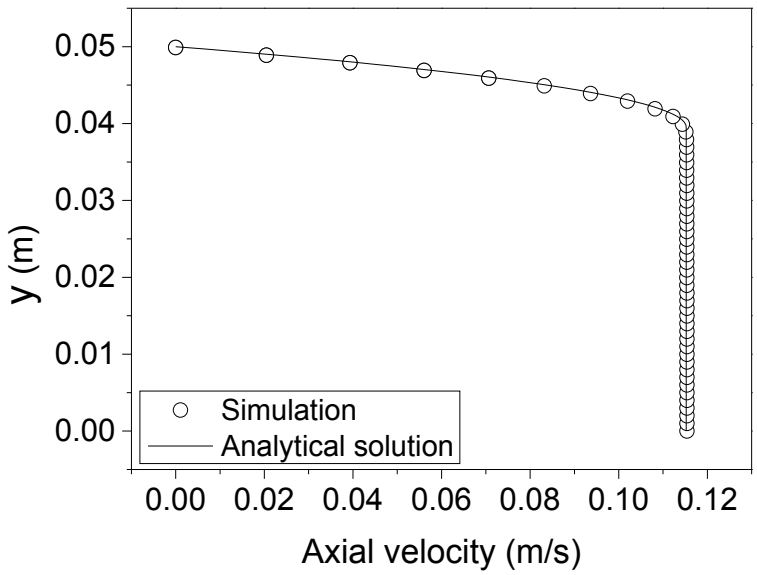

Figure 3 Velocity profiles from the centreline of pipe to the pipe wall.

Figure 3 shows the velocity profiles of pipe flow of Bingham fluid from both simulation and analytical solutions. The excellent agreement between the simulation results and analytical solution verifies the Bingham model in ANSYS FLUENT.

A.4 Results and discussion

A.4.1 The influence of potential energy of paste on flume test

A series of 2D simulations of flume tests was carried out to investigate the influence of initial potential energy of the paste on the resulting beach profile in flume tests. The schematic of the flume apparatus is shown in **Figure 4**. At the beginning of the flume test, the paste is patched in the reservoir (the big end on the left in **Figure 4**) with a specific aspect ratio (a/b). When the simulation starts, the patched paste will flow due to gravity, and finally stop flowing once the equilibrium profile is reached. Information on this type of flume test can be found elsewhere [63]. The simulation was stopped if the spreading of the front end of the beach profile was less than 0.1 mm/s.

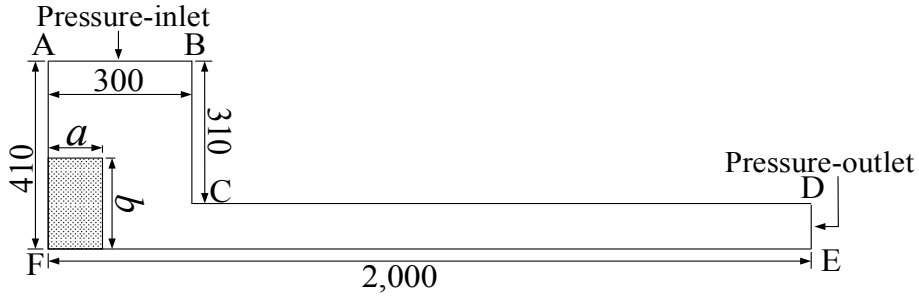

Figure 4 The schematic of setup for the investigations of influence of potential energy on small-scale beach profiles.

To allow variations of the initial potential energy of paste while keeping the same volume of paste in each test, the aspect ratio (a/b) was adjusted with the product of a and b constant. Contours of volume fraction (paste) were saved during the simulations to ensure that the paste did not contact the "irrelevant walls" (AB, BC, CD and DE in **Figure 4**) of the flume.

For the patched paste in **Figure 4**, with the flume width equal to unity, the potential energy of the paste is given by:

$$E_p = \frac{1}{2}\rho g a b^2 \tag{8}$$

where ρ is the density of the paste, g is the gravitational acceleration, a and b are the length and height respectively of the patched area, as shown in **Figure 4**.

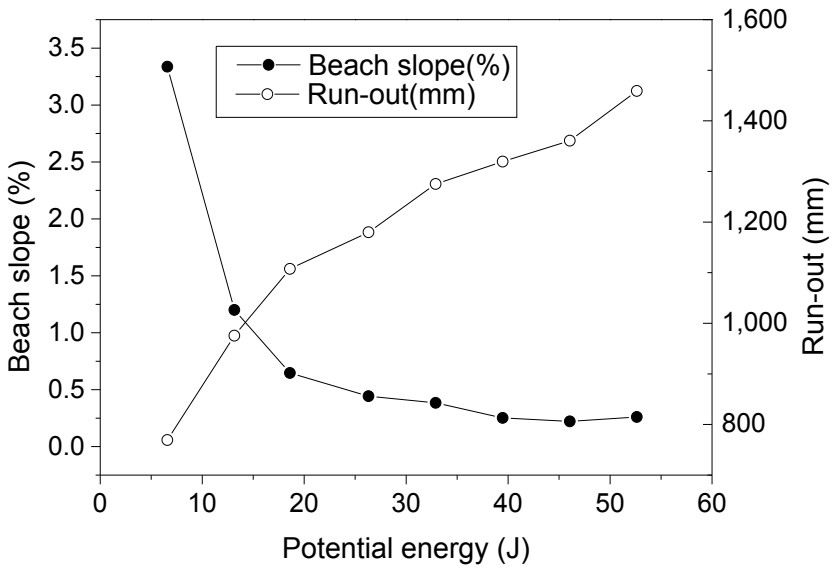

Figure 5 Beach slope and run-out distance versus initial potential energy. The input parameters used are the same as Case 0 in **Table 1**.

Figure 5 summarises the variation of run-out (the beach length of the equilibrium profile in the flume test) and beach slope with the potential energy of paste in the reservoir. The beach slope was obtained by a linear fit for the beach profile. It is clear that with the increment of potential energy the run-out increases significantly, resulting in a reduction of beach slope, which was observed by Sofra and Boger [33, 63] in laboratory flume tests. However it should be noted that the initial paste volume in their flume tests was not fixed when they varied the height of the paste in the reservoir, which means that the volume influence may be mingled with that of potential energy in their results.

A.4.2 The influence of volume of paste on beach slope in flume test

2D simulations of flume tests with the setup shown in **Figure 4** were conducted to study the influence of paste volume on the beach profile.

The height of the patched area (b in **Figure 4**) was fixed at 0.1 m for the six simulations reported in this section, to ensure that the paste in each simulation has equivalent initial potential energy per unit volume. Since the inertial effects are caused by the potential energy in this case, the same initial potential energy per unit volume may yield similar inertial effects in each case, thereby facilitating the analysis of the influence of paste volume on the achieved beach slope. Please note that the term “inertial effects” used in the present work is not identical to the inertia of an object which is solely quantified by its mass. Inertial effects here are the resultant effects caused by inertia. For instance, if

the kinetic energy (per unit volume) of the fluid is higher, then it will be harder to stop the fluid (i.e. more negative work by resistance is required to stop the fluid) due to its inertia, which means that the inertial effects are more significant. Therefore, inertial effects are positively correlated to both density and the magnitude of velocity.

The increase of volume of paste was realised by incrementally extending the length of patched area (a in **Figure 4**) from 0.05 m to 0.3 m. For the 2D simulations of flume tests, the length of the patched area is an indicator of the volume of paste considering the height of patched area was fixed.

In order to analyse the inertial effects in the flume test, the "inertial stress" (Typically "$\rho v^2/l_0$" (l_0 is the characteristic length) which is referred to as the inertial force (per unit volume) is used to get the rough orders of magnitude of the inertial term in momentum equations [111]. As "ρv^2" has a similar expression to inertial force and the same unit of stress (Pa), it is referred to as inertial stress, which can be construed as the kinetic energy per unit volume of a flow in terms of energy) was used as an indicator to evaluate the importance of inertial effects. The typical inertial stress I_{av} (Pa) in a flume test is given by:

$$I_{av} = \rho(\frac{L-a}{T_f})^2 \tag{9}$$

where L (m) is the run-out of paste in flume test, a (m) is the length of patched area, T_f (s) is the flow time required to reach the final equilibrium state, and ρ (kg/m3) is the

density of the paste used in the flume test.

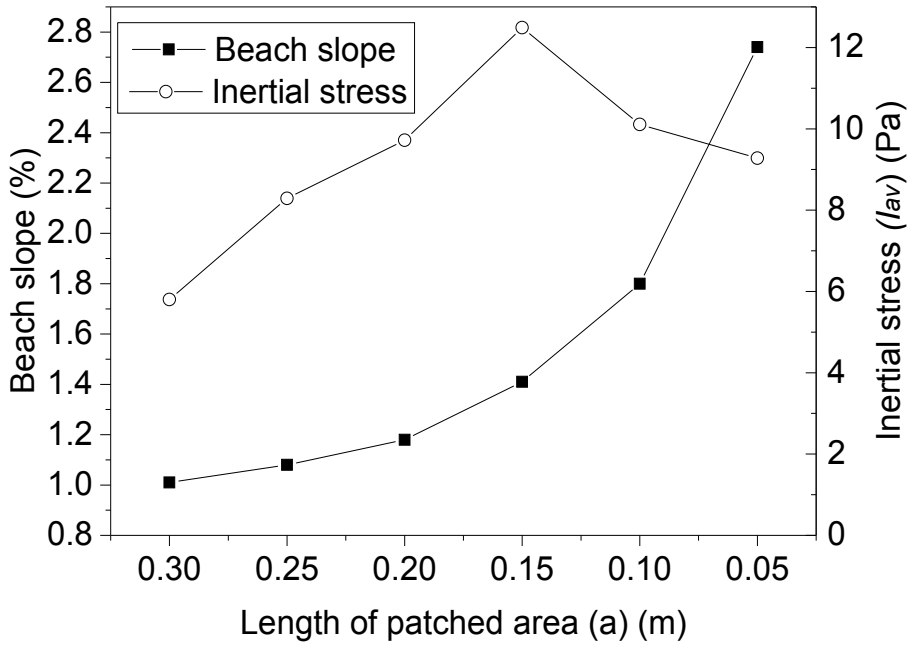

Figure 6 Length of patched area versus beach slope and inertial stress in 2D flume tests. The parameters used are listed in **Table 1**.

Figure 6 demonstrates the influence of inertial tress and the volume of paste, characterised by "length of patched area", on the beach slope based on 2D flume test simulations. Compared to the yield stress (33.28 Pa) of the paste used in the six simulations, the inertial stresses are indeed significant, as shown in **Figure 6**. However does this indicate that the inertial effects play a more important role than the volume in the beach slope formation, or even dominate the tendency of the beach slope variation curve in **Figure 6**?

When the length of patched area is less than 0.15 m, the inertial stress is increasing with the reduction of paste volume. If the inertial effects paly a dominant role in the beach

slope formation, the beach slope should have decreased with the decline of volume as the inertial effects (or inertial stress) tend to increase the run-out, thus reducing the beach slope. However it is clear that the beach slope of the deposition profile increases with the decrease of paste volume, which suggests that the influence of paste volume is more predominant over that of inertial effects.

For the length of patched area larger than 0.15 m, although the inertial stress presents a slight decrease as shown in **Figure 6**, the relatively high values of inertial stress implies that the inertial effects would 'push' the paste to flow further and thus reduce the beach slope. However the beach slopes keep increasing with the reduction of the paste volume according to the beach slope variation curve in **Figure 6**. Therefore the beach slope tends to increase with the reduction of paste volume.

Overall, the flume test simulation results indicate that the beach slope of paste is dependent on the scale of flow, which has been interpreted by Simms et al. [34, 37] using lubrication theory.

A.4.3 The influence of yield stress and viscosity of paste on flume test

In this section, three 2D simulations (Case 0, Case1, Case 2) of flume tests were conducted to study the influence of yield stress and viscosity on beach profile. The parameters used in these cases are listed in **Table 1**.

Figure 7 illustrates the variation from the base case (Case 0) of beach slope and run-out. Generally the increase of yield stress and viscosity reduces the run-out distance and hence leads to a steeper beach slope, as shown in **Figure 7**. Moreover, it can be seen that both the beach slope and run-out distance are more affected by yield stress than viscosity. However, it should be noted that an increase of approximately 25% of the beach slope was caused by a 20% increase of viscosity, which means that the influence of viscosity on beach profile is still significant.

Table 1 The input parameters of paste for simulations of flume test

Cases	Yield stress (τ_y, Pa)	Viscosity (μ_0, Pa·s)	Density (ρ, kg/m^3)
Case 0	33.28	0.4	1,342.6
Case 1	40	0.4	1,342.6
Case 2	33.28	0.48	1,342.6

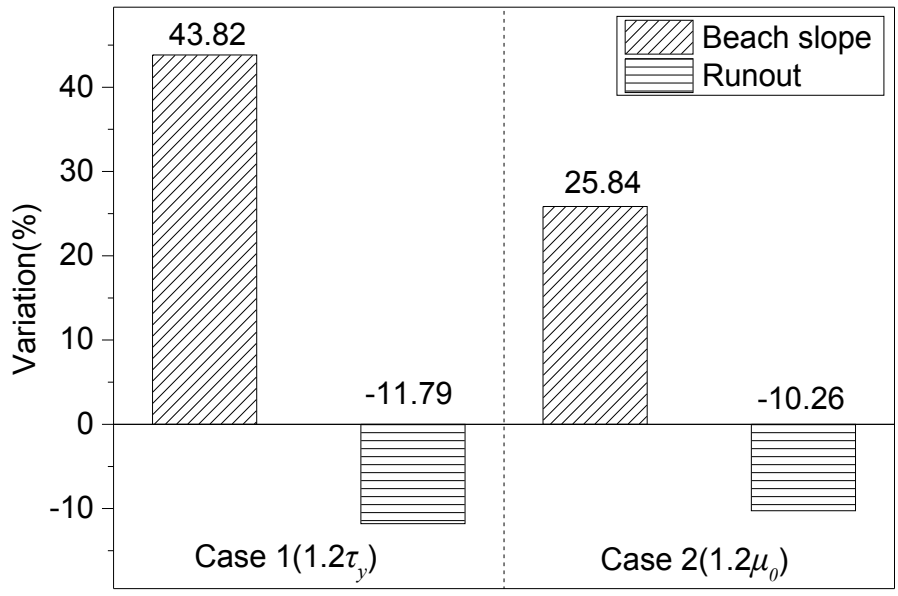

Figure 7 The variation of beach slope and run-out distance with an increase of 20% of yield stress and viscosity from three 2D simulations of flume test. The input parameters for Case 1 and 2 and the base case (Case 0) are listed in **Table 1**.

A.4.4 The influence of flume width on flume test results

Three three-dimensional (3D) simulations of flume tests with flume widths of 0.1 m, 0.2 m and 0.3 m were carried out to investigate the influence of flume width on beach slope. To make the results comparable, the width of the patched fluid varied with the flume width while the length (a in **Figure 8**) and height (b in **Figure 8**) were fixed at 100 mm and 250 mm, respectively. In other words, both the volume of paste per unit width and the potential energy of paste per unit volume were identical in the three simulations. To reduce the "useless" volume of the computational domain occupied by air, a stair-like flume was designed and utilised, as shown in **Figure 8**. There was no contact between the paste and the irrelevant walls (BC, CD, DE, EF and FG in **Figure 8**) during the simulations. The parameters of the paste used in the three simulations are the same as Case 0 listed in **Table 1**.

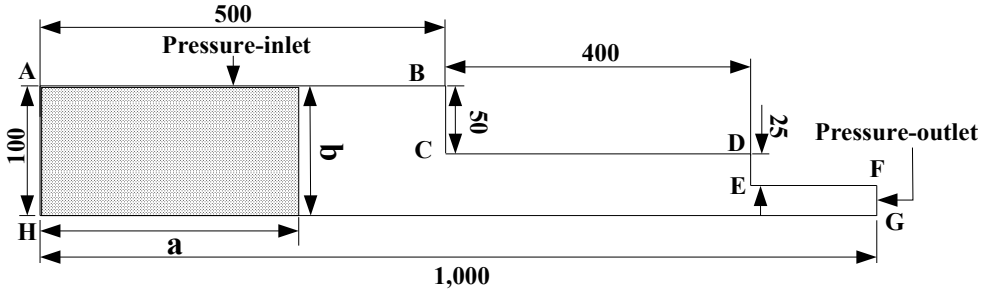

Figure 8 The schematic of setup of 3D flume test simulations (side view).

Figure 9 shows the isometric and top views of the beach at the final stage from the 3D simulation of the flume test with a width of 10 cm. The tongue-shaped front end of the profile clearly indicates the effects of sidewall friction during the flume test. The

intersection between the flume and the symmetric plane is shown in **Figure 10**. It is noted that the intersecting line between the plane of symmetry and the free surface of the deposited paste is reported as the final profile for the 3D simulation of flume tests.

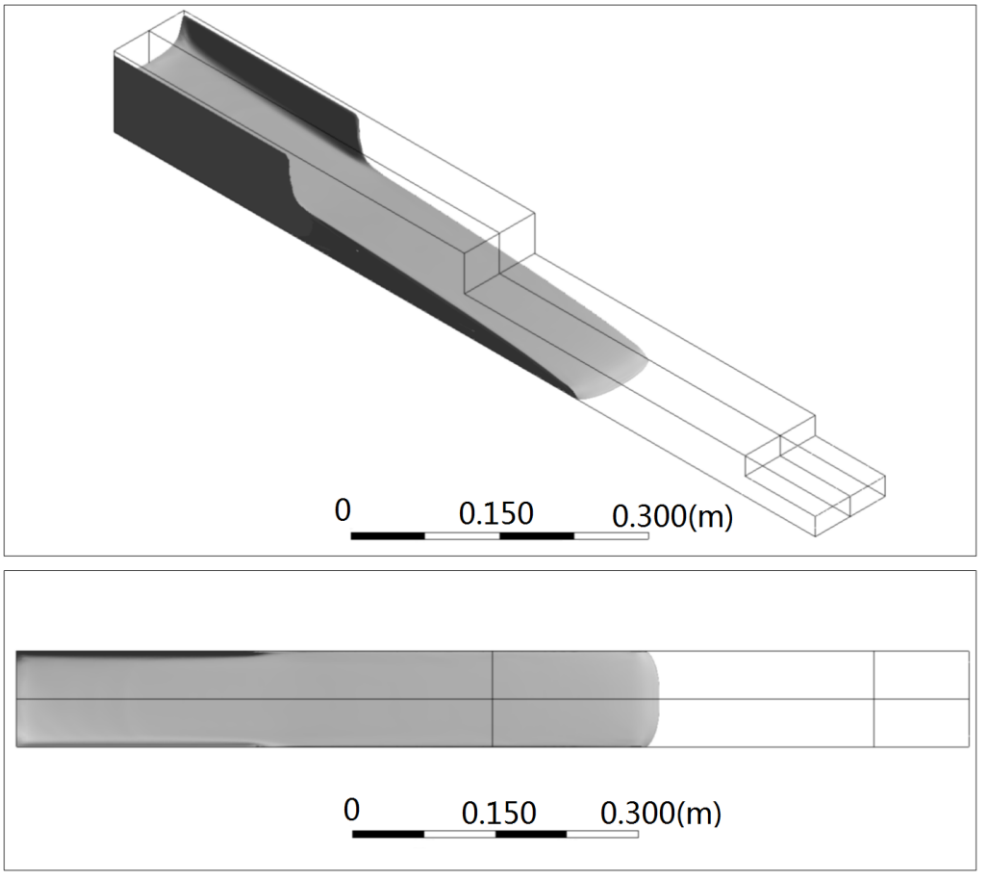

Figure 9 Isometric view (a) and top view (b) of the final state from 3D simulations of the flume test with a width of 10 cm. The volume fraction of paste for the isosurface is 0.5.

Figure 11 illustrates the beach profiles from the 3D simulations of flume tests of different widths and the corresponding linear fit results. Some data points at both ends of the profiles were neglected when the linear fit was performed in order to reduce the "end effects" of the profile on the beach slope, thereby obtaining good fitting. As shown in

Figure 11, the run-out of paste increases while the beach profile decreases with the increment of flume width, which has been described by Fourie and Gawu [26].

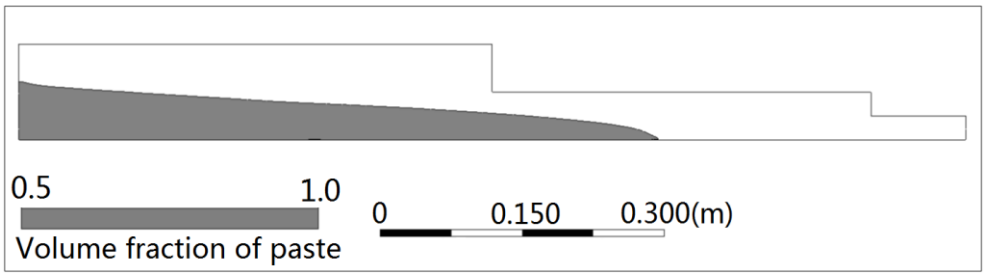

Figure 10 The intersection between symmetry plane and the flume (width = 10 cm) at the final state from 3D simulation of the flume test.

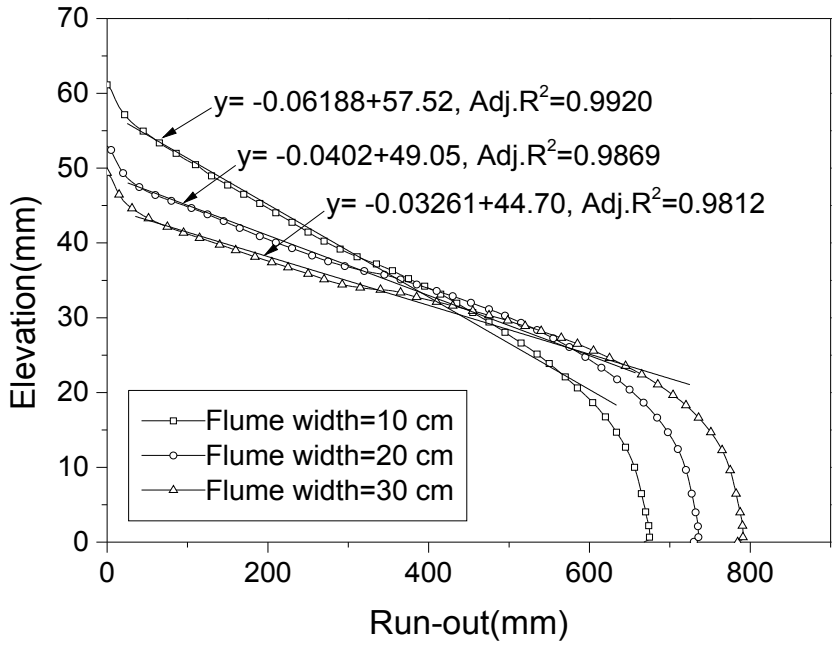

Figure 11 Beach profiles from 3D simulations of flume tests at three different flume widths. The input parameters for the three simulations are the same as Case 0 listed in **Table 1**.

Detailed information about the influence of flume width on beach slope and run-out in flume tests are presented in **Figure 12**. Compared to the run-out of the paste, beach profile is more affected by the flume width ranging from 10 cm to 30 cm, with the same volume

of paste per unit width.

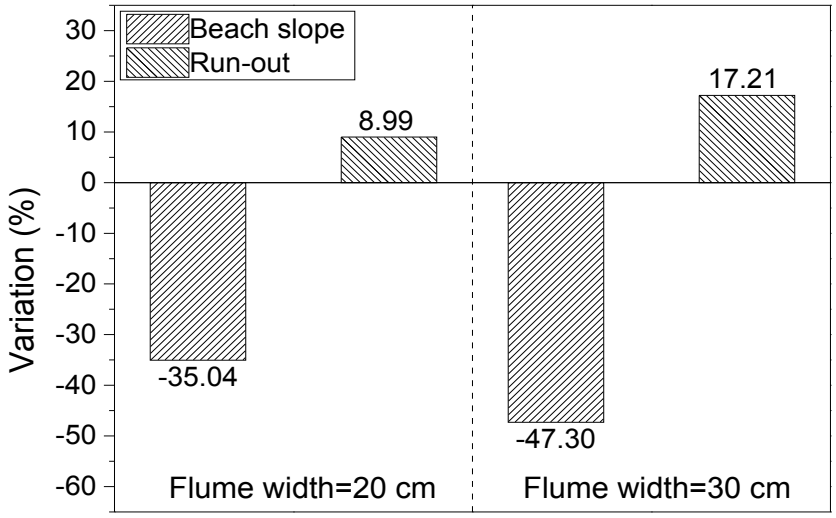

Figure 12 The variation of beach slope and run-out with the increase of flume width from 3D simulation of flume tests. Note: The input parameters for the base flume test (flume width = 10 cm) are listed in **Table 1**.

A.5 Conclusions

Based on the work presented in this paper, several conclusions may be arrived at:

1. The potential energy of paste in a flume test, which corresponds to the discharge flow rate at an operational site, increases the run-out distance and decreases the beach slope angle.
2. The beach slope decreases with an increase of the material volume, which indicates that the beach slope of paste is flow-scale dependent.
3. Although yield stress has more influence on the beach slope than viscosity (for the same percentage change in these parameters), the influence of viscosity on beach

slope is also significant. Therefore, viscosity should be taken into account when beach slope predictions are performed.

4. The influence of flume width on the beach profile increases as the flume width decreases.
5. Generally, the conclusions from CFD simulations are consistent with those from laboratory flume tests and theoretical analyses, which indicates that CFD simulations may provide a new method for beach slope prediction.

Acknowledgements

The authors acknowledge iVEC for providing advanced computing resources located at iVEC@Murdoch (Murdoch University, Perth, Australia).

REFERENCES

[1] D. V. Boger, "Rheology of slurries and environmental impacts in the mining industry," *Annual review of chemical and biomolecular engineering,* vol. 4, pp. 239-257, 2013.
[2] D. Luppnow and J. Moreno, "Esperanza project – drivers for using thickened tailings disposal," in *Proceedings of the 11th International Seminar on Paste and Thickened Tailings (Paste 2008)*, Kasane, Botswana, 2008, pp. 189–198.
[3] B. Busani, A. M. Copeland, R. Cooke, and M. Keevy, "A holistic approach to optimise process water retention and residue disposal for Orapa mines," in *Proceedings of the 9th International Seminar on Paste and Thickened Tailings (Paste 2006)*, Limerick, Ireland, 2006, pp. 147–156.
[4] J. Oxenford and E. R. Lord, "Canadian experience in the application of paste and thickened tailings for surface disposal," in *Proceedings of the 9th international Seminar on Paste and Thickened Tailings (Paste 2006)*, Limerick, Ireland, 2006, pp. 93-106.
[5] A. B. Fourie, "Perceived and realised benefits of paste and thickened tailings for surface deposition," in *Proceedings of the 15th International Seminar on Paste and Thickened Tailings(Paste 2012)*, Sun City, South Africa, 2012, pp. 53-64.
[6] D. J. Cooling, " Improving the sustainability of residue management practices – Alcoa World Alumina Australia," in *Proceedings of the 10th International Seminar on Paste and Thickened Tailings (Paste 2007)*, Perth, Australia, 2007, pp. 3–16.
[7] G. E. Blight and A. B. Fourie, "Catastrophe revisited–disastrous flow failures of mine and municipal solid waste," *Geotechnical & Geological Engineering,* vol. 23, pp. 219-248, 2005.
[8] E. I. Robinsky, *Thickened tailings disposal in the mining industry*: EI Robinsky Associates, 1999.
[9] E. I. Robinsky, "Thickened discharge - A new approach to tailings disposal," *CIM bulletin,* vol. 68, pp. 47-53, 1975.
[10] E. I. Robinsky, "Tailings disposal by the thickened discharge method for improved economy and environmental control," in *Tailings Disposal Today, proceedings of the Second International Tailing Symposium*, Denver, Colorado, USA, 1978, pp. 75-92.
[11] R. J. Jewell, A. B. Fourie, and E. R. Lord, *Paste and Thickened Tailings – A Guide*: Australian Centre for Geomechanics, 2002.
[12] R. J. Jewell, "Thickened tailings in Australia – drivers," in *Proceedings of the 7th International Seminar on Paste and Thickened Tailings (Paste 2004)*, Cape Town, South Africa, 2004.
[13] R. J. Jewell and A. B. Fourie, *Paste and Thickened Tailings – A Guide, 2nd edition*: Australian Centre for Geomechanics, Perth, 2006.
[14] D. V. Boger, "Environmental rheology and the mining industry," in *Proceedings of*

the Sixth International Symposium on Mining with Backfill, Brisbane, Australia, 1998, pp. 15–17.
[15] D. V. Boger, "Rheology and the resource industries," *Chemical Engineering Science,* vol. 64, pp. 4525-4536, 2009.
[16] Q. D. Nguyen and D. V. Boger, "Application of rheology to solving tailings disposal problems," *International Journal of Mineral Processing,* vol. 54, pp. 217-233, 1998.
[17] E. C. Bingham, "An investigation of the laws of plastic flow." vol. 13, ed: Bulletin of the Bureau of Standards, 1916, pp. 309 - 353.
[18] E. C. Bingham, *Fluidity And Plasticity*. New York: Mcgraw-Hill Book Company,Inc., 1922.
[19] M. P. Davies and S. Rice, "An alternative to conventional tailings management–"dry stack" filtered tailings," in *Proceeding of Tailings and Mine Waste'01*, 2001, pp. 411-420.
[20] S. G. Vick, *Planning, design, and analysis of tailings dams*. Vancouver: BiTech, 1990.
[21] U. S. E. P. A. (EPA), "Technical Report: Design and Evaluation of Tailings Dams," Office of Solid Waste Special Waste Branch1994.
[22] T. Fitton, "Tailings beach slope prediction," PhD thesis, RMIT University, 2007.
[23] E. I. Robinsky, S. L. Barbour, G. W. Wilson, D. A. Bordin, and D. G. Fredlund, "Thickened Sloped Tailings Disposal - An Evaluation of Seepage and Abatement of Acid drainage," in *Proceedings of the Second International Conference on the Abatement of Acid Drainage*, Montreal, Quebec, 1991.
[24] M. P. A. Williams, K. D. Seddon, and T. G. Fitton, "Surface disposal of paste and thickened tailings – a brief history and current confronting issues," in *Proceedings of the 11th International Seminar on Paste and Thickened Tailings (Paste2008)*, Kasane, Botswana, 2008, pp. 143–164.
[25] A. B. Fourie, "Paste and thickened tailings: has the promise been fulfilled?," in *GeoCongress 2012: State of the Art and Practice in Geotechnical Engineering*, 2012, pp. 4126-4135.
[26] A. B. Fourie and S. K. Y. Gawu, "The validity of laboratory flume data for predicting beach slopes of thickened tailings deposits," in *Proceedings of the 13th International Seminar on Paste and Thickened Tailings (Paste 2010)*, Toronto, Canada, 2010, pp. 241-254.
[27] X. Huang and M. H. Garcia, "A Herschel–Bulkley model for mud flow down a slope," *Journal of fluid mechanics,* vol. 374, pp. 305-333, 1998.
[28] G. Lauber and W. Hager, "Experiments to dambreak wave: Sloping channel," *Journal of hydraulic research,* vol. 36, pp. 761-773, 1998.
[29] B. Nsom, "Horizontal viscous dam-break flow: experiments and theory," *Journal of Hydraulic Engineering,* vol. 128, pp. 543-546, 2002.
[30] N. Balmforth, R. Craster, P. Perona, A. Rust, and R. Sassi, "Viscoplastic dam breaks and the Bostwick consistometer," *Journal of non-newtonian fluid mechanics,* vol. 142, pp. 63-78, 2007.

[31] C. Ancey and S. Cochard, "The dam-break problem for Herschel–Bulkley viscoplastic fluids down steep flumes," *Journal of Non-Newtonian Fluid Mechanics,* vol. 158, pp. 18-35, 2009.
[32] R. B. Minussi and G. d. F. Maciel, "Numerical experimental comparison of dam break flows with non-Newtonian fluids," *Journal of the Brazilian Society of Mechanical Sciences and Engineering,* vol. 34, pp. 167-178, 2012.
[33] F. Sofra and D. V. Boger, "Slope prediction for thickened tailings and pastes," in *Proceedings 8th International Conference on Tailings and Mine Waste, 16-19 January 2001*, Fort Collins, Colorado, USA, 2001, pp. 75-83.
[34] J. Henriquez and P. Simms, "Dynamic imaging and modelling of multilayer deposition of gold paste tailings," *Minerals Engineering,* vol. 22, pp. 128-139, 2009.
[35] M. Engman, A. Sellgren, A. Sundqvist, T. Wennberg, and I. Goldkuhl, "Users perspective on the design of high density base metal tailings handling systems," in *Proceedings 11th International Conference on Tailings and Mine Waste*, Vail, Colorado, USA, 2004, pp. 45-54.
[36] G. E. Blight, R. R. Thomson, and K. Vorster, "Profiles of Hydraulic-Fill Tailings Beaches, and Seepage through Hydraulically Sorted Tailings," *Journal of the South African Institute of Mining and Metallurgy,* vol. 85, pp. 157-161, 1985.
[37] P. Simms, "On the Relation Between Laboratory Flume Tests and Deposition Angles of High Density Tailings," in *Proceedings 10th International Seminar on Paste and Thickened Tailings (Paste 2007)*, Perth, Australia, 2007, pp. 329-335.
[38] J. Henriquez, A. Vandervoort, and P. Simms, "Imaging and Modelling of Flows of Gold Paste Tailings During Deposition—Laboratory Study and Field Scale Predictions," in *Proceedings 12th International Seminar on Paste and Thickened Tailings (Paste 2009)*, Perth, Australia, 2009, pp. 31-38.
[39] G. E. Blight, "The master profile for hydraulic fill tailings beaches," *Proceedings of the ICE-Geotechnical Engineering,* vol. 107, pp. 27-40, 1994.
[40] C. M. Boldt, "Beach characteristics of mine waste tailings," US Department of the Interior, Bureau of Mines1988.
[41] X. S. Fan and J. Masliyah, "Laboratory Investigation of Beach Profiles in Tailings Disposal," *Journal of Hydraulic Engineering-Asce,* vol. 116, pp. 1357-1373, 1990.
[42] A. B. Fourie, "Beaching and permeability properties of tailings," in *Hydraulic Fill Structures*, Fort Collins, 1988, pp. 142-154.
[43] J. A. Wates, C. Stevenson, and A. R. Purchase, "The effect of relative densities on beaching angles and segregation on gold and uranium tailings dams," in *Proceedings of the International Conference on Mining and Industrial Waste Management*, Johannesburg, South Africa, 1987.
[44] A. L. B. Cavalcante, L. F. M. Ribeiro, and A. P. de Assis, "Experimental and Physical Analysis Applied to Tailing Dams," *Electronic Journal of Geotechnical Engineering,* vol. 18, pp. 485-495, 2013.

[45] A. A. G. Küpper, N. R. Morgenstern, and D. C. Sego, "Laboratory tests to study hydraulic fill," *Canadian Geotechnical Journal,* vol. 29, pp. 405-417, 1992.
[46] A. A. G. Kupper, N. R. Morgenstern, and D. C. Sego, "Comparison between Various Flume Tests Used for Hydraulic-Fill Studies," *Canadian Geotechnical Journal,* vol. 29, pp. 418-425, 1992.
[47] A. B. Fourie and S. K. Y. Gawu, "Post-depositional behaviour of high-density tailings," in *International Seminar on Paste and Thickened Tailings (Paste 2004)*, Cape Town, South Africa, 2004, p. 16.
[48] M. P. A. Williams, "Australian experience with the central thickened discharge method for tailings disposal," in *Proceedings of the Second International Conference on Environmental Issues and Management of Management of Waste in Energy and Mineral Production*, Calgary, Canada, 1992.
[49] K. R. Wood and G. W. Mcdonald, "Design and operation of thickened tailings disposal system at Les Mines Selbaie," *CIM Bulletin,* vol. 79, pp. 47-51, 1986.
[50] N. Pashias, D. V. Boger, J. Summers, and D. J. Glenister, "A fifty cent rheometer for yield stress measurement," *Journal of Rheology,* vol. 40, pp. 1179-1189, 1996.
[51] A. B. Fourie, "Preventing catastrophic failures and mitigating environmental impacts of tailings storage facilities," *Procedia Earth and Planetary Science,* vol. 1, pp. 1067-1071, 2009.
[52] B. J. A. Stuckert, "Model study of sloped tailings deposits," Master thesis, University of British Columbia, 1982.
[53] A. Paterson, "Pipeline transport of high density slurries: a historical review of past mistakes, lessons learned and current technologies," *Mining Technology,* vol. 121, pp. 37-45, 2012.
[54] S. K. Y. Gawu and A. B. Fourie, "Assessment of the modified slump test as a measure of the yield stress of high-density thickened tailings," *Canadian Geotechnical Journal,* vol. 41, pp. 39-47, 2004.
[55] S. Clayton, T. G. Grice, and D. V. Boger, "Analysis of the slump test for on-site yield stress measurement of mineral suspensions," *International Journal of Mineral Processing,* vol. 70, pp. 3-21, 2003.
[56] N. Pashias, D. V. Boger, K. J. Summers, and D. J. Glenister, "A fifty cent rheometer for waste management of environmentally sensitive ore tailings," *Mineral Processing and Extractive Metallurgy Review,* vol. 20, pp. 115-122, 2000.
[57] R. B. Bird, G. Dai, and B. J. Yarusso, "The rheology and flow of viscoplastic materials," *Rev. Chem. Eng,* vol. 1, pp. 1-70, 1983.
[58] Q. D. Nguyen and D. V. Boger, "Measuring the flow properties of yield stress fluids," *Annual Review of Fluid Mechanics,* vol. 24, pp. 47-88, 1992.
[59] G. R. Cokelet, E. Merrill, E. Gilliland, H. Shin, A. Britten, and R. Wells Jr, "The rheology of human blood—measurement near and at zero shear rate," *Transactions of The Society of Rheology (1957-1977),* vol. 7, pp. 303-317, 1963.

[60] G. Scott Blair, "The success of Casson's equation," *Rheologica Acta,* vol. 5, pp. 184-187, 1966.
[61] E. Merrill, B. Koo, E. Salzman, J. Lindon, and D. Brier, "The erythrocyte sedimentation rate of blood reconsidered," in *AI Ch. E. Symposium Series*, 1978, p. 74.
[62] Q. D. Nguyen and D. V. Boger, "Direct yield stress measurement with the vane method," *Journal of Rheology,* vol. 29, pp. 335-347, 1985.
[63] F. Sofra and D. V. Boger, "Environmental rheology for waste minimisation in the minerals industry," *Chemical Engineering Journal,* vol. 86, pp. 319-330, 2002.
[64] G. Christensen, "Modelling the flow properties of fresh concrete: the slump test," PhD thesis, Princeton University, 1991.
[65] P. Simms, M. P. A. Williams, T. G. Fitton, and G. I. McPhail, "Beaching angles and evolution of stack geometry for thickened tailings - a review," in *Proceedings of the 14th International Seminar on Paste and Thickened Tailings (Paste 2011)*, Perth, Australia, 2011, pp. 323-338.
[66] T. G. Fitton and K. D. Seddon, "Related Atterberg Limits to Rheology," in *Proceedings of the 15th International Seminar on Paste and Thickened Tailings(Paste 2012)*, Sun City, South Africa, 2012, pp. 273-284.
[67] H. A. C. Meintjes, "Interpretation of flume tests for non-segregating paste tailings," in *Proceedings of the 7th International Seminar on Paste and Thickened Tailings (Paste 2004)*, Cape Town, South Africa, 2004, p. 6.
[68] R. J. Jewell, "Putting beach slope prediction into perspective," in *Proceedings of the 15th International Seminar on Paste and Thickened Tailings (Paste 2012)*, Sun City, South Africa, 2012, pp. 85-92.
[69] S. Mizani, X. He, and P. Simms, "Application of lubrication theory to modeling stack geometry of high density mine tailings," *Journal of Non-Newtonian Fluid Mechanics,* vol. 198, pp. 59-70, 2013.
[70] J. Gao and A. B. Fourie, "Using the flume test for yield stress measurement of thickened tailings," *Minerals Engineering,* 2015.
[71] *ANSYS FLUENT 15.0 User's Guide, Southpointe, 275 Technology Drive, Canonsburg, ANSYS Inc., USA.*, ANSYS Inc., 2013.
[72] J. Gao and A. B. Fourie, "Spread is better: An investigation of the mini-slump test," *Minerals Engineering,* vol. 71, pp. 120-132, 2015.
[73] N. Roussel, C. Stefani, and R. Leroy, "From mini-cone test to Abrams cone test: measurement of cement-based materials yield stress using slump tests," *Cement and Concrete Research,* vol. 35, pp. 817-822, 2005.
[74] *ANSYS FLUENT 15.0 Theory Guide, Southpointe, 275 Technology Drive, Canonsburg, ANSYS Inc., USA.*, ANSYS Inc., 2013.
[75] S. Osher and J. A. Sethian, "Fronts propagating with curvature-dependent speed: algorithms based on Hamilton-Jacobi formulations," *Journal of computational physics,* vol. 79, pp. 12-49, 1988.

[76] E. Olsson, G. Kreiss, and S. Zahedi, "A conservative level set method for two phase flow II," *Journal of Computational Physics,* vol. 225, pp. 785-807, 2007.
[77] C. W. Hirt and B. D. Nichols, "Volume of Fluid (VOF) Method for the Dynamics of Free Boundaries," *Journal of Computational Physics,* vol. 39, pp. 201-225, 1981.
[78] M. Sussman and E. G. Puckett, "A coupled level set and volume-of-fluid method for computing 3D and axisymmetric incompressible two-phase flows," *Journal of Computational Physics,* vol. 162, pp. 301-337, 2000.
[79] S. Osher and R. P. Fedkiw, "Level set methods: an overview and some recent results," *Journal of Computational physics,* vol. 169, pp. 463-502, 2001.
[80] M. Sussman, "A second order coupled level set and volume-of-fluid method for computing growth and collapse of vapor bubbles," *Journal of Computational Physics,* vol. 187, pp. 110-136, 2003.
[81] K. F. Liu and C. C. Mei, "Approximate equations for the slow spreading of a thin sheet of Bingham plastic fluid," *Physics of Fluids a-Fluid Dynamics,* vol. 2, pp. 30-36, Jan 1990.
[82] K. F. Liu and C. C. Mei, "Slow Spreading of a Sheet of Bingham Fluid on an Inclined Plane," *Journal of Fluid Mechanics,* vol. 207, pp. 505-529, 1989.
[83] E. Buckingham, "On physically similar systems; illustrations of the use of dimensional equations," *Physical Review,* vol. 4, pp. 345-376, 1914.
[84] F. Sofra, "Minimisation of bauxite tailings using dry disposal techniques," PhD thesis, University of Melbourne, 2001.
[85] A. Chryss, T. Fitton, and S. Bhattacharya, "Turbulent flow of non-Newtonian tailings in self-formed channels on tailings stacks," in *Proceedings of the 9th International Seminar on Paste and Thickened Tailings (Paste 2006)*, Limerick, Ireland, 2006, pp. 429-38.
[86] T. Fitton, A. Chryss, and S. Bhattacharya, "Tailings beach slope prediction: a new rheological method," *International Journal of Surface Mining, Reclamation and Environment,* vol. 20, pp. 181-202, 2006.
[87] A. Chryss, A. B. Fourie, A. Monch, D. Nairn, and K. D. Seddon, "Towards an integrated approach to tailings management," *Journal of the Southern African Institute of Mining and Metallurgy,* vol. 112, pp. 965-969, 2012.
[88] T. Kokado, T. Hosoda, and T. Miyagawa, "Study on a Method of Obtaining Rheological Coefficients of High-Flow Concrete with Numerical Analysis," in *Proceedings-Japan Society of Civil Engineers*, 2000, pp. 109-126.
[89] C. F. Ferraris and F. De Larrard, "Modified slump test to measure rheological parameters of fresh concrete," *Cement Concrete and Aggregates,* vol. 20, pp. 241-247, 1998.
[90] EFNARC, "The European guidelines for self compacting concrete-dpecification, production and use," ed. http://www.efnarc.org/publications.html: EFNARC Publications, 2005, p. 63.

[91] N. Tregger, L. Ferrara, and S. R. Shah, "Identifying viscosity of cement paste from mini-slump-flow test," *Aci Materials Journal,* vol. 105, pp. 558-566, 2008.
[92] A. Bouvet, E. Ghorbel, and R. Bennacer, "The mini-conical slump flow test: Analysis and numerical study," *Cement and Concrete Research,* vol. 40, pp. 1517-1523, 2010.
[93] Y. Tanigawa and H. Mori, "Analytical study on deformation of fresh concrete," *Journal of Engineering Mechanics-Asce,* vol. 115, pp. 493-508, 1989.
[94] Y. Tanigawa, H. Mori, and K. Watanabe, "Computer simulation of consistency and rheology tests of fresh concrete by viscoplastic finite element method," in *Proceeding of RILEM Colloquium: Properties of concrete*, 1990, pp. 301-308.
[95] N. Roussel and P. Coussot, ""Fifty-cent rheometer" for yield stress measurements: From slump to spreading flow," *Journal of Rheology,* vol. 49, pp. 705-718, 2005.
[96] N. Roussel, "Correlation between yield stress and slump: Comparison between numerical simulations and concrete rheometers results," *Materials and Structures,* vol. 39, pp. 501-509, 2006.
[97] L. N. Thrane, "Form filling with self-compacting concrete," PhD thesis, Technical University of Denmark, 2007.
[98] N. Q. Dzuy, "Rheology of concentrated bauxite residue suspensions," PhD, Monash University, 1983.
[99] Q. D. Nguyen and D. V. Boger, "Yield stress measurement for concentrated suspensions," *Journal of Rheology,* vol. 27, pp. 321-349, 1983.
[100] M. Keentok, "The measurement of the yield stress of liquids," *Rheologica Acta,* vol. 21, pp. 325-332, 1982.
[101] P. Uhlherr, K. Park, C. Tiu, and J. Andrews, "Yield stress from fluid behaviour on an inclined plane," *Advances in Rheology,* vol. 2, pp. 183-190, 1984.
[102] ANSYS FLUENT 14.0 Theory Guide, Southpointe, 275 Technology Drive, Canonsburg, ANSYS Inc., USA. [Online].
[103] D. Youngs, "Time-dependent multi-material flow with large fluid distortion," *Numerical methods for fluid dynamics,* vol. 24, pp. 273-285, 1982.
[104] ANSYS FLUENT 14.5 User's Guide, Southpointe, 275 Technology Drive, Canonsburg, ANSYS Inc., USA. [Online].
[105] ANSYS FLUENT 14.0 UDF Manual, Southpointe, 275 Technology Drive, Canonsburg, ANSYS Inc., USA. [Online].
[106] J. D. Dent and T. E. Lang, "A biviscous modified Bingham model of snow avalanche motion," *Annals of Glaciology,* vol. 4, pp. 42-46, 1983.
[107] J. M. Brethour, "Incremental elastic stress model," Flow Science technical note 64 (FSI-03-TN64), Flow Science, Inc.2003.
[108] T. C. Papanastasiou, "Flows of materials with yield," *Journal of Rheology,* vol. 31, pp. 385-404, 1987.
[109] E. Buckingham, "On plastic flow through capillary tubes," in *Proc. Am. Soc. Test. Mater*, 1921, pp. 1154-1156.

[110] M. Reiner, *Deformation and flow: an elementary introduction to theoretical rheology*. London,: H. K. Lewis, 1949.
[111] R. B. Bird, W. E. Stewart, and E. N. Lightfoot, *Transport phenomena*, 2 ed. New York: John Wiley & Sons, 2007.
[112] N. Tregger, L. Ferrara, and S. Shah, "Empirical relationships between viscosity and flow-time measurements from minislump tests for cement pastes formulated from SCC," in *5th International RILEM Symposium on Self-Compacting Concrete*, 2007, pp. 273-278.
[113] N. Roussel, "Three-dimensional numerical simulations of slump tests," *Annual Transaction of the Nordic Rheology Society,* vol. 12, pp. 55-62, 2004.
[114] D. V. Boger, "Rheology and the minerals industry," *Mineral Processing and Extractive Metallurgy Review,* vol. 20, pp. 1-25, 2000.
[115] T. L. H. Nguyen, N. Roussel, and P. Coussot, "Correlation between L-box test and rheological parameters of a homogeneous yield stress fluid," *Cement and Concrete Research,* vol. 36, pp. 1789-1796, 2006.
[116] J. Wendt, *Computational fluid dynamics: an introduction*: Springer Science & Business Media, 2008.
[117] P. Coussot, S. Proust, and C. Ancey, "Rheological interpretation of deposits of yield stress fluids," *Journal of Non-Newtonian Fluid Mechanics,* vol. 66, pp. 55-70, 1996.
[118] B. S. Palmer and R. J. Krizek, "Thickened slurry disposal method for process tailings," in *Geotechnical Practice for Waste Disposal'87*, 1987, pp. 728-743.
[119] M. Yuhi and C. C. Mei, "Slow spreading of fluid mud over a conical surface," *Journal of Fluid Mechanics,* vol. 519, pp. 337-358, 2004.
[120] G. E. Blight, M. J. Robinson, and J. A. C. Diering, "The flow of slurry from a breached tailings dam," *Journal of the South African Institute of Mining and Metallurgy,* vol. 81, pp. 1-8, 1981.
[121] E. Olsson and G. Kreiss, "A conservative level set method for two phase flow," *Journal of computational physics,* vol. 210, pp. 225-246, 2005.
[122] F. J. Kelecy, "Coupling momentum and continuity increases CFD robustness," *ANSYS Advantage,* vol. 2, pp. 49-51, 2008.
[123] W. D. Whetham, "On the alleged slipping at the boundary of a liquid in motion," in *Proceedings of the Royal Society of London*, 1890, pp. 225-230.
[124] M. A. Day, "The no-slip condition of fluid dynamics," *Erkenntnis,* vol. 33, pp. 285-296, 1990.
[125] S. Prabhakara and M. Deshpande, "The no-slip boundary condition in fluid mechanics," *Resonance,* vol. 9, pp. 61-71, 2004.
[126] P. Coussot, "Steady, laminar, flow of concentrated mud suspensions in open channel," *Journal of Hydraulic Research,* vol. 32, pp. 535-559, 1994.
[127] S. G. G. Stokes, *Mathematical and physical papers* vol. 1. Cambridge: Cambridge University Press, 1880.
[128] T. Kokado, T. Hosoda, T. Miyagawa, and M. Fujii, "Study on a method of

evaluating a yield value of fresh concrete with a slump flow value," *Proceedings of the Japan Society of Civil Engineers,* pp. 19-29, 1997.
[129] E. P. Bostwick, "Consistometer," United States Patent, 1942.
[130] L. E. Charlebois, "On the flow and beaching behaviour of sub-aerially deposited, polymer-flocculated oil sands tailings: a conceptual and energy-based model," Master thesis, The University of British Columbia (Vancouver), 2012.
[131] P. Coussot, *Rheometry of pastes, suspensions, and granular materials: applications in industry and environment*: John Wiley & Sons, 2005.
[132] B. Derakhshandeh, S. G. Hatzikiriakos, and C. P. J. Bennington, "The apparent yield stress of pulp fiber suspensions," *Journal of Rheology,* vol. 54, pp. 1137-1154, 2010.
[133] S. Mizani, S. Soleimani, and P. Simms, "Effects of polymer dosage on dewaterability, rheology, and spreadability of polymer-amended mature fine tailings," in *Proceedings of the 16th International Seminar on Paste and Thickened Tailings (Paste 2013)*, Belo Horizonte, Brazil, 2013, pp. 117-131.
[134] W. Ren, K. Sury, and S. Clingman, "Enhanced thickened tailings performance via additional chemical treatments," in *Proceedings of the 17th International Seminar on Paste and Thickened Tailings (Paste 2014)*, Vancouver, Canada, 2014, pp. 245-255.
[135] S. Mizani, P. Simms, A. Dunmola, C. Côté., and G. Freeman., "Rheology for surface deposition of polymer-amended fine tailings," in *Proceedings of the 17th International Seminar on Paste and Thickened Tailings (Paste 2014)*, Vancouver, Canada, 2014, pp. 295-306.
[136] R. Haldenwang and P. Slatter, "Experimental procedure and database for non-Newtonian open channel flow," *Journal of Hydraulic Research,* vol. 44, pp. 283-287, 2006.
[137] J. Burger, R. Haldenwang, and N. Alderman, "Experimental database for non-Newtonian flow in four channel shapes," *Journal of Hydraulic Research,* vol. 48, pp. 363-370, 2010.
[138] R. Haldenwang, P. T. Slatter, and R. P. Chhabra, "An experimental study of non-Newtonian fluid flow in rectangular flumes in laminar, transition and turbulent flow regimes," *Journal of the South African Institution of Civil Engineering,* vol. 52, pp. 11-19, 2010.
[139] I. D. Sutalo, A. Bui, and M. Rudman, "The flow of non-Newtonian fluids down inclines," *Journal of Non-Newtonian Fluid Mechanics,* vol. 136, pp. 64-75, 2006.
[140] R. Y. Guang, M. Rudman, A. Chryss, and S. Bhattacharya, "DNS of turbulent non-newtonian flow in an open channel," in *Seventh International Conference on CFD in the Minerals and Process Industries*, Melbourne, Australia, 2009.
[141] R. Guang, M. Rudman, A. Chryss, P. Slatter, and S. Bhattacharya, "A DNS investigation of non-Newtonian turbulent open channel flow," *AIP Conference Proceedings,* vol. 1225, pp. 179-184, 2010.
[142] R. Guang, M. Rudman, A. Chryss, P. Slatter, and S. Bhattacharya, "A DNS

investigation of the effect of yield stress for turbulent non-newtonian suspension flow in open channels," *Particulate Science and Technology,* vol. 29, pp. 209-228, 2011.

[143] R. Guang, M. Rudman, A. Chryss, P. Slatter, S. Bhattacharya, R. Jewell*, et al.*, "Direct numerical simulation (DNS) investigation of turbulent open channel flow of a Herschel-Bulkley fluid," in *Proceedings of the 14th International Seminar on Paste and Thickened Tailings (Paste 2011)*, 2011, pp. 439-452.